Advancing Efficiency and Stability of Lead, Tin, and Lead/Tin Perovskite Solar Cells: Strategies and Perspectives

Dhruba B. Khadka,[1*] Yasuhiro Shirai,[1] Masatoshi Yanagida,[1] James W. Ryan,[2] Zhaoning Song,[3] Bobby G. Barker Jr.,[4] Tara P. Dhakal,[5] and Kenjiro Miyano[1]

[1]Photovoltaic Materials Group, Center for GREEN Research on Energy and Environmental Materials, National Institute for Materials Science (NIMS), 1-1 Namiki, Tsukuba, Ibaraki 305-0044, Japan
[2]Department of Chemistry, Swansea University, Singleton Park, Swansea SA2 8PP, UK
[3]Department of Physics and Astronomy and Wright Center for Photovoltaics Innovation and Commercialization, University of Toledo, 2801 W Bancroft St, Toledo, OH 43606, USA
[4]Department of Chemistry and Physics, Augusta University (GE 3041), USA
[5]Department of Electrical and Computer Engineering Material Science and Engineering, and Center for Autonomous Solar Power (CASP), Binghamton University, Binghamton, NY 13902, USA

Corresponding Author

*E-mail: KHADKA.B.Dhruba@nims.go.jp

ABSTRACT

Halide-perovskite-based solar cells (HPSCs) have established themselves as a promising photovoltaic technology in a remarkably short time. The rapid improvement in HPSCs can be attributed to the unique material and optoelectronic properties of metal halide perovskite semiconductors coupled with a very knowledgeable and experienced PV community. This review briefly summarizes the chemistry of halide perovskites, delving into the fundamental aspects of crystal structure and optical bandgap, followed by a more in-depth report on the advancements in HPSCs efficiencies, thanks to structural regulation, interfacial modulation, and thin-film engineering. We mainly focus on three metal halide perovskites topics: i) high performance Pb-based perovskites, ii) Sn-based perovskites and their associated challenges, and iii) emerging work on mixed composition Pb-Sn perovskites. For each of these domains, we examine the effects stemming from the tuning of the monovalent A-site and the halide site. Additionally, we discuss various approaches aimed at passivating defects in the bulk film and at the interface, along with carrier transport engineering. Our discussions also encompass the broader implications for device performance, stability and material toxicity. Finally, we provide perspectives on the future directions and the commercial feasibility of perovskite photovoltaic technologies.

Key words: perovskite solar cells, interface engineering, device stability, Sn-Pb perovskite, tin perovskite

1. Introduction

Photovoltaic (PV) technology, which harnesses solar energy to generate electricity without causing harm to the environment, has garnered considerable interest as a green energy technology. Although the photovoltaic effect was uncovered by French physicist Alexandre-Edmond Becquerel in 1839, PV technology came to mainstream only after the invention of the first practical silicon solar cells at Bell Laboratories in 1954.[1] Today, silicon-based PV technology has achieved a power conversion efficiency (PCE) of 26.8%,[2] approaching the theoretical limit of single-junction solar cells. As low-cost alternatives, thin-film and emerging PV technologies were widely explored based on various photo-absorber materials such as chalcogenide-based semiconductors (CdTe, copper indium gallium sulfide (CIGS), copper zinc tin sulfide (CZTS)), organic semiconductors, quantum dots, dyes, and halide perovskites (HPs). Although all these prevailing PV technologies are still inferior to market-dominant Si-PVs in terms of efficiency and stability, they can be produced with a lower carbon footprint and quicker energy payback time, which promises a bright future for various PV technologies.

Halide perovskites have emerged as one of the most promising light-absorbing materials in the last decade. Miyasaka and coworkers first reported on the application of HPs in dye-sensitized solar cells in 2009.[3] Since then, the PCE of halide perovskite solar cells (HPSCs) has skyrocketed from 3.8% to an impressive 26% (certified) by tailoring device structure and fabrication approach,[4] as well as engineering material composition,[5,6] functional additives,[7,8] interfaces,[9,10] charge carrier transport and charge extraction.[11,12] As for Pb-HPSCs, recent research has been focused on operational device stability and large-area submodules. With the knowledge of materials chemistry and interface engineering, the structural stability under thermal, light, and humidity stress have been investigated to resolve the device stability issues,[13–16] in addition to enhancement in device performance toward the theoretical limit.[16–19] All these technical advances in low-cost fabrication methods, high PCEs, and enhanced device stability are driving HPSCs towards commercialization. Yet, the long-term operational stability and toxicity of Pb HPs have raised concern for their widespread application.[20] Therefore, it is paramount to develop stable and environmentally friendly HPSCs.

To address the toxicity issue of Pb-HPSCs, so far, the alternative candidates primarily encompass group IV metals (tin (Sn) and germanium (Ge)) including group V metals (bismuth (Bi) and antimony (Sb)) and copper (Cu). The trivalent HP candidates (Bi^{3+} and Sb^{3+}) are air-stable and environmentally friendly.[21,22] However, because of their +3 valence states, Bi/Sb-based multidimensional perovskite materials, such as $Cs_3Bi_2I_9$ and $Cs_3Sb_2I_9$, show higher bandgaps (~2 eV) and exciton binding energy, which is undesired for harvesting sunlight and carrier transport,[22] limiting the PCE of these Bi/Sb-based HPSCs.[23–26] Being in the same group (IVA) as Pb, Sn^{2+} and Ge^{2+} metal ions are more favorable candidates as non-toxic alternatives. However, Ge^{2+} easily loses its lone pair electrons due to its $4s^2$ electronic configuration, compromising chemical stability and limiting the PCE of Ge-based HPSCs below 1%.[27] Compared with Ge-HP films, which are most likely to suffer from the instability of Ge^{2+} and are easily oxidized into Ge^{4+}, Sn-based HPs show much-improved stability.[28] Although the stability of Sn-based HPs is still inferior to Bi/Sb HPs, Sn-HPs are the most promising candidate to substitute toxic Pb-HPs owing to excellent optical and electrical properties, especially HPSCs.

Indeed, both Sn and Pb possess the same valence states and comparable ionic radius. Therefore, the substitution of Sn to Pb hardly alters the perovskite crystal structure. Sn-HP derivatives have favorable or even better

photoelectric properties than Pb-HPs with their suitable bandgap (1.2–1.4 eV) close to the theoretical limit, smaller exciton binding energy, and higher charge-carrier mobility.[29] Exploiting the experiences in developing Pb-HPSCs, Sn-HPSCs have progressed device PCE to 14.81% after materials chemistry modifications and interface engineering.[30] Noting that the efficiencies of Sn-HPSCs still lag behind Pb-HPSCs, multiple efforts are currently centered on advancing Sn-based devices as ideal alternatives to Pb-HPs. On the other hand, benefiting from the progress of Pb or Sn- HPSCs, Pb-Sn mixed binary HPs have also made significant advances. Mixed Sn-Pb HPs possess the unique advantage of having an optimal bandgap (~1.2 eV), which is favorable for tandem HPSCs. In the current scenario, Pb- and Sn-Pb -based HPSCs have demonstrated competitive device performance,[31] and an accelerated effort into advancing multijunction HPSCs or tandem device structures has been made.[32,33]

In this review, we discuss the fundamental properties of Pb and Sn-based HP materials and their application in state-of-the-art HPSCs. A number of methods have been successfully introduced for the improvement in device efficiency and stability. We have categorized the widely adopted fabrication techniques; (i) A and X-site engineering, (ii) multifunctional additive engineering, (iii) interfacial passivation by organic molecules molecular passivation, (iv) 2D/3D perovskite composite, (v) strain modulation, and (vi) carrier transport engineering. We mainly review recent advancements in device efficiency and stability, with an emphasis on the material chemistry approaches employed to optimize bulk and interfacial properties. Lastly, we highlight prospective routes to develop efficient and stable HPSCs using various derivatives of HPs as a primary photo-harvesting layer.

2. Fundamental of Metal Halide Perovskite

2.1 Crystal Structure and Tolerance Factor

Gustavus Rose discovered the mineral calcium titanate ($CaTiO_3$) in the Ural Mountains of Russia in 1839. The mineral was named after Lev Alekseyevich Perovski, a Russian mineralogist.[34] The term perovskite has since been used for materials with the ABO_3 structure, in the case of metal oxide perovskites, and more recently ABX_3 for metal halide perovskites, where A is a monovalent cation, B a divalent metal cation, and X a monovalent halide anion. C. K. Møller can be attributed to the discovery of the first halide-based perovskite structure, $CsPbX_3$, in 1958.[35] While the first metal-organic hybrid halide perovskite was reported by Weber in 1978.[36] A variety of halide perovskite derivatives have since been explored.[37,38]

A variety of anions can be utilized for forming metal halide perovskites. In general, the monovalent cation, A could be organic or inorganic preferably, Cs^+, Rb^+, methylammonium (MA^+), or formamidinium (FA^+); the divalent B site is usually occupied by Pb^{2+} in high efficiency solar cells but Sn^{2+}, or Ge^{2+} can also be used, and the monovalent anion X sites comprise I^-, Br^-, or Cl^-. As depicted in Figure 1, the optimal crystal structure is a cubic lattice with the B metal sixfold coordinated by X in BX_6 octahedra, and A-12-fold coordinated by X anions in AX_{12} cubo-octahedra. The tuning of these components can greatly alter the structural and electronic properties of HPs and is crucial when tailoring HPs for certain applications. For example, the bandgap is particularly influenced by the choice of ions used, *vide infra*.

It is also important to understand how the choice of ions influences the structural stability of the perovskite crystal structure. The equilibrium crystal structure can be evaluated using two parameters, Goldschmidt's tolerance (t) and the octahedral factor (μ) as defined below.[39]

Tolerance (t)= $\frac{R_A+R_X}{\sqrt{2}(R_B+R_X)}$ (1)

and

Octahedral factor (μ) = $\frac{R_B}{R_X}$ (2)

where R_A, R_B, and R_X are the ionic radii of the corresponding ions, respectively. A table showing the values of a series of frequently explored perovskites is shown in Figure 1a (Table 1). The tolerance factor is helpful for understanding the structural transition in stoichiometric engineering. Materials with a t~1 and μ between 0.44 and 0.90 retain a highly symmetric cubic structure, α phase (Figure 1b). At finite temperature, the cubic structure may exist in the range of 0.8< t <1.107, otherwise the cubic structure is unstable. When the A cation is undersized or the B cation is oversized, the perovskite structure undergoes distortion (t<1). The crystal lattice then changes from the high-symmetry cubic phase to a low-symmetry tetragonal or orthorhombic phase with distorted octahedral BX_6 as depicted in Figure 1b. For t >1, the three-dimensional (3D) B-X network destabilizes resulting in the hexagonal phase.

The monovalent A-cation plays a significant role in templating the inorganic framework, with its size regulating the tilting of the BX_6 octahedra and the structural distortions deviating from the ideal X–B–X bond angles. Substituting A-sites with different sizes in halide perovskite, where the B site consists of either Pb, Sn or Ge, alters the symmetry and formation energy. For example, if we consider Cs^+, the largest group-I element, it is still not large enough to hold the stable cubic phase at room temperature and tends to transform $CsPbI_3$ into the orthorhombic perovskite structure. That is why replacing Cs with larger molecules, MA^+ or FA^+, leads to optimal tolerance factor values and the stable cubic phase. When an oversized organic A cation is included (t>1), the 3D structure transforms to low-dimensional perovskite structures, such as layered 2D perovskites, including Ruiddlesden–Popper perovskites, Dion–Jacobson perovskites, and the alternating-cation perovskites.[40]

Besides these structures, many alternative Pb-free perovskites have been explored by substituting the B^{2+} cations with different valencies. Alternative structures will be formed as depicted in Figure 1c. For example, as B^{2+} is replaced by B^{4+}, it leads to the A_2BX_6 vacancy ordered perovskite crystal that forms a vacancy with one-half of the octahedral B cation. This structure has been reported with Sn^{4+},[41,42] Bi,[4+43] and Ti^{4+}.[44,45] Considering the B^{3+} cation, it can form a 2D layered perovskite, $A_3B_2X_9$ (e.g., $Cs_3Sb_2I_9$, $Cs_3Bi_2I_9$, $Rb_3Sb_2I_9$), where a vacancy substitutes one of every three octahedral B cation sites.[23,26,46–48] Another alternative double-perovskite structure has also been engineered by mixing monovalent (B^+) and trivalent (B^{3+}) cations in place of the divalent metal cation with the general formula $A_2B^+B^{3+}X_6$. The most explored double perovskites are $Cs_2(Ag,Bi)Br_6$,[49] $Cs_2AgSbCl_6$,[50] $Cs_2(Ag,In)Cl_6$,[51] and $MA_2(Ag,Bi)Br_6$.[52,53] All of the above-mentioned stable alternatives have been used for solar cell devices but device efficiencies have not come close to the more established Pb and Sn based ABX_3 perovskites.[46,54–57]

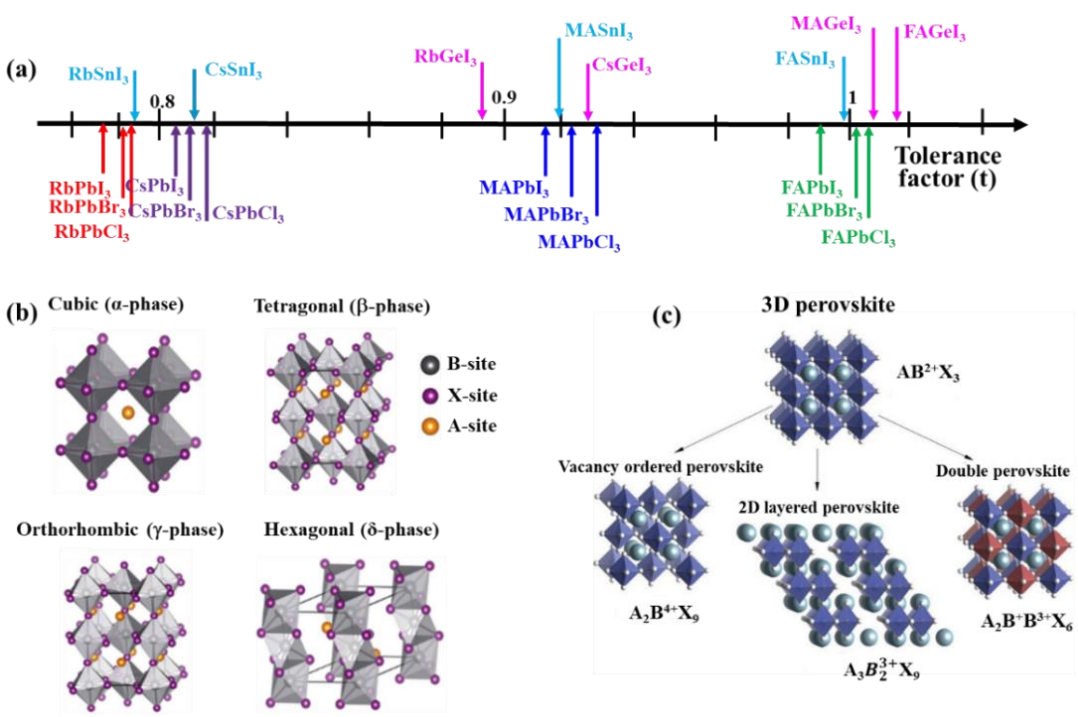

Figure 1. Variations in the perovskite crystal structures. (a) Tolerance factor of perovskite derivatives (summarized in Table 1). Inspired by the report.[58] (b) Perovskite crystal phases: cubic, tetragonal, orthorhombic, and hexagonal. Reproduced with permission.[59] Copyright 2020, Springer Nature. (c) Alternative structural derivative of perovskite, standard perovskite (top), vacancy ordered perovskite, 2D layered perovskite, and double perovskite. Reproduced with permission.[60] Copyright 2016, American Chemical Society.

Table 1. Tolerance factor for Pb, Sn, and Ge- based halide perovskites (Eqn 1 and 2; ionic radius data ref.)[58]

Tolerance factor (t)	Ionic radius	R_B (pm)	Pb			Sn			Ge		
			119			115			75		
	Octahedral factor (μ)		0.541	0.607	0.647	0.523	0.587	0.625	0.341	0.383	0.408
	R_A (pm) ↓	R_X (pm) →	I	Br	Cl	I	Br	Cl	I	Br	Cl
			220	196	184	220	196	184	220	196	184
FA	253		0.987	1.008	1.020	0.998	1.021	1.033	1.134	1.172	1.193
MA	216		0.909	0.925	0.933	0.920	0.937	0.946	1.045	1.075	1.092
Cs	167		0.807	0.815	0.819	0.817	0.825	0.830	0.928	0.947	0.958
Rb	152		0.776	0.781	0.784	0.785	0.791	0.795	0.892	0.908	0.917

2.2 Optical Bandgap and Electronic Band Structure

Metal halide perovskites have unique properties which are attributed to a combination of the perovskite crystal symmetry and its electronic band structure. First principle calculations indicate that the valence band maximum (VBM) of $APbX_3$ is derived from the strong antibonding character between the Pb-6s and X-p orbitals, while the conduction band minimum (CBM) is mainly formed from the Pb-6p orbitals with negligible coupling to X-s orbitals.[59,60] The electronic structure of halide perovskites embodies a distinctly hybrid nature, comprising both ionic and covalent

characteristics. Its orbital symmetry promotes a strong dipole transition moment between the valence and conduction bands. The antibonding nature in the VBM contributes to the defect-tolerant nature of lead halide perovskites, as iodide's dangling bond, which is formed by a vacancy in the lead cation, resonates within the VBM. Importantly, due to the lone-pair s-orbitals, HPs have a direct band structure with a stronger p-p optical transition as compared to conventional semiconductor materials such as GaAs and CdTe, whose direct bandgaps (E_g) derive from a p-s transition.[61] Regarding perovskite crystal phases, α-phase HP has a similar band structure to both β and γ phase HPs suggesting Pb-I-Pb bond distortion does not affect the electronic structure significantly.[61] While in the δ-phase, the Pb-I bonds are broken and the 3D [Pb-I] framework is destroyed due to weaker coupling between Pb s and I p orbitals. This weaker coupling results in a lowering of the VBM, leading to a wide E_g as observed in experiments.[62–64]

The optical bandgap of a HP is typically determined by its chemical composition ABX_3. A-site cations do not have a direct role in confining the basic band structure in HPs but change the lattice spacing and the overlapping of Pb-X orbitals. A recent report by Park and co-workers suggests a contrasting point, and states that the electronic structure at the band edge of HP is influenced by the s-orbital state of A-site ions.[65] Nonetheless, it is widely observed that the A-site is more sensitive to stabilizing the perovskite structure and lattice change. For $APbI_3$ HPs, replacing MA with a larger FA cation reduces the bandgap from 1.52 to 1.48 eV. On the contrary, substituting MA with a smaller size Cs increase in E_g to 1.67 eV (Figure 2a). Indeed, the size of A- cation plays a critical role in regulating the bond length and electron cloud interaction between B and X ions. A-site cations exert an indirect influence on the electronic structure which is manifested by altering the volume of the ABX_3 lattice or introducing distortions within the ideal perovskite structure with a change in the B-X bond. With a longer B-X bond length, the overlap of electron clouds between B and X atoms decreases, resulting in a lower E_g.

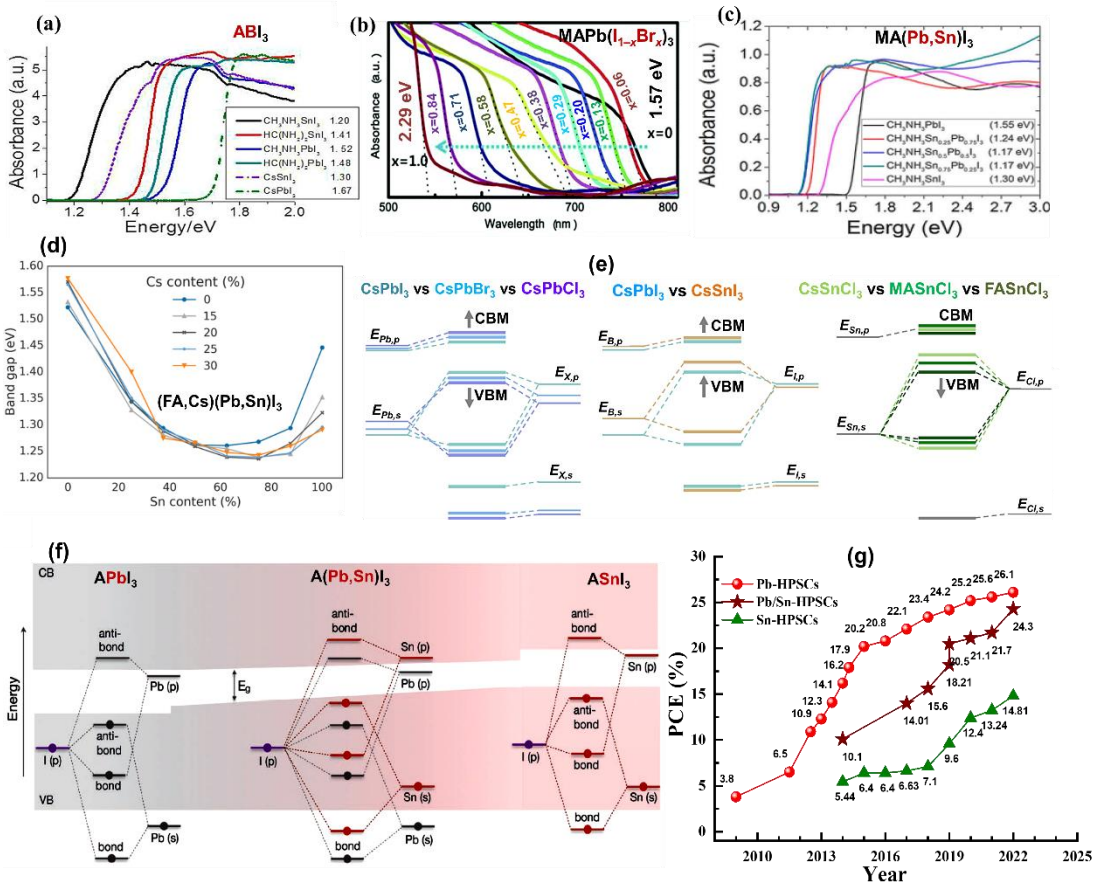

Figure 2. Relations between perovskite composition and bandgap. UV–vis absorption spectra; effect of (a) A and B -site in ABI_3. Reproduced with permission.[66] Copyright 2013, American Chemical Society. (b) X-site engineering in of $MAPb(I,Br)_3$ ($E_g(x)=E_g(0)+0.39x+0.33x^2$). Reproduced with permission.[6] Copyright 2013, American Chemical Society. (c) effect of B (Pb-Sn)-site alloying $MA(Pb,Sn)I_3$.[67] Copyright 2014, ACS. (d) Bandgap of Pb-Sn mixed perovskites with varying fractions of (FA/Cs). Reproduced with permission.[68] Copyright 2017, American Chemical Society. (e) Schematic energy levels in ABX_3 perovskites; represents (i) trends in changing X-site, (ii) trends in changing B-site and (iii) tends in changing A-sites, where the arrow indicates shifting of energy level upon substitution. Reproduced under the terms of the CC-BY license.[69] Copyright 2019, The Authors, Springer Nature. (f) Schematic of the origin of the bandgap bowing in $A(Pb_{1-x}Sn_x)I_3$, shaded regions indicate the VBM and CBM with bold lines showing the molecular orbital picture of the formation of electronic bands. Reproduced with permission.[70] Copyright 2018, American Chemical Society. (g) Efficiency progress of Pb, Pb/Sn, and Sn-based HPSCs.[71–73]

For the X-halide site, the bandgap shows a blue shift when replacing I with Br and a further blue shift when Cl takes its place (Figure 2b).[74–77] The position of the Pb 6p atomic level has a predominant influence on the CBM, shifting upwards when transitioning from I to Br to Cl. As the Pb-X distances decrease from I-Br to Cl, the electron localized on a Pb atom becomes more confined, resulting in an increase in its energy. This shifts the CBM level upwards for smaller halogen atomic size, while the VBM is significantly influenced by higher electronegativity. The strength of

Pb,*s*/X,*p* hybridization is slightly enhanced as halogen size decreases. Consequently, the X,*p* level determining the VBM level undergoes a downward shift, resulting in a substantial increase in the E_g with decreasing halogen size.

As the B-site (Pb^{2+}) is mixed with smaller cations (Sn^{2+}), it dominantly affects the E_g of HPs. Despite being akin to $APbI_3$, the size and electronic structure of Sn affect the band structure and E_g of $ASnX_3$ films.[78] As depicted in Figure 2a, $MASnI_3$ and $FASnI_3$ lowered E_g to 1.20 and 1.41 eV, respectively. Similarly, the bandgap of $CsSnI_3$ is 1.30 eV and the E_g is increased to 1.60 eV for $CsGeI_3$.[28] With reference to electronic structure, DFT calculations suggest that the binding strength of Sn^{2+}(s) and Sn^{2+}(p) atomic orbitals are less than those of the corresponding Pb^{2+} states. By substituting Pb with Sn, upwards shift in atomic levels is observed, which can be attributed to the smaller electronegativity of Sn. As depicted in Figure 2e, both VBM and CBM move upwards. Due to the smaller splitting between s and p states in an Sn atom compared to a Pb atom, the upward shift of the s level is larger than that of the p level. Consequently, the upward shifting of VBM is more than the CBM level. Thus, the energy band edges of $ASnI_3$ exhibit a weaker binding compared to Pb^{2+}-analogues, resulting in a reduction in E_g.[69]

The B-site alloying HP system has documented the bandgap bowing trend for Pb-Sn alloying HPs with either A-site atoms: MA, FA, or Cs.[67,68,79] The E_g of Pb-Sn alloyed HPs can be tuned from ~1.55 to 1.17 eV, making them optimal E_g absorber layers for harvesting the solar spectrum (Figure 2c).[67] It is worth noting that achieving an optimal bandgap for a single-junction solar cell falls within the range of 1.1 to 1.4 eV. This desirable range can be attained through alloying Sn and Pb in an HP system (Figure 2c, d). This bandgap bowing results from loosely bounded Sn-s and Sn-p atomic orbitals than corresponding Pb states. Hence, in the case of Pb/Sn-alloyed HP materials, the VBM originates from interactions between Sn-s and I-p orbitals, whereas the CBM is predominantly influenced by the Pb-p and I-p orbitals. And hence, the E_g reduced compared to the corresponding pristine perovskites (Figure 2f). Besides that, there could be a small contribution of lattice strain and local relaxation in an alloyed film which could modify the band edge shifts.[68]

3. Lead-Based HPSCs

Since the initial report from the Miyasaka group on HPSCs utilizing a $MAPbI_3$ light absorbing layer,[80] there has been a remarkable increase in the PCE of Pb-HPSCs, soaring from 3.8 to ~26.1%[81] (Figure 2g). A couple of years on from the first report using HP as a sensitizer in dye-sensitized solar cells, mesoporous (Gratzel and Park;[82] Miyasaka and Snaith [83]) and planar device structures were introduced. The device performance scaled through an array of advances based on optimizing film growth and crystallization,[84,85] solvent engineering,[4,86–89] film composition,[5,90] additive engineering,[7,91] surface defect passivation,[92,93] and carrier transport engineering.[94–96] Keeping aside the device structure and crystallization approach, in this review, we discuss the strategies for bulk and interface modulation of Pb-HPSCs for simultaneous improvement in PCE and operational stability, as summarized in Table 2.

Table 2. Summary of the strategies used for the advancement of Pb-HPSCs.

Strategies	Materials	Pb-HP	Device structure	PCE (%) (Control to target)	Stability data (Target device)	Year	Ref.
A-site engineering		$(Cs,FA,MA)Pb(Br,I)_3$	FTO/c-TiO_2/Li-m-TiO_2/Pb-HP/Spiro-OMeTAD/Au	17.42 to 21.17	~86% of PCE_0 @ t~250 h	2016	[5]
	MDAI	$(MDA,Cs,FA)PbI_3$	FTO/c-TiO_2/m- TiO_2/Pb-HP/Spiro-OMeTAD/Au	22.72 to 25.17	Unencapsulated: 85 °C, dark, 25% RH; ~80% of	2020	[80]

					PCE_0 @ t~1300 h		
	FASCl	$(FAS,FA)PbI_3$	FTO/NC-TiO_2/m- TiO_2/Pb-HP/spiro-OMeTAD/Au	19.59 to 23.11	Unencapsulated: 85 ºC, argon ambient, dark, ~92.5% of PCE_0 @ 1000 h	2021	[8]
X-site engineering	Ammonium tetrafluoroborate ($NH4BF_4$)	$(FA,MA)Pb(I,Br)_3$	FTO/SnO_2/Pb-HP/Spiro-OMeTAD/MoO3/Au	17.55 t0 20.16	Encapsulated: MPPT, ~86% of PCE_0 @ 300 h	2019	[81]
	Methylammonium thiocyanate (MASCN)	$FAPbI_3$	ITO/SnO_2/Pb-HP/Spiro-MeOTAD/Au	17.95 to 23.21	Encapsulated: MPPT, ~90% of PCE_0 @ 500 h	2020	[82]
	X-additive: FACOOH Passivation: Octylammonium iodide (OAI)	$FAPbI_3$	FTO/c-TiO_2/Li-m-TiO_2/Pb-HP/OAI/Spiro-OMeTAD/Au	23.92 to 25.6%.	Unencapsulated: 60 ºC, 20% RH, dark; >80% of PCE_0 @ t~1000 h	2021	[83]
Additive	OAI	$(OA,MA)PbI_3$	FTO/c-TiO_2/mp-TiO_2/Pb-HP/PTAA/Au	18.4 to 20.6	Unencapsulated: 85 ºC, dark; ~80% of PCE_0 @ t~760 h	2018	[84]
	4-chlorophenyltrifluoroborate potassium salt (4-ClPTFBK)	$(MA,FA)Pb(I,Br)_3$	FTO/SnO_2/Pb-HP/Spiro-OMeTAD/Au	22.63 to 24.50	Unencapsulated: 85ºC, dark; ~86% of PCE_0 @ t~1000 h	2023	[85]
	Imidazole (MZ-1)	$(Cs,FA,MA)Pb(I,Br)_3$	ITO/SnO_2/Pb-HP/Spiro-OMeTAD/Li-TFSI /Ag	21.01 to 24.61		2023	[86]
	Ionic liquid: Methylammonium butyrate (MAB)	$(FA,MA)Pb(I,Br,Cl)_3$	FTO/SnO_2/Pb-HP/Spiro-OMeTAD/Au	23.03 to 25.10	Unencapsulated: 85 ºC, 25% RH; ~ 84% of PCE_0 @ t~800 h	2023	[87]
Passivation (multifunctional molecules)	Pentafluorophenylethylammonium iodide (FEAI)	$(Cs,FA,MA)PbI_3$	FTO/c-TiO_2/Pb-HP/FEAI/Spiro-OMeTAD/Au	19.97 to 22.09	Encapsulated: MPPT, 40% RH; ~ 90% of PCE_0 @ t>1000 h	2019	[88]
	Cyclohexylethylammonium iodide (CEAI)	$(Cs,FA,MA)Pb(I,Br)_3$	FTO/c-TiO_2/Pb-HP/CEAI/Spiro-OMeTAD/Au	20.99 to 23.57	Unencapsulated: MPPT, RT, N_2-ambient; 96% of PCE_0 @ t~1500 h	2021	[89]
	Ferrocenyl-bis-thiophene-2-carboxylate ($FcTc_2$)	$(Cs,FA,MA)Pb(I,Br)_3$	ITO/PTAA/Pb-HP/$FcTc_2$/C_{60}/BCP/Ag	23.0 to 25.0	Encapsulated: 85 ºC/85% RH; 95% of PCE_0, @ t~1000 h	2022	[90]
	Pentafluorophenylhydrazine (5F-PHZ)	$(Rb,Cs,FA)PbI_3$	ITO/NiO_x/MeO-2PACz/Pb-HP/5F-PHZ/C60/BCP/Ag	18.10 to 22.29	Encapsulated: MPPT, RT; 93% of PCEo @ t~1000 h	2023	[10]
	2-amino-5-bromobenzamide (ABA)	$CsPb(I,Br)_3$	ITO/NiO_x/Pb-HP/ABA/PCBM/BCP/Ag	18.46 to 20.38	Unencapsulated: air ambient, 25% RH; 83% of PCE_0 @300 h	2023	[91]
Passivation (LD perovskite)	2D-HP with Oleylammonium iodide (OAI)	$(Cs,FA,MA)PbI_3$	ITO/2PACz/Pb-HP/OAI HP/C_{60}/BCP/Ag	22.3 to 24.3	Encapsulated: damp-heat; 95% of PCE_0 @ t~1200 h	2022	[92]
	2D-HP: $BA_2MA_{n-1}PbnI_{3n+1}$)	$(Cs,FA,MA)Pb(I,Br)_3$	ITO/SnO_2/Pb-HP/2D-HP/Spiro-OMeTAD/Li-TFSI-tBP/Au	21.0 to 24.5	Encapsulated: 65ºC/75% RH; 99% of PCE_0 @ t~2000 h	2022	[17]
	Phenyltrimethylammonium iodide (PTMAI)	$CsPbI_3$	FTO/c-TiO_2/Pb-HP/PTMAI/Spiro-OMeTAD/Au	19.10 to 21.0	Unencapsulated: air ambient, 25% RH; ~83% of PCE_0 @ t~2000 h	2022	[93]
Contact engineering	ETL: TiO_2-nanorods	$(Cs,FA,MA)Pb(Br,I)_3$	ITO/c-TiO_2/nr-TiO_2/PMMA:PCBM/Pb-HP	20.83 to 23.17	Encapsulated: damp-heat; 92%	2021	[94]

			/PMMA/P_3HT:CuPc/Au		of PCE_0 @ t~1000 h		
	Porous insulating contact (PIC)-Al_2O_3	$(Cs,FA,MA)Pb(I,Br)_3$	ITO/SAM/PIC-Al_2O_3/Pb-HP/LiF/C_{60}/BCP/Ag	~23.0 to 25.56	Unencapsulated: 85 ºC, N_2-ambient, 20%-RH; ~98% of PCE_0 @ t~1000 h	2023	[95]
	Self-assembled monolayers	$(Cs,FA,MA)Pb(I,Br)_3$	ITO/SAM/Pb-HP/F-PEAI/C_{60}/BCP/Ag	22.63 to 25.40	Encapsulated: damp-heat; ~95% of PCE_0 @ t~500 h	2023	[96]
	n-type band bending: Propylamine hydrochloride (PACl)	$CsPbI_3$	FTO/P_3CT/Pb-HP/PACl/PCBM/BCP/Ag	14.43 to 20.17	Unencapsulated: RT, air ambient, 20% RH; 97% of PCE_0 @33 days	2023	[97]

3.1. Pb-HPSCs: A and X- Site Engineering

A primary aspect of A or X-site engineering is the modulation of structural and opto-physical properties of the HP film for enhanced device performance and stability. $MAPbI_3$, the HP commonly used in HPSCs, suffers from intrinsic instability during operation due to the volatilization of MA (methylammonium).[98,99] This instability has prompted researchers to explore alternative HP compositions. Among these alternatives, the mixed cations Pb-HPs, such as $(Cs,MA,FA,Rb)PbI_3$, have emerged as highly effective in enhancing both stability and efficiency, consequently dominating the forefront of research in this field.[5,100] For the mixed cation strategy, the combination of different cations in the A-site of the perovskite structure leads to the formation of a perovskite alloy with improved properties (e.g., suppression of the non-photoactive δ-phase and surface or grain boundary defects). However, some recent studies propose an alternative viewpoint, suggesting that the mixed cations may coexist as microcrystals rather than forming a fully alloyed composite structure.[101] NMR analysis revealed that the cations; Cs, MA, and FA could form an alloyed composite, but alkali ions (K and Rb) with smaller radii grew with a non-perovskite phase and stayed either on the surface or between grains as a mixed phase, serving as a passivating species.[101,102] Moving away from organic cations entirely, all inorganic $CsPbI_3$ offers superior material stability and is considered as priority in the $APbI_3$ family for improved device stability.[93,103,104] Yet, its bandgap is larger than the optimal bandgap for single-junction solar cells and is mainly considered for tandem applications.[105,106]

Strain in HPs plays a crucial role in dictating both device efficiency and stability of devices,[107,108] and can be modulated via A-site engineering. A good example of this has been demonstrated by Seok and colleagues, where they revealed that by substituting Cs and methylenediammonium (MDA) cations into FA-sites of $FAPbI_3$, the lattice strain is effectively reduced (Figure 3a) by more than 70% compared to pristine HPs. This reduction in strain led to several beneficial effects, including an increase in carrier lifetime and a decrease in defect concentration. As a result, the PCE exceeded 25% with superior device stability.[80] Importantly, the magnitude of strain is relatively high in HP compared to other photovoltaic materials: such as residual strain values of up to ~2.4% for α-$FAPbI_3$[18] whereas the PCE of Si and CIGS devices drops substantially when residual strains exceed ~1%.[109,110] The high magnitude of strain in perovskite materials can be correlated to the device stability of HPSCs. As documented in a report,[111] due to their mechanical fragility, perovskites are highly susceptible to strain, making strain engineering a critical factor in enhancing

device stability for photovoltaic applications

Park and coworkers reported an extensive review on modifying HPs through A-site engineering, as depicted in Figure 3b.[65] The effect that the size of the A-site cation has on chemical and optoelectronic properties was succinctly discussed. A-site cation engineering is crucial for tuning the material properties of HP, including the thermodynamic stability of polymorphic HP, impeding ionic migration at the interface and grain boundaries by electrostatic interactions, strain engineering, interface energy band modification, interface passivation, and surface modification. Undersized alkali cations, such as Rb and K, possess strong electropositive properties that effectively bind and immobilize excessive and undercoordinated halide ions, thereby suppressing undesired ion migration.[112] The introduction of alkali cation doping elevates the formation energy of mobile halide interstitial defects.[113] Besides partial alloying in A-sites, the bulky cations can segregate on grain boundaries and surfaces by virtue of their functional characteristics. Bulky cations also serve as physical barriers that enhance the activation energy for ion migration by obstructing low-energy migration pathways along the grain boundaries. Additionally, ammonium-based cations can electrostatically bind to negatively charged defects (such as A cation vacancies and undercoordinated halides), preventing their migration and deactivating their charge-trapping capability. For instance, Zhu et al. employed formamidine disulfide dihydrochloride (FASCl) as a potent oxidant and a localized electron scavenger to capture electrons.[8] It is found that substituting FA^+ with FAS^{2+} eliminates strongly localized electrons from iodine vacancies and mitigates the formation of deep traps. The addition of FASCl stabilizes the black α-phase $FAPbI_3$ and retards crystallization, and promotes the formation of compact, highly crystalline HP layers with large grain sizes, resulting in enhanced efficiency and stability Figure 3c-e.

Besides cation-modulation strategies, X-site engineering also significantly affects the optoelectronic properties of HPs. As discussed in the previous section, the X-site tunes the tolerance factors, bandgap, and formation energy. The bandgap and formation energies gradually increase with a decrease in halogen size.[114] Despite the variation in absolute bandgap in different reports, when going from iodine to chlorine, the bandgap of $MAPbX_3$, $FAPbX_3$, and $CsPbX_3$ ranges between 1.58–3.06 eV, 1.48–3.02 eV, and 1.75–2.90 eV, respectively.[115] Due to the higher phase transition energy of the mixed halide, halide engineering is not only beneficial for tuning device performance but also for stability with optimal compositional engineering.[116,117] It is demonstrated that defects associated with iodide, such as interstitial iodide and iodide vacancies, pose challenges due to their low formation energy. However, these defects can be passivated by incorporating smaller halides, leading to improved optoelectronic quality and defect dynamics of HPs. Nevertheless, the application of mixed halide hybrid perovskites can be limited due to the potential occurrence of halide segregation induced by various factors such as light, heat, electric fields, etc. The non-uniform distribution of halide significantly lowers the open-circuit voltage, V_{OC}, in HPSCs.[118] A detailed study by Hoke et al. found that phase segregation occurs in mixed halide perovskite films under light irradiation, resulting in the formation of minority iodide-rich and majority bromide-enriched domains.[119] The segregated phases deteriorate the optical properties of the film and lead to a reduction in the bandgap. Moreover, the minority domains in the HP film act as recombination trap centers which are detrimental to device performance. To address the phase segregation issue, HP films with thresholds in halide composition have been proposed.[120,121] With optimal triple halide engineering, wide bandgap HPSCs demonstrated superior stability and prevented phase segregation under illumination.[122,123] A strategy of halide engineering could

play a vital role in the fabrication of tandem devices using perovskite subcells with various bandgaps.

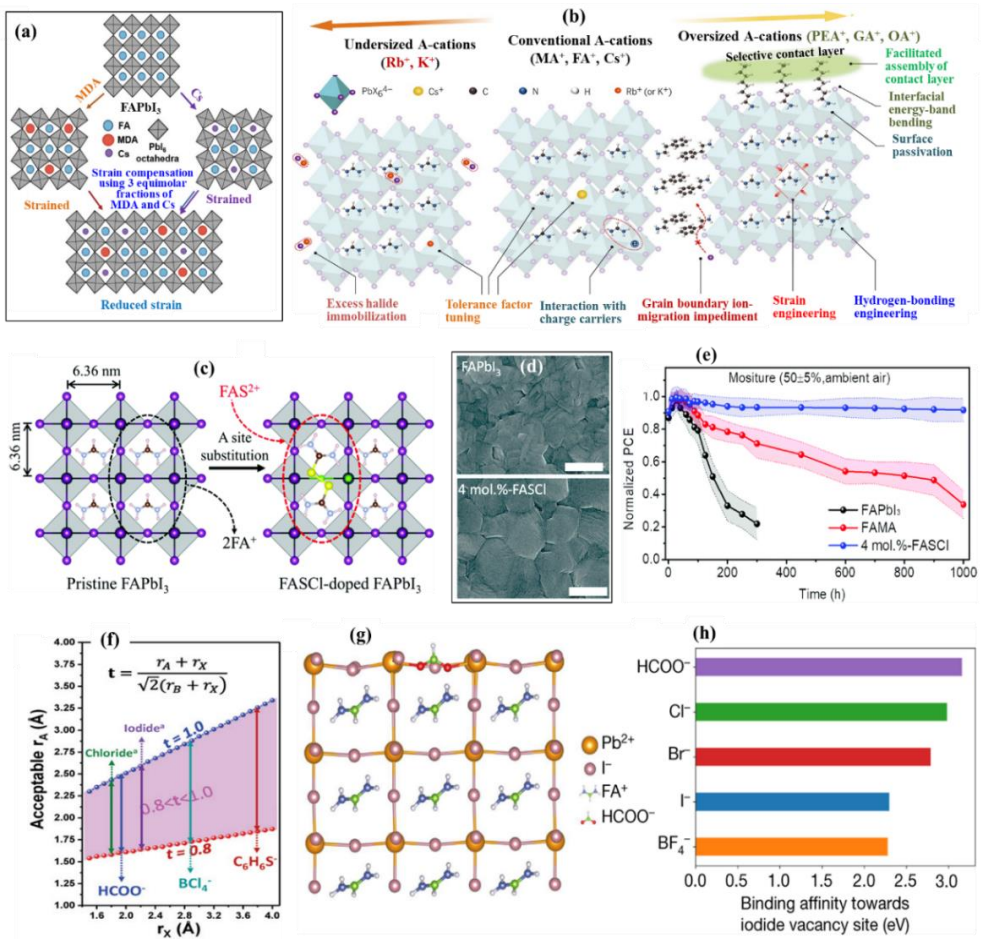

Figure 3. A-site and X-site engineering for Pb-HPs. (a) Schematic illustration of lattice strain engineering using Cs^+ and MDA^{2+} in $FAPbI_3$. Reproduced with permission.[80] Copyright 2020, Science. (b) effect of A-site alloying with various sizes of cations for tuning optoelectronic properties. Reproduced with permission.[65] Copyright 2022, Science. (c) Structure of pristine and FASCl-doped $FAPbI_3$ perovskite, (d) effect on film growth, and (e) device stability. Reproduced with permission.[8] Copyright 2021, Royal Society of Chemistry. (f) Plot of the range of acceptable A-site ionic radii that satisfy tolerance factor ($0.8 > t > 1.0$). Reproduced with permission.[115] Copyright 2019, Wiley-VCH. (g) Lattice structure for the passivation of an iodine vacancy at the $FAPbI_3$ surface by an $HCOO^-$ as pseudohalide. (h) Binding strengths of pseudohalides/anions with the V_I at the surface. Reproduced with permission.[83] Copyright 2021, Springer Nature.

Incorporating pseudohalogens in the X-site, is another strategy to passivate defects and improve material stability. In this instance, pseudohalogens with higher electronegativity and electron affinity compared to halides are used.[115,124] Although only limited pseudohalides have been explored in HPSCs to date, pseudohalide anions, such as SCN^-, CH_3COO^-, BF_4^-, PF_6^-, and $HCOO^-$ have shown unique advantages in aspects of tuning the growth, properties,

and stability of HP films resulting improvement in device performance.[81,83,125–128] Unlike monatomic ions, the ionic radii for polyatomic ions are not as well defined.[115] For non-spherical ions, the ionic volume remains constant rather than the ionic radius for different crystals comprising the same anion.[129] These pseudohalide additives can also regulate the hydrogen and halogen bonding in the HP crystal lattice. As depicted in Figure 3f, Walker et al. have documented that the range of acceptable A-site anions increases as r_x increases. Thus, incorporating larger polyatomic anions in the X-site of the HP lattice allows for larger cations to be used in the A site, following the criteria $0.8 > t > 1.0$.

For instance, SCN^- derivatives have been used in precursor solutions to prepare high-quality HP films with improved device efficiency and stability due to the quenching of bulk and interfacial defects.[130–132] The addition of NH_4SCN promotes the formation of the black trigonal phase α-FAPbI3 with improved crystallinity, while simultaneously inhibiting the formation of the yellow hexagonal phase δ-FAPbI3.[133] Chen et al. documented that the partial substitution of iodide with PF_6^- forms an $FA_{0.88}Cs_{0.12}PbI_{3-x}(PF_6)_x$ interlayer, which could suppress the trap density.[127] Similarly, the HP with BF_4^- substitutions ($FA_{0.83}MA_{0.17}Pb(IBr)_{3-x}(BF_4)_x$) showed lattice expansion and strain relaxation.[81] Importantly, BF_4^- suppressed nonradiative recombination and reduced the charge transport loss, resulting in a significant increase in device PCE. Similarly, Jeong et al. incorporated a $HCOO^-$ anion as a pseudohalide into α-$FAPbI_3$, which exerted a higher binding affinity towards iodide vacancies compared to other anions like Cl^-, Br^-, and BF_4^- (as shown in Figure 3g, h). The $HCOO^-$ functional group can form two Pb–O coordination bonds with lead cations, effectively eliminating halide vacancy defects at both grain boundaries and the surface of HP films. This led to a notable increase in the PCE from 23.92 to 25.6%.[83] $HCOO^-$ incorporation lowered the density of halide vacancies, which inhibited photoinduced iodine loss under illumination leading, to improvement in device stability. Indeed, the polyatomic anions are too active to directly substitute the true halide anions in perovskite lattices. These functional molecules play a crucial role in regulating the nucleation and growth of the HP crystals. They are present at the grain boundaries and surfaces of the HP film as passivating agents, thereby leading to improved performance of HPSCs.

The pseudohalide anion engineering could pave a universal way to achieve highly efficient and stable HPSCs. There is still ample opportunity to identify and/or develop suitable candidates for tailoring the crystallinity and defect engineering through the modulation of cations/anions within the crystal lattice, for achieving superior device stability in HPSCs.

3.2 Pb-HPSCs: Additive Engineering and Molecular Passivation/Post-treatment

Despite their unique defect tolerance characteristic, perovskites are prone to degradation. The presence of detrimental traps is attributed to the low defect formation energy and reduced activation energy for ionic migration, occurring on the surface, grain boundaries, and within the bulk of the material. Besides crystalline deformation, recombination centers in HP films are detrimental to device performance and stability. Additive engineering and passivation strategies are recognized as effective and convenient approaches for improving the crystal quality and phase stability of perovskites, defect mitigation, and moisture resistivity. With this regard, numerous reports have used functional additives and passivation methods to customize crystallization, address defects within the bulk materials or at the surface and modify interface energetics. Additive engineering is done with functional ammonium salts, ionic liquids,

Lewis's acid-like metal cations, fullerene derivatives, and Lewis bases categorized by their donor type (such as O-donor, S-donor, and N-donor). Additionally, low-dimensional perovskites are employed to enhance device performance and stability.[134,135] Multifunctional additives have been reported for excellent defect passivation in HPSCs.[136,137] For example, Zhong et al. have used halogenated phenyl trifluoroborate potassium salts (4-XPTFBK) as multifunctional additives (Figure 4a), which simultaneously improved the crystallization process of the perovskite film and reduced the trap density in perovskites.[85] The dipole moment of the C-Cl bond is the highest one among the four carbon-halogen bonds, which may allow it to better regulate the electronic properties of the π-coupling system. As displayed in Figure 4b, organic potassium salts induce a strong coordination between the multifunctional group and the undercoordinated Pb^{2+}, halide vacancies, and FA^{+} ions which passivated the defects and suppressed the formation of cation vacancies through strong interactions and hydrogen bonding, realizing the full-structure and multi-site passivation effect.

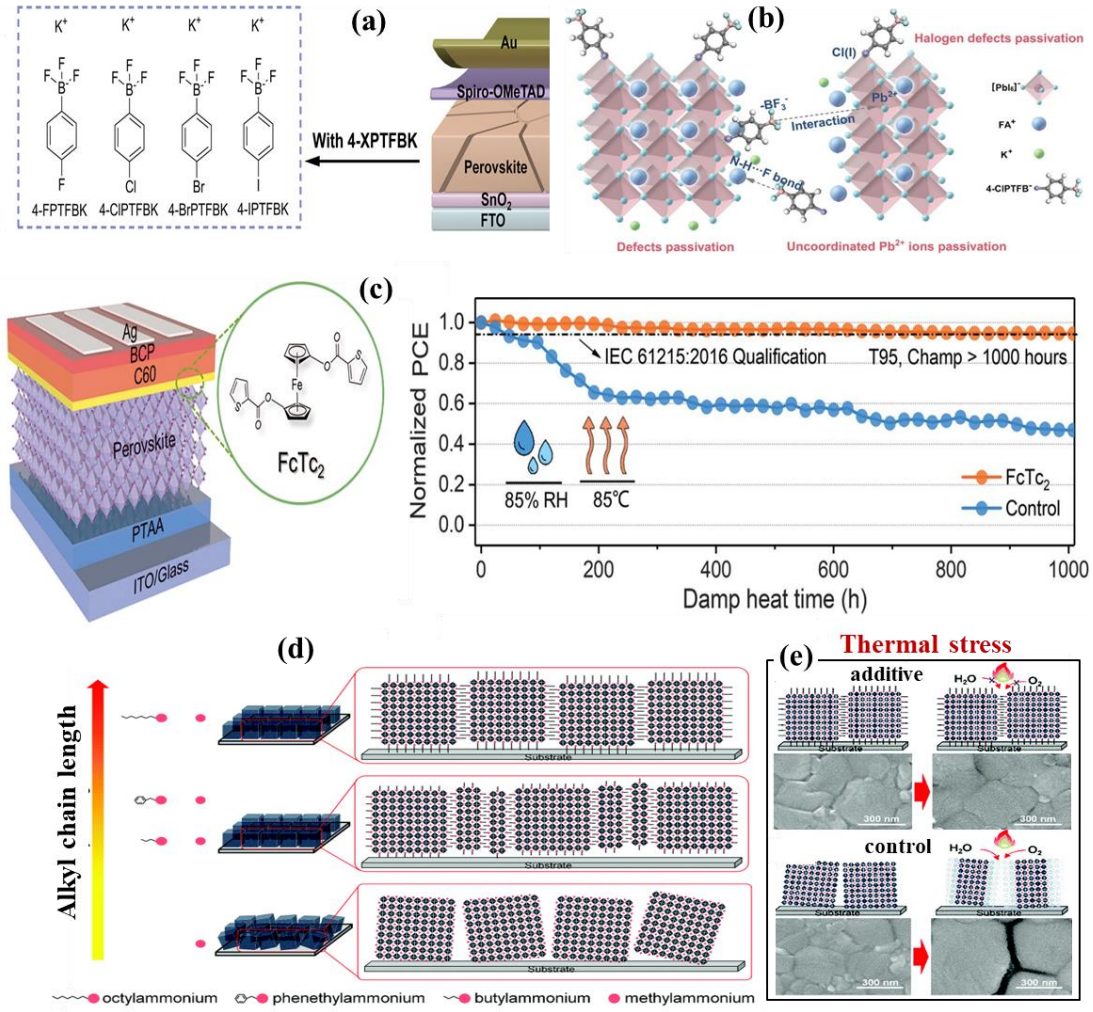

Figure 4. Advanced additive engineering and molecular passivation strategies for Pb-HPs. (a) Molecular structures of potassium 4-halogen-phenyl trifluoroborate (4-XPTFBK) (X = F, Cl, Br, I) additives and device structure;

(b) defect passivation chemistry with 4-XPTFBK additive. Reproduced with permission.[85] Copyright 2023, Wiley-VCH. (c) Schematic of interfacial passivation using $FcTc_2$ as functional molecules and stability under humidity and heat stress. (e) Schematic illustration of the stabilization of surface ions by $FcTc_2$ under heat and light. Reproduced with permission.[90] Copyright 2022, Science. (d) Crystal growth of perovskite with varying alkyl chain functional additive. (e) Illustration of the perovskite degradation under thermal stress and SEM images (control and additive). Reproduced with permission.[84] Copyright 2022, Royal Society of Chemistry.

Ionic liquids (ILs) can also be incorporated to improve device efficiency and stability. IL additives in HP control the film formation dynamics and modify the interface and defect chemistry of the perovskite film.[138] ILs consist of larger cations and/or anions with a weak electrostatic force; they are highly polar in nature and possess high ionic conductivity. Recently, IL additives in HPSCs have been utilized to enhance device performance and stability.[139] For example, Chao et al. have used an IL with acetate (Ac^-) anions, along with methylammonium acetate as an additive in the precursor solution. This combination of acetate ILs and methylammonium acetate facilitated a coordination exchange between I^- and Ac^- ions, creating reaction sites for the introduction of FAI.[140] This interaction between Ac^- and Pb^{2+} via C=O···Pb chelation leads to the formation of a relaxed Pb–I bond, which enables the insertion of FA into a soft Pb–I framework. Thus, it stabilizes the film, even when fabricated in ambient air, which is a desirable characteristic for the industrial processing of perovskite solar cells. Similarly, Snaith and colleagues achieved prolonged operational stability of HPSCs by incorporating a significant amount of 1-butyl-3-methylimidazolium, an ionic liquid, into the perovskite precursor.[141] This IL additive strongly inhibited ion migration in the perovskite film, contributing to the improved stability of the devices. Zhong and colleagues used protic amine carboxylic acid as IL additives in the Pb-HP precursor that achieved device PCE > 25%.[142] This ionic liquid comprising the carboxyl and ammonium functional group passivates the undercoordinated lead ions, halide vacancies, and organic vacancies, eliminating the deleterious nonradiative recombination.

Similarly, multidentate additives utilized in the perovskite precursor play a pivotal role in both modulating film growth and passivating defects within the material. Park and co-workers have used bipyridine and tridentate ligands as additives in perovskite precursor solutions.[143] The degree of interaction between PbI_2 and multidentate additives played a crucial role in the crystallization process. The bidentate and tridentate ligands of pyridine derivatives have rather effective roles in modulating grain growth and defect passivation. Interestingly, Tan and co-workers reported an effective lattice-matching chelation strategy to modulate the strain of the crystal lattice of perovskite films using an organic bidentate imidazole (MZ-1) salt.[86] This demonstrated significantly improved PCE ~24.61% with improved long-term thermal stability. This advancement is attributed to the firmly anchored and passivated perovskite lattice, resulting in compressive-strained perovskite films, which modified energy alignment for efficient charge carrier transport and decreased nonradiative recombination.[86]

The use of functional molecules to passivate the perovskite surface has been popularly employed in HPSCs.[144–146] It is important to design or modify the interface as issues related to surface defect chemistry and interfacial ionic diffusion play a dominant role in device performance and stability. It is known that molecular

passivators have shown remarkable potential owing to their tunable electrochemical and optophysical properties, and hydrophobicity in perovskites. Li et al. demonstrated a new functionalized molecular passivator, an organometallic compound, $FcTc_2$that induced a strong interaction between perovskite and $FcTc_2$.[90] The PCE of HPSCs was enhanced from 23.0%) to 25.0% with $FcTc_2$ passivation. It is beneficial for both the passivation of surface defects and the stabilization of surface components in perovskite, resulting in high stability in damp heat tests as depicted in Figure 4c. Similarly, Zhu et al. demonstrated reactive surface engineering through the treatment of 3-(aminomethyl) pyridine (3-APy), which facilitated a reaction between 3-APy and FA cation on the surface.[147] These reactive molecular passivators reduced perovskite surface roughness and induced an n-type surface, improving the device figure of merits. Halogen bond interactions also play a crucial role in the formation and properties of HP films. The potential of supramolecular modulation via the halogen bonding interactions with HPs has been explored using multifunctional fluorinated molecules.[10,148–151] The multifunctional fluorinated molecules have also demonstrated excellent passivating effects in the performance and stability of HPSCs.[10,150] Gratzel and co-workers have used pentafluorophenylethylammonium iodide (FPEAI) as a surface passivator on the 3D HP layer in which the perfluorinated moiety strongly enhances hydrophobicity, thus protecting the HP from ambient moisture. FPEAI also facilitated efficient hole extraction, and inhibited interlayer ion migration.[88] Importantly, fluoroarene-based molecular passivation forms a 2D layer at the surface by consuming the non-perovskite phase (hexagonal polymorph) as a 3D/2D overlayer.[88,148]

It is known that ammonium halide-based cations have demonstrated remarkable potential owing to their tunable electrochemical and optophysical properties, and hydrophobicity. Aliphatic and aromatic ammonium halides, in particular, have been widely used in the HP surface treatment.[91,152,153] Seok and his colleagues discovered a significant dependence between the alkyl chain length of surfactants and the structural evolution of perovskites, even when considering long organic cations, as depicted in Figure 4d. This study demonstrated the structural evolution of HP by controlling the formation of 2D layered structures at grain boundaries which boosts the PCE offering long-term thermal and humidity stability. Thermal degradation of the HP triggered by heat or electron beam stress initiated at the GBs was significantly reduced by the presence of octylammonium cations at the GBs, in contrast to butylammonium (BA) and phenethylammonium (PEA) cations (Figure 4e).[84] Interestingly, the hydrophobicity of octylammonium impedes detrimental ionic migration and H_2O infiltration. Additionally, they revealed the impact of interfacial engineering by employing alkylammonium halides with varying alkyl chain lengths.[154] With an increase in alkyl chain length from butylammonium iodide (BAI) to OAI, and further to dodecylammonium iodide (DAI), the electron-blocking capability and humidity resistance was substantially enhanced. However, the distinction between OAI and DAI in these aspects is not significantly pronounced. With these alkylammonium halides, the 2D structure formed on the 3D HP film acts as a passivation layer, showing an optimal device performance of HPSCs post-treated with OAI. Subsequently, various derivatives of octylammonium salts have been reported to show superior device properties with suppressed iodine migration.[155]

Similarly, Hagfeldt and his team introduced a newly designed ammonium salt, cyclohexylethylammonium iodide (CEAI), for interfacial engineering purposes. CEAI incorporates a "chair" conformation cyclohexane and an

ethylammonium group substituted in the equatorial position. This innovative compound facilitated the formation of a 2D perovskite interlayer with the integration of the cyclohexylethyl group through CEAI treatment. This modification resulted in a notable enhancement in surface hydrophobicity, ultimately leading to the exceptional stability of the perovskite film.[89] Moreover, Paetzold group introduced a dual passivation strategy involving the utilization of phenethylammonium chloride (PEACl) as both an additive and for surface treatment. This approach enabled simultaneous passivation of grain boundaries and the interface. By implementing this strategy, the activation energy for ion migration was significantly increased, leading to improved stability of the HPSCs against light, humidity, and thermal stress.[156] In addition, Shin and his colleagues reported using anion engineering with phenethylammonium to exert control over the structural and electrical properties.[126] They demonstrated that incorporating mixed anions in the form of phenethylammonium salts led to the formation of a 2D phase located at the grain boundaries of the 3D hybrid perovskite host. This 2D phase acted as a passivation agent, effectively enhancing the performance and stability of the system.

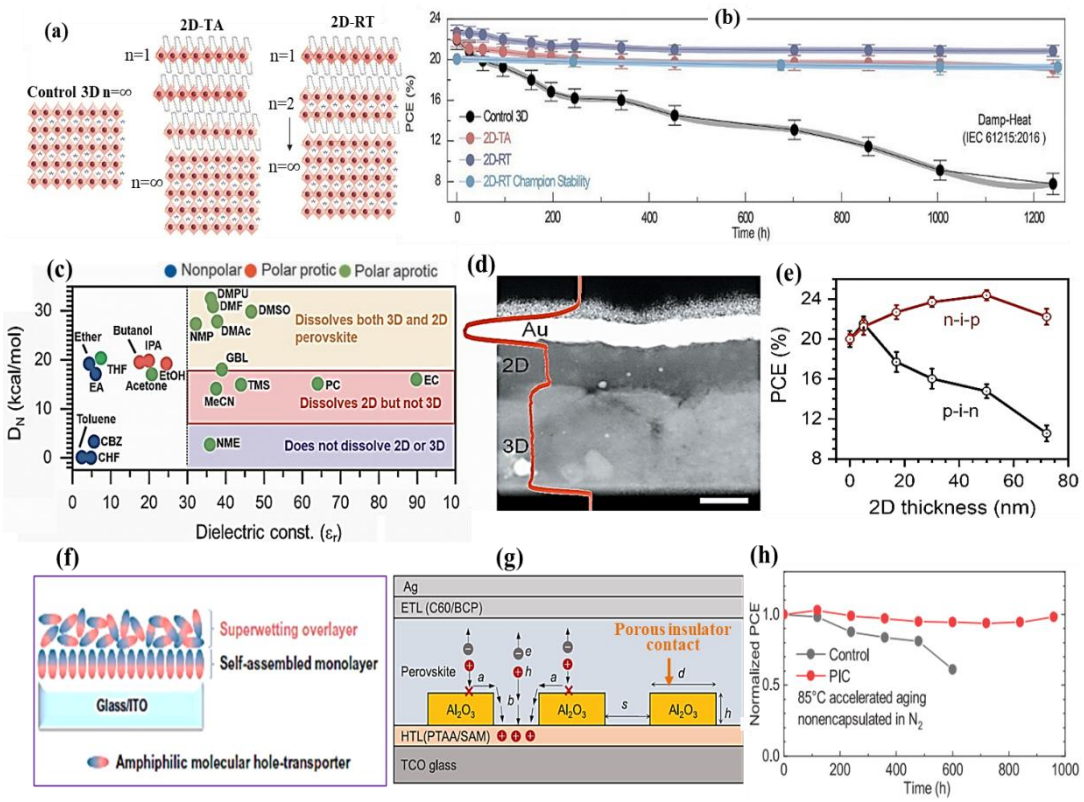

Figure 5. 2D/3D perovskite and interfacial passivation strategies for Pb-HPs. (a) Schematic illustration of 2D perovskite passivation with different n layers under thermal annealing at 100°C (TA) and room temperature process (RT). (b) Device stability during the damp-heat test of control and tailored-dimensionality 2D/3D heterojunctions. Reproduced with permission.[92] Copyright 2022, Science. (c) Evaluation of the dielectric constant (ε_r) and the Gutmann number (D_N) assessing the dissimilarities in solubility between the 3D and 2D HPs when forming a bilayer stack of 3D/2D. (d) Cross-sectional HR-TEM image of the 3D/2D HP stack with the overlaying intensity profile (red). (e) PCE

of both n-i-p and p-i-n planar 3D/PP-2D exhibiting variation with respect to the thickness of the 2D HP layer. Reproduced with permission.[17] Copyright 2022, Science. (f) Schematic depiction of the bilayer stack of amphiphilic molecular hole transporter on an ITO-glass substrate. Reproduced with permission.[96] Copyright 2023, Science. (g) Schematic of device structure with the porous insulating contact. The parameters *h*, *d*, and *s* represent the local Al_2O_3 dielectric mask's height, width, and local opening width, respectively. (h) corresponding device stability data. Reproduced with permission.[95] Copyright 2023, Science.

3.3. Pb-HPSCs: 2D/3D Heterostructure/Passivation

Noting the benefits of the 2D interlayer, researchers also have focused on 2D perovskite engineering in 3D HPSCs.[157,158] 2D phase formed on 3D perovskite improved efficiency and stability relative to 3D analogs due to higher formation energies and favorable intermolecular bonding between ligand molecules, and their ability to suppress ion migration. A 2D interlayer repels water by virtue of its hydrophobic ligand.[159] The growth of 2D perovskite layers on the upper surface of 3D perovskites forms a 2D/3D perovskite heterojunction. This heterojunction serves as an effective means to passivate surface defects and mitigate ion migration within the material.[159] Li et al. used a dimensionally graded perovskite formation approach using butylammonium bromide by spin coating on top of a 3D HP film which formed a self-passivated 2D/3D HP layer in bulk, covered by a graded mixed dimensional, wider bandgap 2D perovskite. It effectively suppresses the non-radiative recombination loss in both the bulk and at the interface of the HP.[153] Sargent group made an interesting observation of progressive dimensional reduction, starting from 3D down to 1D, when treating 3D hybrid perovskites with vinylbenzylammonium ligand cations.[160] They propose that these ligands incorporate into the 3D lattice in a sequential manner, driven by phenyl ring stacking. This process progressively bisects the 3D perovskite, resulting in lower-dimensional fragments and the formation of stable interfaces. This structural modification leads to improved carrier extraction and enhanced device efficiency, with a reported efficiency of 20% for 3D-only perovskite and 22% for the 2D/3D hybrid system. Moreover, Azmi et al. reported hydride 3D perovskite-based solar cells by modifying the dimensions of 2D HP layers using oleylammonium iodide molecules as depicted in Figure 5a.[92] These 2D layered passivated trap states and hindered ion migration. The study demonstrated the effectiveness of this approach by fabricating inverted HPSCs of PCE exceeding 24.3% that retained over 95% of their initial value even after being subjected to damp-heat test conditions for more than 1000 hours (Figure 5b). The improved stability was attributed to the presence of a thicker 2D-HP overlayer.

Furthermore, Mohite group[17] reported a new strategy to directly form a 2D perovskite by selecting suitable solvents for dissolving 2D phase with intact of 3D perovskite (Figure 5c). It is found that by using solvents with the right dielectric constant and donor strength, they were able to selectively grow pure 2D phases with controlled thickness and composition on 3D substrates without causing dissolution (Figure 5d). Directly growing 2D passivation layers on 3D HP has been shown to enhance the PCE of HPSCs. The HPSC achieved a remarkable PCE retention of 24.5% over 2000 hours under continuous light at 55°C and 65% relative humidity, with minimal degradation of less than 1%. Importantly, the PCE as a function of 2D HP thickness shows a different critical thickness for n-i-p and p-i-n device configurations (Figure 5e). In the n-i-p structure, the PCE decreased beyond a 2D-50 nm thickness. This reduction can be attributed to the limited transport of free charge carriers from the 3D material to the 2D passivation layer, which is

constrained by the diffusion length of less than 100 nm for a polycrystalline 2D material. In contrast, for p-i-n devices, the PCE experienced a significant decrease beyond a 2D passivation layer thickness of 5 nm, as the passivation layer hindered the extraction of electrons.

Furthermore, regarding carrier transport layer (CTL) engineering, the material and optophysical properties of CTL are important for the growth of high-quality perovskite films, the interface quality, and optimal band alignment.[12,161–164] Many reports have demonstrated the crucial role of the carrier transport layer in achieving high-efficiency Pb-HPSCs with superior device stability.[96,165,166] Wu and co-workers reported an amphiphilic molecular hole transporter, (2-(4-(bis(4-methoxyphenyl)amino)phenyl)-1-cyanovinyl)phosphonic acid, that features a multifunctional cyanovinyl phosphonic acid group and forms a superwetting underlayer for perovskite deposition (Figure 5f).[96] This approach yielded high-quality HP films with minimized defects at the buried interface, resulting in PCE as high as 25.4% with a significant increase in an open-circuit voltage of 1.21 V and a fill factor of 84.7%. Similarly, a carrier transport engineering strategy was found to be effective for improving the fill factor (FF) of large area HPSCs. For example, White and co-workers introduced a nanopatterned electron transport layer to form nanoscale localized charge transport pathways, which is effective for defect passivation and excellent charge extraction. It achieved a significantly high FF of 0.839 for larger area HPSCs (1 cm^2).[94] Catchpole and co-workers used nitrogen-doped titanium oxide for engineering electron transport dynamics in larger area Pb-HSPC demonstrating a record value of FF (~86.68%) close to the theoretical limit (90.2%).[167] Peng et al. reported a new strategy for carrier transport engineering with a porous insulator contact using alumina nanoplates (Figure 5g) which reduced surface recombination in the HPSCs and enhanced PCE from 23.0 to 25.56% and superior device stability (Figure 5h) compared with a conventional method.[95]

3.4. Lead Toxicity Issues in Pb-HPSCs

Pb-HPSCs have comparable device efficiency to silicon PV but offer the added benefit of a significantly shorter energy payback time. However, the competitive market has set a barrier to Pb-HPSCs due to their susceptibility to heat and moisture instability and concerns about lead toxicity. Lead, known for its harmful effects to both humans and the environment, is among the top ten chemicals of public health concern. Since lead salts comprising in HPs have high solubility in water, it is more lethal to the living being. Comparatively, heavy metal compounds commonly used in solar cells, such as CdS, PbS, and CdTe, exhibit much lower solubility products (K_{SP})ranging from 10^{-27}–10^{-34}, whereas that for PbI_2 is on the order of 10^{-8}.[168] Due to high solubility of Pb, it easily pollutes land and aquatic ecosystems. Once polluted, the harm to the earth and human beings is almost eternal. As per protocols set by the environmental protection agency in the United States, the limit of Pb content level is 1.5 μg/m^3 in air and 15 μg/L in water. Since Pb has a detrimental effect on the nervous system, it is deleterious to children which may lead to behavioral problems, learning deficits, and low IQ.[169] Pb pollution also affects the health of the adult human body. Therefore, it is imperative to set strict standards in using technology and monitor Pb leakage problems.

In this regard, Abate and colleagues thoroughly investigated the biological impact of Pb from Pb-HP contaminating the soil by analysing plants.[170] It is found that Pb leaking into the ground enters the plant grown on it and reached the food cycle more effectively compared to other lead-comprising compounds. The risk of Pb-

contamination can be controlled by recycling the used HPSCs and device encapsulation.[171] Despite employing protective techniques, both physical and chemical encapsulation, external factors like pressure, heat, and UV rays can still cause degradation. As a result, the ability of the encapsulation to safeguard Pb-HPSCs may be compromised.

Therefore, HPSC research has now primarily focused on developing Pb-free or reduced Pb (Pb-Sn) HPSCs to overcome the toxicity issue. Interestingly, there are some low-toxicity constituents with perovskite structures having attractive properties, such as Sn[172] and Ge-based HPs,[27,173–176] some double perovskites,[42,177,178] and some Bi/Sb-based halides[23,24,179] with structures alike to Pb-HP.[180] Particularly, Sn or Pb-Sn mixed HPSCs are considered prominent candidates due to an ideal optical bandgap with promising optoelectronic properties, but the poor chemical stability of tin is a big impugning factor. In the following sections, we will discuss the experimental prospective HPSCs with Sn and less-Pb-based perovskites, including strategies for improving their materials characteristics, stability, and device efficiency.

4. Lead-Free HPSCs

4.1. Tin (II)-Based HPSCs

Sn^{2+} has a comparable ionic radius and electronic properties to Pb^{2+}. Indeed, the Sn-HP comprises the closest crystallographic and photophysical properties to Pb-HP. Sn-HPs have a direct E_g ranging from 1.2–1.4 eV, making them highly promising for achieving high performance close to the Shockley-Queisser (SQ) limit, with a potential power conversion efficiency (PCE) of ~33%.[181] A notable observation, and critical issue in the field, is that the Sn^{2+} cation, readily undergoes oxidation to Sn^{4+}. In contrast, the heavier Pb^{2+} cation remains stable due to the presence of stable $6s^2$ electrons, exhibiting a stronger inert pair effect.[182] The crystallization rate of Sn-HP is faster, leading to lower film quality characterized by a higher defect density, primarily attributed to the elevated Lewis acidity of Sn^{2+}. This also leads to severe degradation of film and devices and serves as a significant barrier to realizing commercially viable Sn-HPSCs. Considering these challenges, researchers have extensively investigated strategies in Sn-HPSCs to enhance device performance through materials engineering and through employing functional additives.[183] These additives serve multiple purposes such as suppressing Sn oxidation,[182] regulating film growth,[184,185] and improving carrier transport.[186] However, the certified record efficiency of Sn-HPSCs is still below 15%.[30] Currently, Sn-HPSCs with the inverted (p-i-n) structure have demonstrated superior device efficiencies and stability compared to the regular (n-i-p) configuration.[187] The FA-based Sn-HP absorber layer with coadditive engineering demonstrated better efficiency and stability compared to the MA and Cs-based Sn-perovskite. In this section, we will discuss multiple chemical engineering techniques, such as additives, composition modification, surface passivation, and 2D/3D heterostructure, as summarized in Table 3, which have been used to overcome the issues of Sn-HPSCs.

Table 3. Summary of the strategies used for the improvement of Sn-HPSCs.

Strategies	Materials	Sn-HP	Device structure	PCE (%) (Control to target)	Stability data (Target device)	Year	Ref.
A-site engineering	CsI	$(Cs,FA)SnI_3$	ITO/PEDOT:PSS/Sn-HP/C_{60}/BCP/Ag	3.74 to 6.08	100 °C, N_2-ambient, ~68% of PCE_0 @ t~250 h	2018	[188]
	GAI and $EDAI_2$	$(EDA,GA,FA)SnI_3$	ITO/PEDOT:PSS/Sn-HP/C_{60}/BCP/Ag	7.1 to 9.6	60% RH, ~80% of PCE_0 @ t~96 h	2018	[189]

	RbCl	$(Rb,FA)Sn(I,Cl)_3$	ITO/PEDOT:PSS/Sn-HP/PCBM/AZO/Ag	3.12 to 5.89	Encapsulated, RT, ambient air, ~70% of PCE_0 @ t~600 h	2020	[190]
	FAI	(FA,MA)SnI3	ITO/PEDOT: PSS/Sn-HP/C60/BCP/Ag	4.29 to 8.12	N_2-glovebox, ~80% of PCE_0 @ t~400 h	2020	[190]
	Ethylammonium iodide (EAI), $EDAI_2$, GeI_2	$(FA,EA, EDA)SnI_3$	FTO/PEDOT:PSS/Sn-HP/C_{60}/BCP/Ag/Au	9.03 to 13.24	-	2020	[191]
	($EDAI_2$ and $EDABr_2$), GeI_2	$(FA,EDA)Sn(I,Br)_3$	ITO/PEDOT:PSS/Sn-HP/C_{60}/BCP/Ag	7.84 to 14.23	100 °C, N_2 atmosphere; >92% of PCE_0 @ t~4000 h	2022	[192]
X-site engineering	FASCN	$(FA,PEA)Sn(I,SCN)_3$	ITO/PEDOT:PSS/Sn-HP/PCBM/Al	5.09 to 8.17	Unencapsulated, N_2-glovebox storage, >90% of PCE_0 @ t~1000 h	2018	[193]
	PEASCN	$(FA,PEA)Sn(I,SCN)_3$	ITO/PEDOT: PSS/Sn-HP/PCBM/BCP/Ag	4.52 to 9.65	Encapsulated, RT, air ambient; ~56% of PCE_0 @ t~1200 h	2021	[194]
	FACHOO	$FASn(I,CHOO)_3$	ITO/PEDOT: PSS/Sn-HP/C_{60}/BCP/Ag	5.80 to 12.11	N_2-glovebox storage; ~68% of PCEo@ t~3400 h	2022	[195]
Additive	Poly(vinyl alcohol) (PVA)	$FASnI_3$	ITO/PEDOT:PSS/Sn-HP/C_{60}/BCP/Ag	6.48 to 8.92	Encapsulated, MPPT, RT, air ambient; ~100% of PCE_0 @ t~400 h	2019	[184]
	Hexafluoro-2-propanol and Ethylenediammonium dihypophosphite ($EDAP_2$)	$FASnI_3$ + $EDAI_2$	ITO/PEDOT:PSS/Sn-HP/C60/BCP/Ag	4.9 to 6.8	Dark, 60% RH; ~80% of PCE_0 @ t>70 h	2020	[196]
	SnI_2·$(DMSO)_x$ / NH_4SCN	$(FA,PEA)Sn(I,Br)_3$	ITO/PEDOT:PSS/Sn-HP/ICBA/BCP/Ag	12.2 to 14.6	Encapsulated, N_2-atmosphere stored; ~96% of PCE_0 @ t~100 days	2021	[185]
	Trimethylthiourea	$(FA,PEA)SnI_3$	ITO/PEDOT:PSS/Sn-HP/ICBA/BCP/Ag	10.0 to 14.3	-	2022	[197]
	1-(4-Carboxyphenyl)-2-thiourea	$CsSnI_3$	FTO/c-TiO_2/m-TiO_2/Al_2O_3/NiO_x/m-carbon-Sn-HP	2.04 to 8.03	N_2-glovebox storage; ~90% PCE_0 @ t~3000 h	2022	[198]
	Dipropylammonium iodide (DipI), sodium borohydride ($NaBH_4$)	$FASnI_3$	ITO/PEDOT:PSS/Sn-HP/C_{60}/BCP/Ag	4.72 to 10.61	N_2-glovebox storage, MPPT; ~96% of PCE_0 @ t~1300 h	2022	[199]
	Phenylhydrazine hydrochloride (PHCl)	$FASnI_3$	ITO/PEDOT:PSS/Sn-HP/C_{60}/BCP/Ag	5.6 to 11.4	Unencapsulated, air ambient; ~60 % of PCE_0 @ t~144 h	2020	[182]
	Sulfamic acid (SA)/Imidazolium (IM)	$(FA,IM,Cs)SnI_3$	ITO/PEDOT:PSS/Sn-HP/C_{60}/BCP/Ag	9.80 to 12.50	Unencapsulated, 50% RH, ~99 % of PCEo @ t>3 h	2022	[200]
	4-Fluorobenzylammonium iodide (FBZAI)	$(FA,EDA)(Sn,Ge)I_3$	TO/PEDOT:PSS/Sn-HP/C60/BCP/Cu	11.47 to 13.85%	Unencapsulated, N_2-glovebox storage, ~95% of PCEo @ t~3800 h	2022	[201]
	2-Methyl-2-butanol	FASnI3 +PAI+MACl	ITO/PEDOT:PSS/Sn-HP/C_{60}/BCP/Ag	x to 10	Operational stability, ~92% of PCE_0 @ t~1000 h	2022	[202]
	Bidentate ligand: Formohydrazide (FHZ)	$(FA,Rb)SnI_3$:$EDAI_2$:PEABr	ITO/PEDOT:PSS/Sn-HP/ICBA/BCP/Ag	9.93 to 12.87	Encapsulated, MPPT, RT, ambient air; ~ 62% of PCE_0 @ t~120 h	2023	[203]
Passivation (multifunctional molecules)	Diamine ethane (DAE)	$(FA,EDA)SnI_3$	FTO/PEDOT:PSS/Sn-HP/C_{60}/BCP/Ag	8.09 to 10.18	-	2019	[204]
	Additive: TM-DHP Passivation: EDA	FA0.75MA0.25SnI3	ITO/PEDOT:PSS/Sn-HP/C_{60}/BCP/Ag	9.9 to 11.5	Unencapsulated, RT, N_2-glovebox storage, ~100% of PCE_0 @ t>50 days	2020	[205]
	6-	$FASnI_3$ + $EDAI_2$	ITO/PEDOT:PSS/Sn-	10.40 to 13.64	MPPT	2022	[206]

	Maleimidohexane hydrazide trifluoroacetate		HP/C_{60}/BCP/Ag		illumination, ~75% of PCE_0 @ t~1000 h		
Passivation (2D HP)	Phenylethylammonium iodide (PEAI)	(FA,PEA)SnI_3	FTO/PEDOT:PSS/Sn-HP/C_{60}/BCP/Ag	6.0 to 9.0	-	2017	[207]
	Phenyl ethylammonium chloride (PEACl)- doping	$FASnI_3$	FTO/PEDOT:PSS or NiOx/Sn-HP/C_{60}/BCP/Ag	4.3 to 9.1	-	2020	[208]
	Bulky cation ammonium iodide (BAI)	(FA,GA)SnI_3 + $EDAI_2$	ITO/PEDOT:PSS/Sn-HP/C_{60}/BCP/Ag	8.7 to 10.6	10 cycles- thermal and light stress; ~95% of PCE_0	2021	[209]
	4-Fluoro-phenethylammonium bromide (FPEABr)	(FA,EPEA)Sn(I,Br)$_3$	ITO/PEDOT:PSS/Sn-HP/ICBA/BCP/Al	9.38 to 14.81	Encapsulated, N_2-ambient stored; ~80% of PCE_0 @ t~432 hrs	2021	[30]
	GASCN	(FA,PEA)SnI_3	ITO/NiOx/Sn-HP/C_{60}/BCP/Ag	9.95 to 13.79	N_2-glovebox; ~90% of PCE_0 @ t~1200 h	2022	[210]
	2-Guanidinoacetic acid (GAA)	(FA,PEA)Sn(I,Br)$_3$	ITO/PEDOT:PSS/Sn-HP/ICBA/BCP/Ag	9.34 to 13.70	N_2-glovebox storage, ~93% of PCE_0 @ t~1200 h	2022	[211]
Contact engineering	ETL: PCBM to ICBA	(FA,PEA)SnI_3 +NH4SCN	ITO/PEDOT:PSS/Sn-HP/ETL/BCP/Ag	7.7 to 12.4	-	2020	[186]
	ETL: Pyridine-Functionalized Fullerene	(FA,EDA)SnI_3	ITO/PEDOT:PSS/Sn-HP/C60-Bpy/C_{60}/BCP/Ag	12.29 to 14.14	Encapsulated, N_2-ambient stored, ~80% of PCE_0 @ t~1000 h	2022	[212]
	HTL: P-SnO_x ETL: T-SnO_x + Passivation: EDA	(FA,Cs,DEA,EDA)SnI_3	ITO/PEDOT:PSS or P-SnOx/Sn-HP/T-SnOxC_{60}/BCP/Ag	10.39 to 14.09	-	2022	[213]

4.2. Sn-HPSCs: A and X- Site Engineering

A-site alloying in $ASnX_3$-based HPSCs tunes the tolerance factor that stabilizes the crystal phase, regulates crystal structure, reduces Sn oxidation, and affects the film growth rate resulting in enhanced device efficiency and stability.[187] Simple inorganic cations (Cs or Rb) [188,190] or multifunctional organic cations[189,214] have been used for A-site modification. In this regard, Wu and co-workers incorporated Cs into the $FASnI_3$ lattice, which tuned a tolerance factor t close to 1, shrinking the crystal lattice as depicted in Figure 6a, b.[188] It demonstrated a structural regulation of $FASnI_3$ perovskite that could enhance thermal stability, suppress the oxidation of Sn^{2+}, and improve the device stability.

As with Pb-HPSCs, the film quality of Sn-HP films can be improved by incorporating co-cations into the crystal lattice of $FASnI_3$.[214] This modification leads to a reduction in pinhole concentration, decreased carrier recombination, larger grain size, and enhanced stability. Indeed, compositional engineering with multifunctional co-cations modified the material properties of Sn-HP, such as thermodynamic stability, film crystallinity, and optical bandgap.[215] For example, guanidinium (GA) can occupy the A-site in Sn-HP, whereas it is not suitable in Pb-HP. GA incorporation in the $FASnI_3$ lattice not only improves the film growth and crystallinity but also modifies the energy band alignment as depicted in Figure 6c, d. The GA-incorporated FA-Sn-perovskite device revealed peculiar self-defect quenching properties with a successive improvement in the device parameters for ~2000 hours stored in a glove-box environment (Figure 6e).[189] Similarly, adopting the A-site modification method, Hayase and colleagues achieved a record PCE of 13.24% with $FASnI_3$ with co-cation additive (10 mol% ethylammonium iodide (EAI), 1 mol% $EDAI_2$, and 5 mol% GeI_2) subsequent with ethylenediamine passivation.[191] In same line, Jian et al. used 1 mol% of $EDABr_2$ instead of $EDAI_2$ in $FASnI_3$. This modification proved to be more effective in passivating grain boundaries and surface

Sn vacancies while also reducing the background hole density than $EDAI_2$. The improved performance can be attributed to the synergistic effects of the EDA^{2+} cation and Br^- anion. As a result, the HPSC achieved a PCE of 14.23% and demonstrated long-term stability, retaining approximately 93% of its initial PCE after storing for approximately 4000 hours.[192]

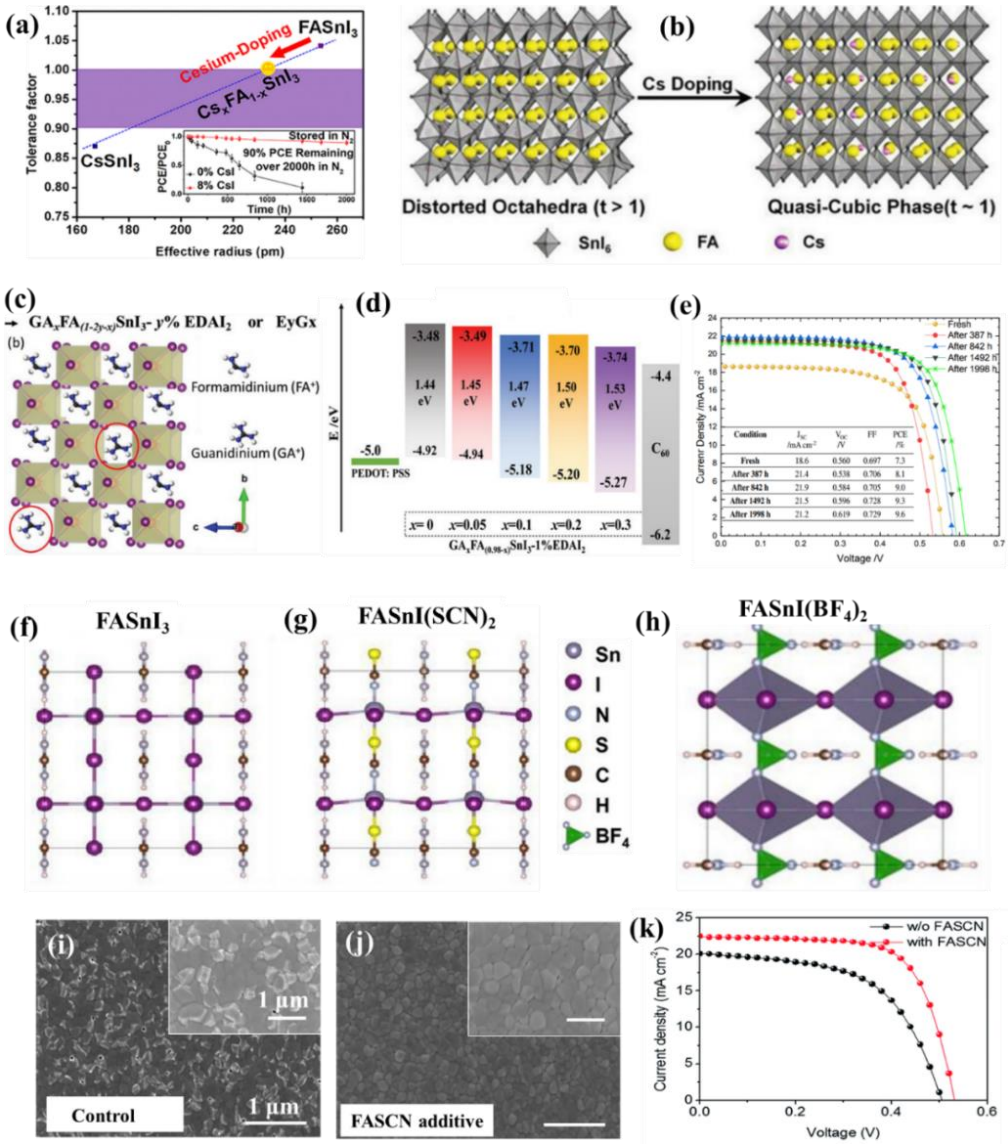

Figure 6. A-site and X-site engineering for Sn-HPs. (a) Tolerance factor and the effective radius in A-site alloyed ($Cs_xFA_{1-x}SnI_3$) Sn-perovskite; (b) Structural transition in $FASnI_3$ with Cs- alloying. Reproduced with permission.[188] Copyright 2018, American Chemical Society. (d) Alloyed Sn-perovskite: (GA, EDAI, FA) SnI_3, (e) energy band diagram of alloyed $FASnI_3$, (f) current–voltage characteristics of respective devices. Reproduced with permission.[189] Copyright 2019, Wiley-VCH. (g) Structural modification of (g) $FASnI_3$ using pseudohalides; (h) SCN^- and (i) BF_4^-. Reproduced with permission.[216,217] Copyright 2020, American Chemical Society. (i,j) SEM images of Sn-perovskite, (k) Current-voltage curve without and with FASCN additive. Reproduced with permission.[193] Copyright 2018, Royal Society of Chemistry.

With regards to the X-site, anion engineering of Sn-HPs affects the crystal lattice and optophysical properties. Kanatzidis and colleagues reported bandgap engineering of Sn-perovskite with mixed halide anions showing a lattice contraction from $MASnI_3$ (~1.30 eV) to $MASnBr_3$ (~2.15 eV), covering much of the visible spectrum,[218] demonstrating a PCE of 5.73% with $MASnIBr_2$ composition. Water and oxygen significantly destabilize Sn-HPSCs due to the high susceptibility of the Sn-X bond, leading to pronounced instability. To address this, Sn–X bonding can be strengthened via X-site engineering with polyatomic anions such as SCN^-, BF_4^-, PF_6^- , and $HCOO^-$ as pseudohalides. Thus, following Pb-HPSCs reports,[125] pseudohalide engineering has also been explored for their Sn counterparts. It stabilizes metal oxidation, passivates trap-assisted recombination, and increases the hydrophobicity of Sn-HPs. Diau and co-workers investigated the effect of varying the tetrafluoroborate to iodine ratios, which suppress the extent of oxidation and enhance the carrier dynamics (Figure 6f-g).[216,217] The pseudohalide incorporation in $FASnI_3$ revealed a remarkable decrease in bond angles and bond lengths. For example, anion SCN^- substitution led to a higher formation energy and greater binding strength that increased the stability relative to pristine $FASnI_3$.[216] Similarly, BF_4^- incorporation led to an enhancement of the B-site metal-octahedron contact. The Sn-X bond length contracted due to stronger electronegativity of super halogen (BF_4^-) resulting in better photostability of $FASnI_3$ film.[217] Moreover, Jang et al. incorporated a formate anion ($HCOO^-$) in $FASnI_3$, which resulted in the formation of a uniform and pinhole-free perovskite film with a low trap density, reduced charge carrier recombination, and improved charge transport owing to the strong interaction between Sn^{2+} and $HCOO^-$.[195] Collectively, these pseudohalide-incorporated Sn-HPSCs demonstrated enhanced PCE and stability. Additionally, Kim et al. discovered that the inclusion of a formamidinium thiocyanate (FASCN) additive effectively regulated oxidation by establishing robust chemical interactions with the tin component (Sn^{2+}).[193] This resulted in the formation of coarser perovskite grains (Figure 6i, j) and enhanced crystallinity, with controlled growth in out-of-the-plane direction significantly influencing device performance and stability (Figure 6k). Khadka et al. employed phenethylammonium thiocyanate (PEASCN) as a functional additive in a $FASnI_3$ precursor. This additive was effective in suppressing Sn oxidation and promoting the formation of a compact film with a larger grain size and higher crystallinity.[194] Wang et al. found that the PEASCN incorporation significantly suppressed Sn^{2+} oxidation, improved electron transport and reduced carrier recombination, resulting in lower voltage deficit with electron transport engineering, showing decent device stability over 2000 h under a nitrogen atmosphere.[219] Despite the many versatilities of pseudohalide for Sn-X bonding engineering, not much work has been done in this area to date. Many polyatomic anion derivatives with suitable cations can be added to the Sn-HP precursor solution. These derivatives could then be incorporated in the Sn-HP crystal lattice or quench defects on the surface and/or at grain boundaries and thus enhancing the optoelectronic properties of the Sn-based perovskite film.

4.3. Sn-HPSCs: Additive engineering and passivation/post-treatment

Additive engineering is a proven strategy in Pb-HPSCs. It has also played a crucial role in controlling the rate of crystallization as well as the self-doping of Sn-HP films. Mathews et al. used SnF_2 to reduce Sn vacancies and carrier density, to effectively prevent metallic behavior.[220] Abate et al. investigated the antioxidative characteristics of SnX_2 derivatives in the Sn-HP precursor solution.[221] SnF_2 was found to be more effective than other halide derivatives for

controlling the extent of Sn^{2+} oxidation. SnF_2 coordinated Sn^{4+} via a ligand exchange reaction forming SnF_4 and SnI_2 rather than producing a redox reaction. Besides that, it also induced excellent morphology and stability.[222] However, an excess amount of SnF_2 has detrimental effects on film morphology, leading to the formation of separate phases. This process can be inhibited using additional functional additives. Moreover, Graham and colleagues investigated antioxidant organic molecules in Sn-perovskites.[223] They discussed how additives attenuate the Sn^{2+}oxidation in Sn-HP films. A particular additive may act as a halide exchanger, coordinator, sacrificial antioxidant, and redox catalyst to inhibit the oxidation of Sn^{2+} in the solution or during crystallization. Therefore, it is advantageous to include multiple additives having different functionalities which could reverse the oxidation of SnI_2 in precursor and film formation while also passivating the surface and grain boundaries after film formation.

Typically, more than two additives have been used in most of high-efficiency Sn-HPSCs reported, including SnF_2.[207] As a good example of this, Mora-Seró and colleagues employed a complex additive system consisting of dipropylammonium iodide and sodium borohydride, as a reducing agent in Sn-HPSCs. This approach resulted in a higher PCE compared to employing the additives individually, along with improved film morphology and operational stability, which maintained 96% of its initial PCE after 1300 h in a N_2 atmosphere (Figure 7a,b).[199] He et al. used an additional functional additive; trifluoroethylamine hydrochloride (TFEACl) along with SnF_2 that improved film morphology, produced a favorable energy band alignment, and diminished the Sn^{4+} content.[224] Similarly, introducing trimethylthiourea and PEAI in a $FASnI_3$ precursor solution resulted in a smooth and compact film by controlling the film crystallization, as depicted in Figure 7c. It is found that the trimethylthiourea in Sn-HP precursor formed a complex through stronger bonding interactions, leading to slower crystallization, Sn-HPSCs made using this strategy delivered a promising PCE of over 14.0% (Figure 7d) and enhanced stability against humid air.[197] Haung et al. used a multifunctional additive phenylhydrazine hydrochloride (PHCl) in $FASnI_3$ which effectively passivated trap states, improved film growth and modified band alignment.[182] Importantly, this multifunctional additive significantly suppressed the extent of Sn^{4+} oxidation due to strong interactions between reductive hydrazine and hydrophobic phenyl.[182] Moreover, the Cl and Br derivatives of phenylhydrazine greatly improved the device stability, with devices retaining 91% of their PCE for 4,800 h under continuous illumination.[225] Kuan et al. developed Sn-HP films using a combination of triple cations (Cs, FA, Imidazolium (IM)) along with a bifunctional additive, sulfamic acid (SA).[200] This additive was crucial in mitigating iodine vacancies and interacting with uncoordinated Sn atoms to improve the surface defects. It revealed that SA, converted from its zwitterionic form to its ammonia/acid form upon irradiation, effectively reduced Sn^{4+} back to Sn^{2+}. Furthermore, additives with fluorinated groups have also been used for regulating the growth of high-quality Sn-HP films. Their high electronegativity tunes the electron cloud density of aromatic amine cations, which is benign for the passivation effect and hydrophobic character. For example, Zhao and co-workers used 4-fluorobenzylammonium iodide (FBZAI) as an additive in the Sn perovskite precursor. [201] Like other additives, it slowed down the crystallization rate and the extent of Sn^{2+} oxidation. A reduction in nonradiative recombination was also reported and ascribed to the modulation of benzylamine and fluorine functional groups.

Moreover, the choice of ligands in Sn-perovskite plays a critical role in modulating the bonding strength with the Sn-atom. Mi and colleagues introduced a series of sulfur ligands, namely N,N-dimethylthioacetamide (DMTA),

N,N,N',N'-tetramethyl thiourea (TMTU), N,N'-dimethylethylene thiourea (DMETU), and 1,3-dimethylimidazoline-2-thione (DMIT) (Figure 7e), into the precursor solution.[226] It was observed that the partial charge on sulfur (S) becomes increasingly negative in the order of DMTA < TMTU < DMETU, owing to better stabilization of the partial positive charge on nitrogen in the same sequence. Similarly, DMIT, with its aromatic imidazolium ring, exhibits the strongest affinity for I_2. These sulfur ligands delay the crystallization rate, which widens the antisolvent dripping window (Figure 7f). Consequently, they enable the formation of pinhole-free films and effectively suppress surface defects, leading to progressively improved device parameters (Figure 7g). Similarly, Khadka et al. used formohydrazide as a bidentate ligand as an antioxidant additive in the precursor solution which is propitious for alleviating of defects in Sn-HP film resulting in the suppression of Sn-oxidation and modulation of the interfacial energy band alignment.[203]

The growth of Sn-HP films can be affected by the nature of bonding using functional additives. For example, Han and coworkers demonstrated a new strategy for retarding the crystallization rate of $FASnI_3$ by introducing OH···I– hydrogen bonding interactions using polyvinyl alcohol (PVA) (Figure 7h).[184] The bonding interactions between PVA and $FASnI_3$ have the effects of directing the crystal orientation by slowing down the crystallization rate, reducing trap states within Sn-HP, and suppressing the migration of the iodide ions. As a result, these improvements significantly enhance both the efficiency and stability of the devices utilizing the PVA-$FASnI_3$ composite. In this regard, there is still much room to explore in the realm of functional additives and the nature of their bonding in Sn-HPSCs.

Wakamiya and co-workers recently reported a new strategy for controlling Sn^{2+} oxidation by modulating the precursor solution. In this report, they demonstrated a method to remove Sn^{4+} from Sn-HP precursor solution using a 1,4-Bis(trimethylsilyl)-2,3,5,6-tetramethyl-1,4-dihydropyrazine (TM-DHP) reductant that acts as a scavenger of Sn^{4+} species that proceeded to form Sn (0) nanoparticles, as depicted in Figure 7i.[205] Through this nanoparticle-based scavenging method, Sn-HPSCs with a $FA_{0.75}MA_{0.25}SnI_3$ absorber and employing interface modification by EDA and $PC_{61}BM$, a PCE of 11.5% was achieved. Similarly, Ning and colleagues reported the $SnI_2{\cdot}(DMSO)_x$ complexes prepared via the interaction between I_2 and DMSO.[185] The streamlined synthesis of the SnI_2 precursor enables the creation of $SnI_2{\cdot}(DMSO)_x$ complexes with improved coordination. They found a significant difference in crystal growth dynamics in two-step and one-step synthesis routes. The tin adducts formed with a one-step synthesis route that regulated tin-halide perovskite growth, avoided SnI_2 phase segregation and formed fewer pinholes of (FA,PEA)$Sn(I,Br)_3$ film. With a high level of coordination, the $SnI_2{\cdot}(DMSO)_x$ complex effectively guided the out-of-plane crystal orientation, forming uniformly homogeneous perovskite films (Figure 7j). This advancement resulted in a record PCE of 14.6%. By adopting a surface passivation method, Yin and co-workers used 6-maleimidohexanehydrazide trifluoroacetate as a surface passivator atop the Sn-HP films. This functional molecule modified the bulk microstructure and modulated the surface chemistry of Sn-HP film, in addition to tuning the Fermi level and nullifying the charged-defect-rich surface.[206] The additive functionalities with reductive hydrazide and carboxyl groups suppressed Sn^{4+} formation. The device with surface reconstruction achieved a PCE of 13.64%, retaining over 75% of the original PCE after 1000 h of illumination (in an environment with an O_2 concentration < 50 ppm).

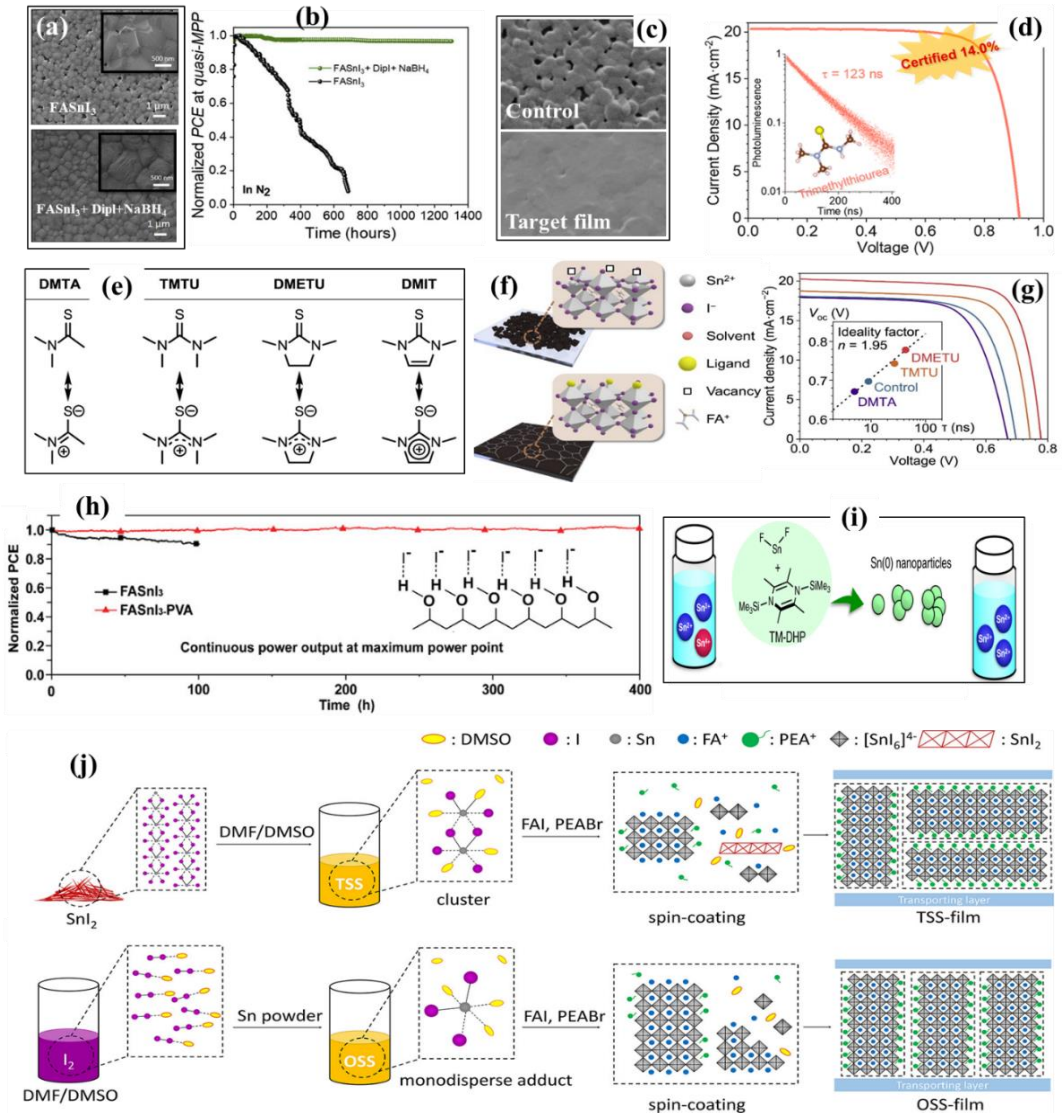

Figure 7. Advanced additive engineering and molecular passivation strategies for Sn-HPs. (a) SEM images of control and additive (DipI+$NaBH_4$) in $FASnI_3$, (b) corresponding device stability in N_2 atmosphere. Reproduced with permission.[199] Copyright 2022, Elsevier Inc. (c) SEM images of control and additive (TMT) in $FASnI_3$, (d) current-voltage characteristics with carrier lifetime inset. Reproduced with permission.[197] Copyright 2022, American Chemical Society. (e) A set of sulfur ligands (DMTA, TMTU, DMETU, DMIT) with characteristics resonant structure, (f) schematic of grain growth, and (g) Typical J–V characteristics of the HPSCs. Inset: Voc vs PL lifetime (τ) of the FASnI3 layer. Reproduced with permission [226] Copyright 2022, Elsevier Inc. (h) Device stability without and with PVA additive; inset O-H and I- hydrogen bonding interaction. Reproduced with permission [184] Copyright 2019, Wiley-VCH. (i) Sn^{4+} scavenging method using TM-DHP additive. Reproduced with permission [205]. Copyright 2020, Springer Nature. (j) two-step synthesis (TSS) and one-step synthesis (OSS) synthetic methods for SnI_2 precursors and corresponding film growth regulation. Reproduced with permission. [185] Copyright 2021, American Chemical Society.

The above examples have all been based on the one-step deposition method and only a few reports have used the two-step deposition method to fabricate Sn-HPSCs, in contrast to Pb-HPSCs.[196,227] Shahbazi et al. reported Sn-HPSCs using a two-step method and solvent engineering.[196] Unlike the two-step process of Pb-HP, FAI dissolved in isopropyl alcohol (IPA) could not convert the SnI_2 layer into a stable $FASnI_3$ layer due to faster crystal growth. However, the co-solvent containing a mixture of hexafluoro-2-propanol, IP, and chlorobenzene is found to be effective for the growth of Sn-HP by decelerating the crystallization rate. Similarly, The Han group successfully demonstrated a two-step deposition method, effectively controlling crystallization kinetics by utilizing solvents with varying polarity (2-Methyl-1-propanol, 3-Methyl-1-butanol, and 2-Methyl-2-butanol).[202] Their findings revealed that the steric hindrance caused by hydroxyl groups in the solvent molecules influenced the film growth dynamics. This two-step method coupled with solvent engineering is effective for fabricating dense and homogeneous Sn-HP in large areas with device efficiency of over 10% for the first time and retained operational stability of over 92% for 1000 h.

There could be multiple reasons for the lower performance of Sn-HPSCs prepared by the two-step method. As widely observed facts, the preparation of Sn-HP films from SnI_2 is not as straightforward as preparing Pb-HP from PbI_2. It means the SnI_2 layer structure is a poorer precursor for perovskite growth than PbI_2. One primary reason could be related to the structural difference between PbI_2 and SnI_2 crystals.[228] SnI_2 film can grow with two phases: α-SnI_2 (monoclinic) in a layered structure but lacking octahedral coordination with halide and β-SnI_2 (hexagonal) structure lacking a layered structure.[228,229] In contrast, a PbI_2 film comprises a layered structure with octahedral coordination. Benefiting from this favorable structure of PbI_2, AX precursors efficiently diffuse through PbI_2 films to grow the Pb-perovskite crystal. The diffusion of the AX precursor in the SnI_2 film is less favorable than that in the PbI_2 film, resulting in low-quality Sn-perovskite films. Besides the poor SnI_2 crystal layer, facile oxidation of Sn^{2+} is also notorious for developing SnI_4 impurities. Moreover, it is claimed that as SnI_2 and PbI_2 are mixed, they crystallize in the PbI_2 structure resulting in efficient conversion to perovskite crystal, which can explain the competitive PCE of Sn-Pb binary perovskites compared to the case with pristine Sn.[230] Therefore, the two-step method requires further solvent engineering and materials chemistry for the growth of pristine Sn-perovskites than is required for Pb and Sn-Pb analogues.[228]

4.4. Sn-HPSCs: 2D/3D Heterostructure/Passivation

Sn-HPSCs have demonstrated a significant improvement in performance and stability using 2D/3D heterostructures. Similar to Pb-HPSCs, the 2D/3D hydride heterostructure of Sn-HPs can be obtained by introducing bulky organic cations.[30,207,210,231–234] Loi and coworkers added PEAI in $FASnI_3$ which formed a homogenous film with highly crystalline and oriented 2D/3D bulk layer.[207] It has been suggested that the organic PEA^+ cations are oriented perpendicularly to the substrate, and the van der Waals interactions of the benzene ring between the interdigitated PEA^+ cations may facilitate self-assembly of the inorganic SnI_6 layers parallel to the substrate, inducing strong orientation and crystallization of the 2D PEA_2SnI_4. This PCE was seen to improve by 50% compared to the pristine 3D $FASnI_3$ film, as shown in Figure 8a. Wang et al. used NH_4SCN as a structure regulator along with EAI to form a quasi-2D-3D Sn-HP film with a hierarchical structure. The air stability of the composite Sn-HP film was significantly improved due to the parallel growth of a surface layer composed of 2D PEA_2SnI_4.[235] Similarly, Li and co-workers used the PEACI

additive which grows quasi-2D crystals of Sn-HP film with more ordered 2D layered Sn-HP crystalline phase (Figure 8b).[208] The formation of a barrier layer at both the surface and grain boundaries of the perovskite crystals effectively shielded the Sn^{2+} ions from oxidation and moisture, protecting the Sn-HP film.

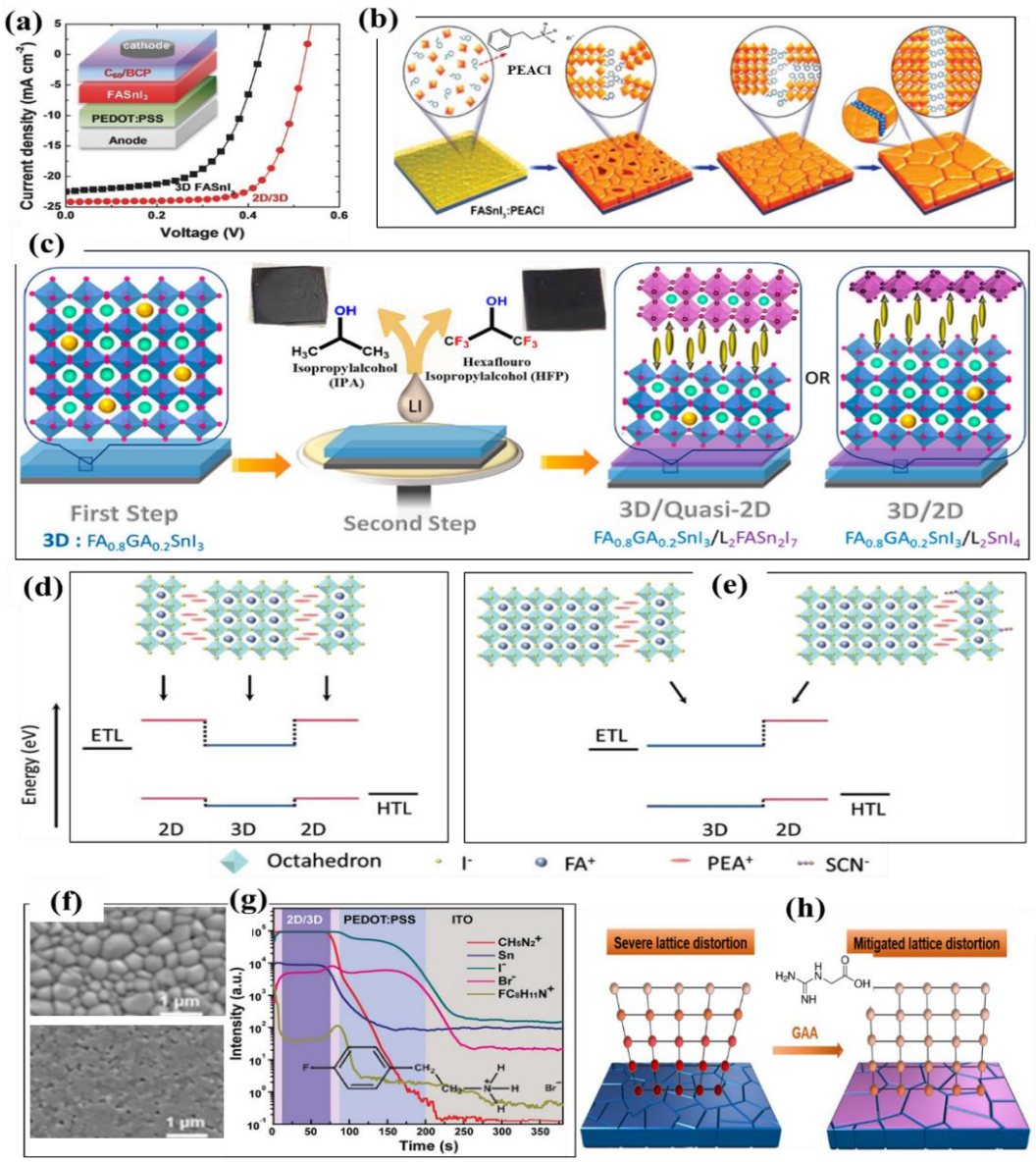

Figure 8. 2D/3D perovskite and interfacial passivation strategies for Sn-HPs. (a) Current-voltage curves of control (3D) and 2D/3D HPSCs. Reproduced with permission.[207] Copyright 2018, Wiley-VCH. (b) Illustration of growth of 2D ordered Sn-perovskite with PEACl.[208] (c) Growth of low-dimensional perovskite phase on 3D (Sn-perovskite) layer using bulky ammonium cations (BAC (L)). Reproduced under the terms of the CC-BY license.[209] Copyright 2021, American Chemical Society. (d, e) Crystal structures of control and 2D/3D vertical heterojunction and energy band alignment with respect to HTL and ETL. Reproduced under the terms of the CC-BY license.[210] Copyright 2022, Wiley-VCH. (f) Morphology of control and 2D/3D hybrid Sn-HP film with FPEABr and (g) spatial distribution of

FPEABr on surface and interface. Reproduced with permission.[30] Copyright 2021, Wiley-VCH. (h) Lattice distortion engineering with GAA modification. Reproduced with permission.[211] Copyright 2022, Wiley-VCH.

Furthermore, Jokar et al. used a sequential solution-processed approach for interfacial treatment. A number of aryl and alkyl bulky ammonium cations (butylammonium (BA), hexylammonium (HA), allylammonium (ALA), cyclohexylammonium (CHA), PEA, anilinium (AN), 2-fluoro-PEA (2F-PEA), and 2F-AN) dissolved in hexafluoro-2-propanol (HFP) were deposited on top of the 3D layer to form a 3D/2D layer (Figure 8c).[209] Importantly, the bulky cations dissolved in IPA destroyed the Sn-HP film displaying pinholes while those dissolved in HFP grew with pinhole-free uniform morphology. Among these devices, the Sn-HPSCs treated with anilinium (AN) exhibited exceptional performance, showcasing self-healing in challenging environmental conditions such as continuous light soaking under one-sun illumination and thermal stress cycles (10 cycles at 20 and 50 °C).

Likewise, Yan and co-workers reported a uniquely controlled stacked quasi-2D (down)–3D (top) double-layered perovskite using PEAI and guanidinium thiocyanate (GuaSCN) additives as depicted in Figure 8d,e.[210] The introduction of GuaSCN additive improved the crystallinity as well as passivated defects resulting in a remarkably high open circuit voltage >1 V in Sn-HPSCs and PCE of 13.79% with decent stability of 90% of the initial PCE for 1200 h storage in a N_2-filled glovebox. Seok and coworkers introduced a new concept involving both surface passivation and strain engineering of Sn-HP films using 2-thiophenemethylammonium iodide (ThMAI).[236] The introduction of ThMAI led to a gradient distribution of out-of-plane compressive strain, which correlated with the vertical compositional inhomogeneity of the film relative to the substrate surface. This approach holds great promise for achieving high-performance devices with improved PCE by adopting an n-i-p architecture. He and colleagues achieved the highest PCE of 14.81% (certified 14.03%) among Sn-HPSCs by incorporating a modified form of PEA called 4-fluoro-phenethylammonium bromide (FPEABr). This modification effectively suppressed Sn^{2+} oxidation by forming a compact microstructure consisting of both 2D and 3D components (Figure 8f).[30] The $FPEA^+$-based 2D tin-perovskite capping layer can offer a reducing atmosphere for vulnerable 3D $FASnI_3$ grains. This approach facilitates the construction of effective 2D/3D microstructures and the FPEABr molecules mainly located on surface or at HTL/perovskite interface (Figure 8g). The functionally incorporated cation $FPEA^+$, shows a distribution rich on the surface and HTL/Sn-HP interface, suggesting a robust, stable, and well-passivated interface formed with 2D/3D heterojunction. Similarly, in their research, Liu and colleagues discovered that incorporating a novel biocompatible chelating agent, 2-guanidinoacetic acid (GAA), in Sn-perovskite can modulate crystallization kinetics. Moreover, GAA effectively regulates lattice strain and controls the phase distribution of the 2D/3D structure, as illustrated in Figure 8h.[211] Importantly, GAA was found to be effective for the mitigation of lattice distortion and Sn/I-related deep defects, which results in a superior device performance with a PCE of 13.70 % with a small voltage deficit of ≈0.47 V and an improved stability.

Regarding the device structure and carrier transport layer engineering, the PCE and device stability of FA-based Sn-HPSCs has been driven mainly by co-additive engineering including, SnF_2 and adopting an inverted (p-i-n) planar device configuration. Diau et al. have documented that the pronounced Sn^{2+} oxidation, p-doping in Sn-HP, and

redox chemistry at metal oxide/Sn-HP interface are the limiting factors of n–i–p configured Sn-HPSCs.[187] In the p-i-n configuration, PEDOT:PSS has been popularly used as the HTL, whereas fullerene derivatives such as C_{60}, PCBM, and ICBA are used as the ETL.[237] Ning and coworkers achieved ultra-high open-circuit voltage using ICBA for 2D/3D-Sn-HPSCs.[186] The LUMO level of the ETL varies with different functional groups in fullerene[238] which affects interfacial binding and band offset. In this regard, Zhu and colleagues reported a multifunctional interface manipulation strategy by introducing pyridine-functionalized fullerene derivatives for ETL engineering.[212] The interface between the functionalized ETL and Sn-HP exhibited a strong bond, resulting in the modulation of energy-level alignment. This bonding also reduced surface defects, suppressed nonradiative recombination, and improved electron extraction efficiency. Sn-HPSCs with ETL modulated interface achieved a PCE of 14.14% while retaining a PCE over 95% under illumination for 1000 hours. Moreover, PEDOT: PSS has been used as a hole transport layer in most of the reports of Sn-HPSCs. Recently, Hayase and colleagues developed a new ambipolar SnO_x by plasma-assistant strategy (P-SnO_x) as an alternative HTL.[213] A champion PCE of 14.09% was achieved by an interfacial modification of Sn-perovskite introduced with the top SnO_x composed of SnO_2 and Sn metal as a protective layer in p-i-n configuration combined with P-SnO_x as HTL.

5. B-Site Modulated: Pb/Sn/Ge-based HPSCs

Although the toxicity issue of Pb-HPSCs can be addressed with Sn-based perovskite, the device performance and stability of Pb-free HPSCs are quite disappointing due to intrinsic instability and uncontrolled crystallization of Sn or Ge -HP. Alternately, B-site modulated perovskites with Pb incorporation in Sn-HP lattice can reduce toxicity. The mixed Sn-Pb- based HP tunes the E_g from 1.2 to 1.6 eV, resulting ideal optical bandgap absorber proposed in the SQ limit and employed as subcells for tandem device structure.[239] In the Sn-Pb HP system, B-site modulation in an octahedral cage of perovskite crystal-induced band bowing with ideal bandgaps (1.2 -1.3 eV). The detailed balanced limit for a single-junction solar cell suggests that Sn–Pb HPSCs have the potential to achieve even more PCEs than Pb-HPSCs. By incorporating a mixture of 50% tin (Sn) and lead (Pb), the bandgap can be tuned to an ideal value of 1.2 eV, which is theoretically associated with an optimal PCE of approximately 32.74%. With Pb content, there is better control of the film growth dynamics.[240] B-site modulated perovskite film has a medium crystallization rate which could minimize nonuniform film growth. Considering the tendency of Sn-HP to undergo oxidation, which can lead to increased defects and instability, it has been found that maintaining an Sn content of approximately 50% is optimal for improving the quality and stability of perovskite films. Benefiting from the advances in Pb and Sn-based HPSCs, the mixed B-sites (Pb/Sn)-based HPSCs have achieved PCE over 24%[71] which is competitive with the highest efficiency of Pb-HPSCs (Figure 2g). This rapid progress of Sn/Pb mixed HPSCs is driven by the adaptation of the advancement on the Pb and Sn-based devices. Leaping from the initial reports on mixed B site -HPSCs with PCE >8%,[67,72] multiple approaches have been explored to scale up the PCE of Sn–Pb PSCs adapting the approach for Sn or Pb-HPSC reports such as A/X-site alloying,[241–243] functional additive,[244] surface treatment,[245] 2D/3D hydride structure,[241][241] carrier transport engineering.[246–248] Efforts have been undertaken thus far to improve the efficiency of Sn–Pb HPSCs, akin to the approaches taken in studies involving both Pb or Pb-based HPSCs as summarized in Table 4.

Table 4. Summary of the strategies used for the improvement of B-site modulated- Pb/Sn/Ge-HPSCs.

Strategies	Materials	Mixed B-site: Sn-Pb-HP	Device structure	PCE (%) (Control to target)	Stability data (Target device)	Year	Ref.
A-site engineering	CsI	$(Cs,FA,MA)(Pb,Sn)I_3$	ITO/PEDOT:PSS/Sn-Pb-HP/C_{60}/BCP/Ag	13.5 to 17.8	-	2017	[68]
	CsI, MAI	$(Cs,FA,MA)(Pb,Sn)I_3$	ITO/NiO_x/Sn-Pb-HP/C_{60}/BCP/Ag	14.80 to 16.77	MPPT, N_2-ambient storage; ~88% of PCE_0 @ t~690 h	2022	[249]
X-site engineering	Octylammonium tetrafluoroborate ($OABF_4$) Passivation: butylenediamine (BDA)	$(FA,Cs)(Pb,Sn)I_3$:PEACl	ITO/PEDOT:PSS/Sn-Pb-HP/$OABF_4$/BDA/C_{60}/BCP/Cu	20.5 to 23.7	MPPT, RT; >88% of PCE_0 @ t>250 h	2023	[242]
Additive	Additive: MASCN + pyrrolidinium thiocyanate (PySCN)	$(FA,MA,Cs)(Sn,Pb)I_3$	ITO/PEDOT:PSS/Sn-Pb-HP/C_{60}/BCP/Ag	18.1 to 20.4	-	2020	[230]
	Ionic liquid - pentylammonium tetrafluoroborate ([PNA]BF_4)	$(FA,MA)(Sn,Pb)I_3$	ITO/PEDOT:PSS/Sn-Pb HP/PCBM/BCP/Ag	16.23 to 20.11	Unencapsulated: N_2-ambient, dark; ~90% of PCE_0 @ t~1200 hrs	2021	[250]
	1-bromo-4-(methylsulfinyl)benzene (BBMS)	$(Cs,FA,MA)(Sn,Pb)I_3$	ITO/PEDOT:PSS/Sn-Pb-HP/C_{60}/BCP/Ag.	18.97 to 22.03	60 ºC, N_2- ambient glovebox storage; ~98% of PCE_0 @ t~2660 h	2022	[251]
	Propane diamine bromide (PDABr)	$(FA,MA)(Pb,Sn)I_3$	ITO/PEDOT:PSS/PMMA/Sn-Pb-HP/PCBM/BCP/Ag	16.23 to 20.41	Unencapsulated: N_2-ambinet glovebox storage; ~95% of PCE_0 @ t~700 h	2022	[252]
	BaI_2 and PEACl	$(Cs,FA)(Pb,Sn)I_3$	ITO/PEDOT:PSS/ Sn-Pb-HP/C_{60}/BCP/Cu	19.6 to 21.2		2022	[253]
	Rubidium iodide (RbI)	$(FA,Cs,Rb)(Sn,Pb)I_3$	ITO/PEDOT:PSS/Sn-Pb-HP/C_{60}/BCP/Cu	18.32 to 20.12	-	2023	[243]
	SnOx-additive	$(FA,MA)(Pb,Sn)I_3$	ITO/PEDOT:PSS/Sn-Pb-HP/C_{60}/BCP/Cu	19.31 to 22.16		2023	[254]
	Trimethylsulfoxonium iodide (TMSI)	$(Cs,FA,MA)(Sn,Pb)I_3$	ITO/PEDOT:PSS/Sn-Pb-HP/C_{60}/BCP/Ag	17.70 to 22.65	N_2-ambient glovebox storage; ~83% of PCE_0 @ t~6000 h	2023	[255]
	dicyandiamide (DCD)	$Cs(Pb,Sn)I_2Br$	ITO/NiOx/Sn-Pb-HP/ZnO/PCBM/Ag	10.53 to 14.17	Unencapsulated: Continuous illumination; ~92% of PCE_0 @ t~600 h	2023	[256]
Passivation (multifunctional molecules)	Additive- TM-DHP Passivation: Maltol	$(Cs,FA,MA)(Sn,Pb)I_3$	FTO/PEDOT:PSS/Sn-Pb-HP/Maltol/C_{60}/ BCP/Ag	18.2 to 21.4	-	2021	[257]
	Additives: NH4SCN + GlyHCl Passivation: piperazine derivatives	$(Cs,FA,MA)(Sn,Pb)I_3$	ITO/PEDOT:PSS/Sn-Pb-HP/PPC_{60}/BCP/Ag	18.30 to 22.70	Unencapsulated, >96% of PCE0; N2-glovebox storage (ISOS D-1), t>2000 hrs	2022	[248]
	Additive: MASCN Passivation:5F-PHZ	$(FA,MA,Cs)(Sn,Pb)I_3$	ITO/PEDOT:PSS/Sn-Pb-HP/IPL/C_{60}/BCP/Ag	16.81 to 19.34	_	2022	[10]
	Additive: GlyHCl Passivation: $EDAI_2$	$(FA,MA,Cs)(Sn,Pb)I_3$	FTO/PEDOT:PSS/Sn-Pb-HP/EDAI2/C_{60}/BCP/Ag	19.6 to 23.6		2022	[244]
	Passivation: (PEAI +$EDAI_2$)	$(FA,MA)(Sn,Pb)I_3$	ITO/PTAA/Sn-Pb/IPL/C_{60}/BCP/Ag	17.07 to 22.51	Unencapsulated: N_2-ambient dark; ~90% of PCE_0 @ t~1600 h	2022	[258]
	Additive: NH_4SCN Passivation: Cysteine hydrochloride (CysHCl)	$(Cs,FA,MA)(PbSn)I_3$	ITO/PEDOT:PSS/Sn-Pb HP/CysHCl/C_{60}/BCP/Cu	18.91 to 22.15		2023	[259]
	Additive: hydrazine sulfate (HS) Passivation: EDA	$(Cs,FA,MA)(PbSn)I_3$	ITO/P_3CT-Cs/Sn-Pb-HP/$EDAC_{60}$/BCP/Ag	20.17 to 23.17	Unencapsulated: N_2-ambient store: ~94% of PCE_0; t~4000 h	2023	[260]
Passivation (LD perovskite)	2D-HP: formed with PEAI	$(FA,MA,Cs)(Sn,Pb)I_3$	ITO/PEDOT:PSS//Sn-Pb-HP/PEAI/PCBM/PEIE/Ag	17.90 to 19.40	Filter spectrum, continuous illumination, ~100% PCE_0 @ t~200 h	2020	[261]
	Quasi 2D: $(PEA)_2GAPb_2I_7$) with (PEAI + GASCN)	$(FA,MA)(Sn,Pb)I_3$	ITO/PEDOT:PSS/Sn-Pb-HP/2D-Hp/C_{60}/BCP/Ag	16.1 to 22.1	NA	2022	[241]
	Passivation:	$(Cs,FA,MA)(Pb,Sn)(I,B$	ITO/Sn-Pb-HP/CF_3-	18.18 to 20.17	N_2-glovebox	2023	[262]

	CF_3-PEAI	r)$_3$	PEAIPCBM/ZrAcac/Cu		storage; ~75% of PCE_0 @ t~700 h		
	2D HP: (4-AMP)PbI_4	(FA,MA) (Sn,Pb)I_3	ITO/PEDOT:PSS/2D-HP/Sn-Pb-Hp/PCBM/BCP/Ag	15.01 to 17.70	-	2023	[263]
Contact or Energy band engineering	ITO to FTO	(Cs,FA,MA)(Pb,Sn)I_3	ITO/PEDOT:PSS/Sn-Pb-HP/PCBM/C_{60}/BCP/Ag	16.74 to 20.40	-	2019	[264]
	HTL: CzAn Additive: PEACl	(Cs,F)(Pb,Sn)I_3	ITO/HTL/PMMA/Sn-Pb-HP/IPL/C_{60}/BCP/Ag	21.02 to 22.61	N_2-glovebox storage; ~96% of PCE_0 @t>1000 h	2022	[247]
	HTL: 2PCz and MPA IPL: EDA	(Cs,FA,MA)(Pb,Sn)I_3	FTO/PEDOT:PSS/Sn-Pb-HP/EDA/PCBM/C_{60}/BCP/Ag	21.37 to 23.32	-	2022	[246]
	Bulk heterojunction with ETL- NIR polymer DTBTI; IPL- GABr	(FA,MA)(Pb,Sn)I_3	ITO/EMIC-PEDOT:PSS/Sn-Pb-HP/GABr/DTBTI/PCBM/C_{60}/BCP/Ag	21.49 to 24.27	Unencapsulated: LED illumination; ~90% of PCE_0 @ t~1000 h	2022	[71]
	HTL- Potassium Citrate dopped PEDOT:PSS; Passivation: $EDAI_2$	(Cs,FA,MA)(Pb,Sn)I_3	ITO/PEDOT:PSS/Sn-Pb-HP/$EDAI_2$/C_{60}/BCP/Ag	20.37 to 22.67	N_2-glovebox storage, 45 °C; ~80% of PCE_0 @ t~800 h	2023	[265]
Sn-Ge -HPSCs		(FA,MA)(Sn,Ge)I_3	ITO/PEDOT:PSS/Sn-Ge HP/PCBM/C_{60}/BCP/Ag/Au	3.31 to 6.90	Unencapsulated; air ambient; ~80% of PCE_0 @ t~1 h	2018	[175]
		(FA,MA)(Sn,Ge)I_3	ITO/PEDOT:PSS//Sn-Ge-HP/PCBM/C_{60}/BCP/Ag	to 7.90	-	2019	[174]

Analogous to Pb-HPSCs, the modulation of A/X-sites, utilization of functional additives, and engineering of interfaces in Sn-Pb perovskite solar cells are crucial factors that significantly influence device efficiency and long-term stability, as listed in Table 4. Accounting for A-site engineering alone, the Sn-Pb-HPSCs also demonstrated improvement in PCE with slightly better device stability.[68,249] X-site engineering by incorporating a small amount of Br and Cl into Sn-Pb HPSCs reduces non-radiative recombination at grain boundaries of Sn-Pb perovskite, leading to better device performances.[266,267] Additionally, Wang et al. used alkylammonium pseudohalide as a functional pseudohalide additive in MA-free Sn-Pb HPSCs, improving the film formation and inhibited iodine vacancies.[242] The device PCE was boosted to 23.7% using an octylammonium (OA^+) cation with a BF_4^- anion in bulk and surface passivation with BDA,which resulted in improved photostability by virtue of the suppressed defect density and slower generation of interstitial iodides and iodine under illumination.

Both inorganic and organic multifunctional molecules have been used as additives in Sn-Pb-HPSCs. Yan and co-workers fabricated the Sn-Pb-HPSCs using MASCN and PySCN as pseudohalide functional additives in two-step deposition method which improved device PCE from 18.1 to 20.4% due to improved film growth and suppression of defect density.[230] Similarly, inorganic additives such as RbI,[243] BaI_2,[253] and SnO_x[254] also have demonstrated significant improvement in film quality by suppressing the Sn-vacancies leading to enhanced device PCE. Ionic salt[250] and reactive functional molecules[251,252,256] were effective in modulating film crystallization. These functional additives reduced surface residual stress and decreased defect state densities. Recently, Jiang et al. used trimethylsulfoxonium iodide as a multifunctional additive in Sb-Pb mixed HP resulting in larger grain and improved crystallinity and defect mitigation.[255] They achieved enhanced PCE from 17.70 to 22.65 % with decent stability, retaining 88% of their initial value after 1200 h of continuous illumination.

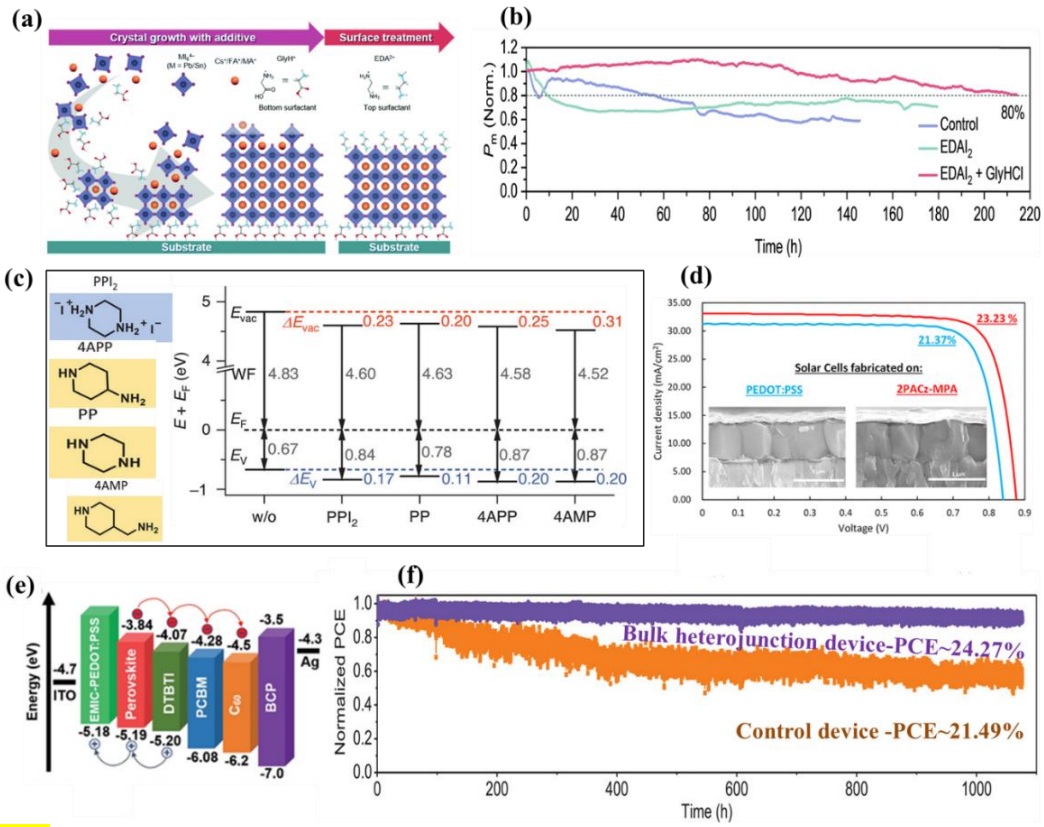

Figure 9. Advanced passivation strategies for Sn-Pb HPs. (a) Schematic of the interface modifications of mixed Sn–Pb HP film by the GlyHCl additive and $EDAI_2$ surface treatment, (b) device stability. Reproduced with permission.[244] Copyright 2021, Wiley-VCH. (c) Surface treatment with passivating functional molecules and its effect in surface energy band. Reproduced with permission.[248] Copyright 2021, Wiley-VCH. (d) Current-voltage curves and Cross-sectional images of devices with different HTLs. Reproduced with permission.[246] Copyright 2021, American Chemical Society. (e) Energy band alignment of Sn-Pb-HP and heterojunction layer, (f) device stability of the control and heterojunction devices. Reproduced with permission.[71] Copyright 2022, Wiley-VCH.

Surface passivation with organic halide salts is also an effective strategy for improving the PCE of Sn-Pb-HPSCs. Zhu et al. used a bulky fluorinated phenmethylammonium salt to passivate the Sn-Pb perovskite film. The passivating molecule introduced a strong interaction with the perovskite reducing the surface and bulk defects in the perovskite due to permeation of the organic halide salt and resulted in an increase in device performance from 20.7 to 22.8 %. Importantly, it achieved 18.0% PCE with a large area (10 cm^2) device with significantly improved device stability under ambient conditions (ISOS-D-1) for non-encapsulated modules.[245] A hydride method with molecular passivation and additive engineering has also been used in Sn-Pb- HPSCs,[10,244,248,257–260] a good example of this coming from the Wakamiya group, where they used 1,4-bis(trimethylsilyl)- 2,3,5,6-tetramethyl-1,4-dihydropyrazine (TM-DHP) as a functional additive and 3-hydroxy-2-methyl-4-pyrone (Maltol) surface treatment for the fabrication of Sn-Pb- HPSCs. They demonstrated enhancement in PCE from 18.2 to 21.4% benefiting from high-quality HP and enhanced charge carrier lifetime.[257] The same group also introduced a bifacial passivation strategy by passivating the

top surface with ethylenediammonium diiodide and the bottom with glycine hydrochloride in Sn-Pb HP as depicted in Figure 9a.[244] It is found that surface dipoles are formed at either interface which promotes crystallinity and reduces trap densities, and facilitates charge extraction. This method demonstrated an excellent device performance of 23.6% and superior stability compared to the control device (Figure 9b). Molecular passivation of Sn-Pb perovskite films was done using reactive molecules with functional groups, such as amine and ammonium; piperazine (PP), 4-aminopiperidine (4APP), and 4-(aminomethyl) piperidine (4AMP) as depicted in Figure 9c.[248] These molecules interacted with the organic cations on the perovskite surface, resulting in surface structural modifications and the adjustment of interfacial energy bands. Along with surface treatment, C_{60} pyrrolidine tris-acid was utilized as the ETL, which exhibited a preference for binding to Sn^{2+} sites on the film surface rather than Pb^{2+}, thereby tuning the carrier transport behavior that ultimately led to device efficiency of 22.7% and excellent stability. Notably, unencapsulated cells retained 96% of their initial efficiency even after more than 2000 hours of storage in a nitrogen environment.

Similar to Pb-HPSCs, there are also a number of exciting results that employ a 2D passivation strategy in Sn-Pb-HPSCs.[241,261–263] Using an ultra-thin 2D perovskite formed with PEAI molecule resulted in an improvement of PCE from 17.90 to 19.40 % along with better operational stability of Sn-Pb-HPSCs.[261] Similarly, trifluoromethyl-phenylethylamine hydroiodide (CF_3-PEAI) isomers were used for forming an ultrathin 2D layer on the surface of Sn-Pb HP films passivating surface defects.[262] It improved device PCE as high as 20.17 % and retained device stability ~ 75% of initial PCE after 700 h. It is reported to be a consequence of passivating 2D layer alongside selective tuning of the perovskite surface polarity by dipole moment engineering, which facilitates electron transport in the HTL-free Sn-Pb-HPSCs. A report by Hao and co-workers documented a regulation of the crystallization growth of Sn-Pb- HP on the 2D perovskite (4-AMP)PbI_4.[263] Although the device PCE (17.70%) is much lower than 2D passivation by molecular surface treatment, this approach is effective for mitigating the buried interface defects and forming formation of better interfacial contact. Moreover, Tong et al. used a quasi-2D passivation strategy in Sn-Pb-HPSCs.[241] The incorporation of mixed bulky organic cations, phenethylammonium (PEA^+), and guanidinium (GA^+), as additives in Sn-Pb perovskite films has resulted in the formation of a quasi-2D structure of $(PEA)_2GAPb_2I_7$. This approach has demonstrated effective defect control, leading to substantial improvements in the structural and optoelectronic properties of the perovskite films. By utilizing this 2D additive engineering, the Sn-Pb perovskite films exhibited a long bulk carrier lifetime of approximately 9.2 μs and a low surface recombination velocity. These advancements ultimately translated into an impressive PCE of 22.1% for single-junction devices. Combining the 2D passivation strategy in Sn-Pb-HPSCs, they achieved highly efficient all-perovskite two-terminal tandems with a remarkable efficiency of 25.5%, high photovoltage of more than 2.1 V and long operational stability.

Similar to Sn-HPSCs, only a few studies have been reported on carrier transport engineering.[246,247,264,265] The improvement in PCE of Sn–Pb HPSCs has been constrained by the selection of the HTL, particularly PEDOT: PSS. Recently, Wang et al. introduced a new alternative, polymer HTL, poly[(phenyl)imino[9-(2-ethylhexyl) carbazole]-2,7-diyl] (CzAn) in place of PEDOT: PSS.[247] Sn-Pb -HPSCs with the CzAn HTL demonstrated PCEs as high as 22.6% using MA-free Sn-Pb HP films prepared with doping optimization and surface passivation. This notable enhancement is primarily attributed to the preparation of MA-free Sn-Pb perovskite with doping and surface passivation

techniques, leading to improved crystallinity and reduced trap-state density. In the same line of thinking, Hayase and co-workers also explored the HTL engineering using 2-(9H-carbazol-9-yl) ethyl] phosphonic acid (2PACz) as hole selective monolayers in Pb-Sn-HPSCs. They demonstrated equivalent PCE (21.39%) to the control device based on the PEDOT: PSS, HTL (21.37%). After further effort on hole transport engineering with hybrid HTL, Sn-Pb -HPSCs with 2PACz and small molecules methyl phosphonic acid (MPA) as the composite HTL, demonstrated a significant enhancement in PCE to 23.3% (Figure 9d).[246] Similarly, adopting a heterojunction structure, Zhou et al. demonstrated an ideal-bandgap Sn-Pb heterojunction HPSCs of excellent PCE of 24.27% using a near-infrared (NIR) polymer (Figure 9e, f). The heterojunction structure showed well-watched interfacial band alignment with cascade-like energy which is effective for charge-extraction. The NIR polymer is not only benign for harvesting the NIR light response but also has a strong interaction with Pb/Sn atoms which mitigates the defects in HP bulk.[71]

In the line of Pb-free mixed B-site HPSCs,[174,175] only a few works have been reported due to much lower efficiency compared to Sn-Pb-based HPSCs. For example, Sn-Ge-alloyed HPSCs have been reported with 5% GeI_2 incorporation which results in PCE of 7.9% with Pb-free B-site alloyed perovskite. It is found that the incorporation of GeI_2 suppresses the Sn^{2+} oxidation and recombination centers within the Sn-Ge HP or at hetero-interfaces.[174] Since Sn^{2+} and Ge^{2+}, both cations have facile oxidation during precursor preparation, film processing, and device operation, it needs extensive studies for controlling the material stability and film crystallization.

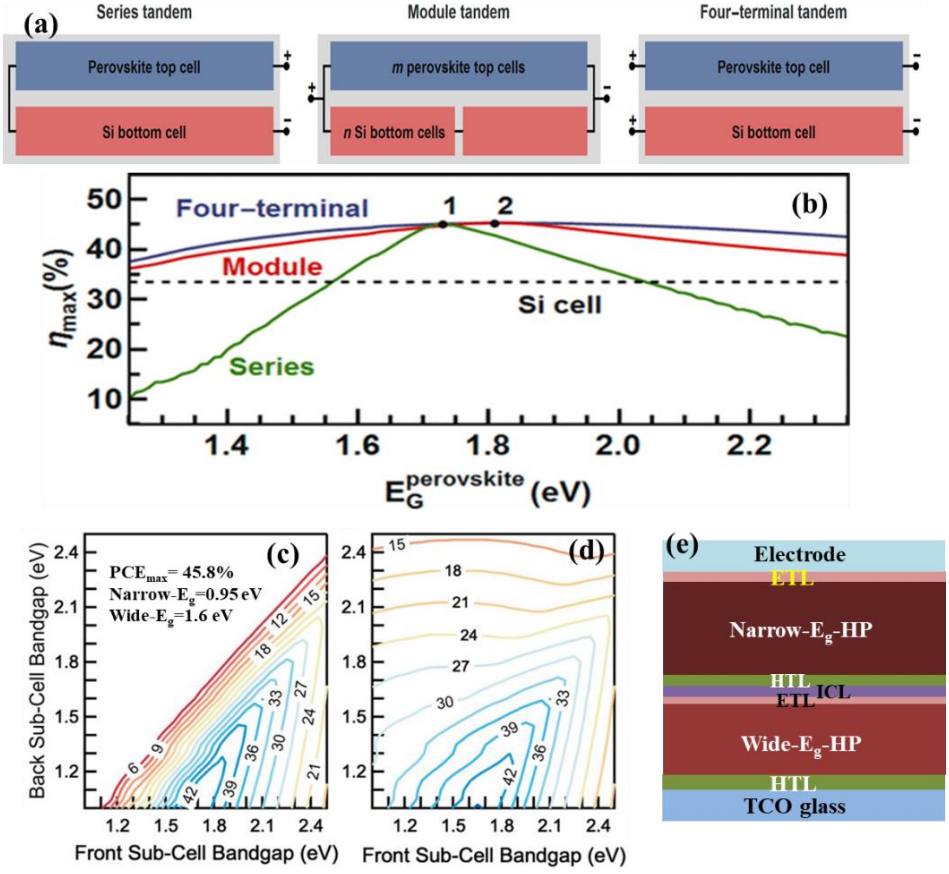

Figure 10. Tandem device applications: (a) Schematic illustration of Si/perovskite tandem device configurations. (b) PCE limit of the corresponding tandem device configurations with different bandgaps of the top cell obtained by detailed-balance calculations. The optimal E_g for the top cell is 1.73 eV (point 1) for a series configuration and 1.81 eV (point 2) for the module and 4-T configuration. The dotted line stands for the SQ limit of Si-PV. Reproduced with permission.[268] Copyright 2016, American Chemical Society. (c) Detailed balance efficiency limits for a 2-T monolithic tandem device (Under standard 1 sun illumination, assuming complete absorption of photons with energy higher than the E_g). (d) Under the same assumptions as in (c), with the exception that the thickness of the wide-E_g sub-cell can be adjusted to allow for the transmission of some photons to the narrow-E_g sub-cell. Reproduced with permission.[269] Copyright 2017, American Chemical Society. (e) Schematic illustration of perovskite/perovskite tandem solar cell.

6. Tandem Configuration -HPSCs

Owing to the wider range of bandgap tunability of HPs (~1.18 - 2.3 eV), they have been used for tandem device configuration (TDC), both in all perovskite configurations and in hybrid with Si or CIGS cells.[32,239,270,271] Detailed-balance calculations have shown that the limiting efficiency of a tandem device, considering an infinite number of subcells, can reach a demonstrated power conversion efficiency (PCE) of up to 69.9% under standard 1 sun illumination.[268,272] In a tandem device, PCE depends on how the subcells are connected. For example, the schematic depicted in Figure 10a displays a simple set of three configurations of perovskite/Si tandem devices. Ehrler and co-worker calculated the limiting PCE of corresponding TDCs showing an optimal PCE of 45.1% for the series and 45.3% for the module and 4T configurations (Figure 10b).226 Because of the current matching issue, the series TDC has a narrow E_g window (1.57-2.04 eV) for the HP top cells for getting higher PCE than the SQ limit of Si- single junction PV while the other the two TDCs demonstrated PCE over the SQ limit of Si-PV with an E_g>1.2 eV. Perovskite/Si tandem solar cells fabricated with solution-processed perovskite on textured silicon wafers, have demonstrated promising device efficiency by tailoring the quality of the perovskite film.[273–275] Recently, De Wolf and coworkers achieved a remarkable record PCE of 33.7% for a perovskite/silicon tandem device which is the best result of all tandem configurations.[2]

Indeed, all-perovskite tandem solar cells offer a compelling combination of low-cost solution processing and the potential for achieving high efficiency than Si-perovskite tandem solar cells.[276] Noting that the SQ limit of single-junction perovskite PCE is up to 33%, it can be scaled up to PCE >45% by combining two perovskite sub-cells having narrow and wide E_g in tandem solar cell configuration. A contour plot of tandem device efficiency with varying E_g of front and back sub-cells is depicted in Figure 10c. Based on this calculation, we can achieve a PCE of 45.8% by matching an absorber layer with E_g ~0.95 eV (narrow E_g) with another absorber with Eg~1.6 eV (wide E_g), assuming all incident light is fully absorbed by each sub-cell.[33,269] However, this narrow widow for high efficiency can be widened if the sub-cell thickness can be varied to allow non-complete absorption in the wide-Eg sub-cell. If the absorber thickness is varied, a wide range of E_g can be used to reach theoretical PCEs>40% (Figure 10d). Combining a narrow E_g sub-cell of 0.9–1.3 eV and another sub-cell with a wide E_g of 1.4–1.8 eV could result in PCE ≥42%. Considering all perovskite TDC (for example, Figure 10e), the tandem solar cells can be obtained by pairing narrow E_g

Sn–Pb -based HP (~1.2 eV) and a wide E_g Pb-HP (~1.6-1.8) to achieve PCE ≥40%. By stacking multiple semiconductor layers, these cells can absorb a broader spectrum of solar radiation, leading to improved overall power conversion efficiency. Due to various hurdles faced with perovskite film growth and connecting carrier transport layer in tandem structures, the PCE of tandem devices with all perovskite configurations has not exceeded the Si/perovskite tandem device. However, recent reports have demonstrated significant progress on perovskite/perovskite tandem devices.[259,277–279] For example, Tan and co-workers have achieved a certified PCE of 26.4% in all-perovskite tandem HPSCs with improved grain surface passivation using multi-functional molecules (e.g., 4-trifluoromethyl-phenylammonium halide) which exceeded the record PCE of the single-junction HPSCs.[280] Furthermore, the same group reported all-perovskite tandem HPSCs with 3D/2D bilayer perovskite heterojunction fabricated by adopting a hybrid evaporation/solution processing method.[281] This fabrication strategy scaled up to a record-high PCE of 28.5%, showing a competitive result to the Si/perovskite tandem solar cells. Despite rapid progress in single junction perovskite devices, the PCE of tandem device configuration is still far lower than the theoretical value and offers great promise.

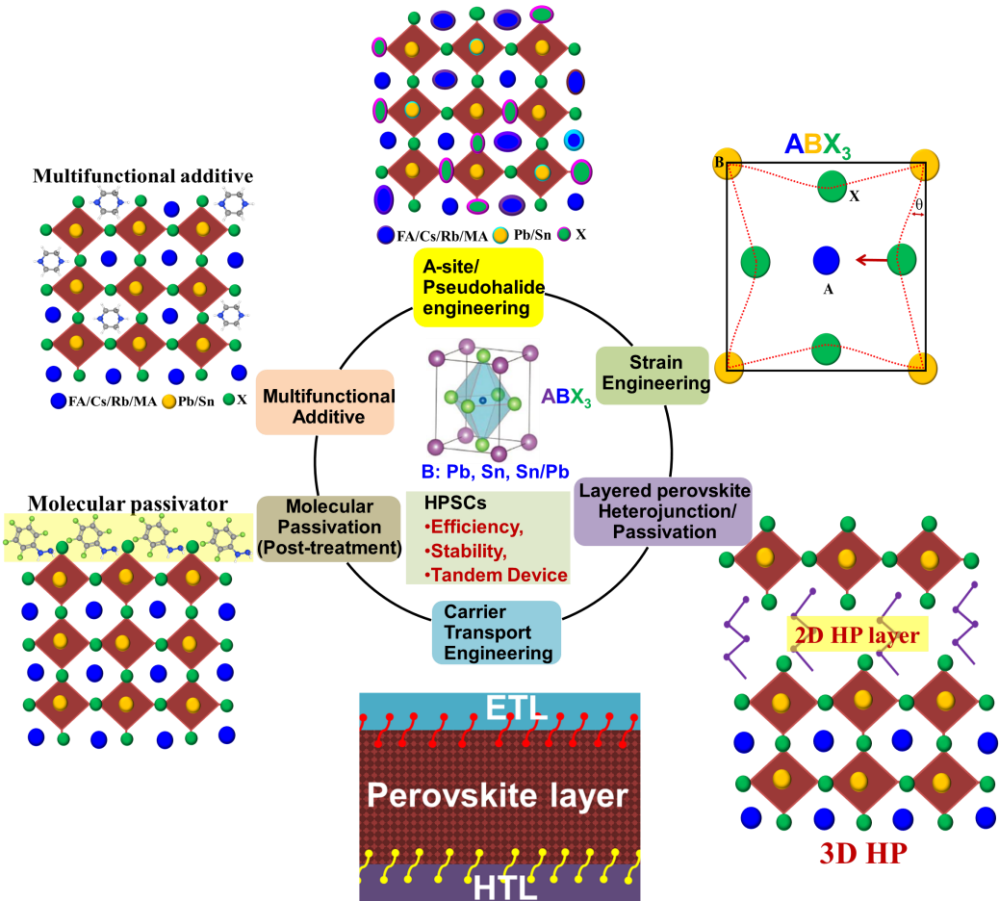

Figure 11. Schematic illustration of strategies for enhancement of device performance and stability of Pb, Sn, Sn/Pb-based HPSCs.

7. Summary and Outlook

Halide perovskite-based solar cells have attracted significant attention due to their startling progress in PCEs compared to other PV technologies. In the cloud of HPSCs reports, this review discusses research on the fundamental of HPs and various methods for advancing the efficiency and stability. The most effective methods for the improvement in device efficiency and stability of Pb-HPSCs are summarized in Figure 11. Despite the startling progress of Pb-based HPSCs, it has imposed a barrier to the commercial application due to their intrinsic instability and toxicity of Pb. Therefore, research on HPSCs focuses on resolving instability and toxicity issues without compromising device performance approaching the theoretical limit. Benefiting from a rich understanding of Pb-HPSCs, Sn, and Sn-Pb mixed-HPSCs have also achieved significant improvement in device performance and stability by adopting similar techniques for material engineering via multifunctional molecular additive and interface passivation/modulation strategies for the device fabrication due to similarities in the electronic properties of Pb and Sn.

As for Pb-HPSCs, the device stability and efficiency have been tailored with chemical engineering and interfacial passivation/modulation, but the lead toxicity issue remains to be addressed. Although Sn-HP derivatives are the most promising candidates, their device efficiency is almost half of Pb-HSPCs due to facile oxidation and faster crystal growth dynamics. These notorious issues of Sn-perovskites have been tried to resolve by introducing reducing agents and multifunctional reactive antioxidative additives. Great efforts must be made to inhibit the oxidation of Sn^{2+} by chemical engineering or structural regulation in future research. Noting the optical bandgap, it is expected to get a competitive device PCE with Sn-HP having stable Sn^{2+} oxidation. Benefiting from the progress in Pb or Sn- HPSCs, Sn-Pb- based HPSCs have demonstrated a competitive PCE to Pb-HSPCs, but device stability is still not as good as Pb-HP. If the problem of Sn oxidation can be overcome, it will lead to a giant leap forward and higher efficiencies than Pb-HPSCs.

Regarding Pb-HPSCs, operational device stability should be the primary focus without compromising device efficiency. Despite encapsulation of the device, the intrinsic instability of perovskite bulk and its interface is a big challenge to be resolved. Extensive insight into strain engineering via bulk or interface modulation using multifunctional molecular additives could be a way to stabilize the perovskite. Interface passivation using stable lower-dimension materials could be crucial in keeping the perovskite bulk intact. Since ion migration and defects in HP play an indelible role, a deeper insight into defect physics and its quenching engineering could give practical ways towards highly efficient and stable Pb-HPSCs.

For Sn-HPSCs, compared to Pb-counterparts, the figures of merit (V_{OC}, short circuit current (J_{SC}), and Fill factor) are much lower. Typical devices have V_{OC} (<1 V) with a voltage deficit > 0.45V. Likewise, despite the absorber layer with optical bandgap (1.2 -1.4 eV) achieving a J_{SC} as high as ~40 mA/cm^2 is possible, the values of reported J_{SC} are < 25 mA/cm^2 for Sn-HPSCs, which is less than 60% of the theoretical value. These parameters could have been limited by defective Sn-HP bulk due to Sn^{2+} oxidation, and less-optimal carrier transport layer. To minimize the V_{OC} loss, firstly, the nonradiative trap density should be controlled by inhibiting oxidation of Sn-HP using a strong reducing agent in the precursor solution, multifunctional additive, and interfacial passivation with 2D/3D hybrid composite. Secondly, interfacial band alignment with self-assembled monolayer or functional fullerene derivates with suitable HOMO and LUMO levels could help for increasing the built-in potential and energy mismatch. Thirdly, the limited

thickness of reported Sn-HP films (200-250 nm) is not thick enough for optical absorption. So, getting thicker Sn-HP film with high optoelectronic quality is important for obtaining a higher J_{SC} close to the theoretical limit.

Furthermore, the knowledge in Pb and Sn- HPSCs can be used to further enhancement of the device efficiency and stability of mixed Sn/Pb-based HPSCs. The tandem device with perovskite subcells can be further improved by optimizing the stack layer quality and interconnecting transport layer engineering. Thus, addressing these issues with extensive insight into material chemistry and defect physics, the HPSCs technology will be a reliable and cost-effective new-generation PV technology in the near future.

Associated Content

Notes

The authors declare no competing financial interest.

Acknowledgements

The authors acknowledge the support under the MEXT Program for Development of Environment Technology using Nanotechnology (GREEN), JSPS KAKENHI grant number JP16K06285. This work was also partly supported by JST-Mirai Program Grant Number JPMJMI21E6, Japan, Hitachi Karata Fund and the Yazaki Foundation for Science and Technology.

References

[1] D. M. Chapin, C. S. Fuller, G. L. Pearson, *J Appl Phys* **1954**, *25*, 676.

[2] National Renewable Energy Laboratory, "Interactive Best Research-Cell Efficiency Chart," can be found under https://www.nrel.gov/pv/interactive-cell-efficiency.html, **2023**.

[3] A. Kojima, K. Teshima, Y. Shirai, T. Miyasaka, *J Am Chem Soc* **2009**, *131*, 6050.

[4] N. J. Jeon, J. H. Noh, Y. C. Kim, W. S. Yang, S. Ryu, S. Il Seok, *Nat Mater* **2014**, *13*, 897.

[5] M. Saliba, T. Matsui, J.-Y. Seo, K. Domanski, J.-P. Correa-Baena, M. K. Nazeeruddin, S. M. Zakeeruddin, W. Tress, A. Abate, A. Hagfeldt, M. Grätzel, *Energy Environ Sci* **2016**, *9*, 1989.

[6] J. H. Noh, S. H. Im, J. H. Heo, T. N. Mandal, S. Il Seok, *Nano Lett* **2013**, *13*, 1764.

[7] Y.-H. Lin, N. Sakai, P. Da, J. Wu, H. C. Sansom, A. J. Ramadan, S. Mahesh, J. Liu, R. D. J. Oliver, J. Lim, L. Aspitarte, K. Sharma, P. K. Madhu, A. B. Morales- Vilches, P. K. Nayak, S. Bai, F. Gao, C. R. M. Grovenor, M. B. Johnston, J. G. Labram, J. R. Durrant, J. M. Ball, B. Wenger, B. Stannowski, H. J. Snaith, *Science* **2020**, *369*, 96.

[8] J. Zhu, S. Park, O. Y. Gong, C. Sohn, Z. Li, Z. Zhang, B. Jo, W. Kim, G. S. Han, D. H. Kim, T. K. Ahn, J. Lee, H. S. Jung, *Energy Environ Sci* **2021**, *14*, 4903.

[9] H. Zhu, Y. Liu, F. T. Eickemeyer, L. Pan, D. Ren, M. A. Ruiz- Preciado, B. Carlsen, B. Yang, X. Dong, Z. Wang, H. Liu, S. Wang, S. M. Zakeeruddin, A. Hagfeldt, M. I. Dar, X. Li, M. Grätzel, *Advanced Materials* **2020**, *32*, 1907757.

[10] D. B. Khadka, Y. Shirai, M. Yanagida, T. Tadano, K. Miyano, *Adv Energy Mater* **2022**, *12*, 2202029.

[11] G. Li, Y. Jiang, S. Deng, A. Tam, P. Xu, M. Wong, H.-S. Kwok, *Advanced Science* **2017**, *4*, 1700463.

[12] D. B. Khadka, Y. Shirai, M. Yanagida, K. Miyano, *ACS Appl Mater Interfaces* **2019**, *11*, 7055.

[13] D. B. Khadka, Y. Shirai, M. Yanagida, K. Miyano, *ACS Appl Energy Mater* **2021**, *4*, 11121.

[14] D. B. Khadka, Y. Shirai, M. Yanagida, K. Uto, K. Miyano, *Solar Energy Materials and Solar Cells* **2022**, *246*, 111899.

[15] S. Ma, Y. Bai, H. Wang, H. Zai, J. Wu, L. Li, S. Xiang, N. Liu, L. Liu, C. Zhu, G. Liu, X. Niu, H. Chen, H. Zhou, Y. Li, Q. Chen, *Adv Energy Mater* **2020**, *10*, 1902472.

[16] I. Gueye, Y. Shirai, T. Nagata, T. Tsuchiya, D. B. Khadka, M. Yanagida, O. Seo, K. Miyano, O. Sakata, *Chemistry of Materials* **2023**, *35*, 1948.

[17] S. Sidhik, Y. Wang, M. De Siena, R. Asadpour, A. J. Torma, T. Terlier, K. Ho, W. Li, A. B. Puthirath, X. Shuai, A. Agrawal, B. Traore, M. Jones, R. Giridharagopal, P. M. Ajayan, J. Strzalka, D. S. Ginger, C. Katan, M. A. Alam, J. Even, M. G. Kanatzidis, A. D. Mohite, *Science* **2022**, *377*, 1425.
[18] Y. Chen, Y. Lei, Y. Li, Y. Yu, J. Cai, M.-H. Chiu, R. Rao, Y. Gu, C. Wang, W. Choi, H. Hu, C. Wang, Y. Li, J. Song, J. Zhang, B. Qi, M. Lin, Z. Zhang, A. E. Islam, B. Maruyama, S. Dayeh, L.-J. Li, K. Yang, Y.-H. Lo, S. Xu, *Nature* **2020**, *577*, 209.
[19] M. Yanagida, Y. Shirai, D. B. Khadka, K. Miyano, *Physical Chemistry Chemical Physics* **2020**, *22*, 25118.
[20] A. Babayigit, A. Ethirajan, M. Muller, B. Conings, *Nat Mater* **2016**, *15*, 247.
[21] B. W. Park, B. Philippe, X. Zhang, H. Rensmo, G. Boschloo, E. M. J. Johansson, *Advanced Materials* **2015**, *27*, 6806.
[22] P. V. Kamat, J. Bisquert, J. Buriak, *ACS Energy Lett* **2017**, *2*, 904.
[23] D. B. Khadka, Y. Shirai, M. Yanagida, K. Miyano, *J Mater Chem C Mater* **2019**, *7*, 8335.
[24] M. G. M. Pandian, D. B. Khadka, Y. Shirai, S. Umedov, M. Yanagida, S. Subashchandran, A. Grigorieva, K. Miyano, *J Mater Chem C Mater* **2020**, *8*, 12173.
[25] S. S. Hosseini, M. Adelifard, M. Ataei, *Journal of Materials Science: Materials in Electronics* **2019**, *30*, 5021.
[26] M. B. Johansson, H. Zhu, E. M. J. Johansson, *Journal of Physical Chemistry Letters* **2016**, *7*, 3467.
[27] I. Kopacic, B. Friesenbichler, S. F. Hoefler, B. Kunert, H. Plank, T. Rath, G. Trimmel, *ACS Appl Energy Mater* **2018**, *1*, 343.
[28] C. C. Stoumpos, L. Frazer, D. J. Clark, Y. S. Kim, S. H. Rhim, A. J. Freeman, J. B. Ketterson, J. I. Jang, M. G. Kanatzidis, *J Am Chem Soc* **2015**, *137*, 6804.
[29] A. Filippetti, S. Kahmann, C. Caddeo, A. Mattoni, M. Saba, A. Bosin, M. A. Loi, *J Mater Chem A Mater* **2021**, *9*, 11812.
[30] B. Yu, Z. Chen, Y. Zhu, Y. Wang, B. Han, G. Chen, X. Zhang, Z. Du, Z. He, *Advanced Materials* **2021**, *33*, 2102055.
[31] A. Yadegarifard, H. Lee, H.-J. Seok, I. Kim, B.-K. Ju, H.-K. Kim, D.-K. Lee, *Nano Energy* **2023**, *112*, 108481.
[32] H. Chen, A. Maxwell, C. Li, S. Teale, B. Chen, T. Zhu, E. Ugur, G. Harrison, L. Grater, J. Wang, Z. Wang, L. Zeng, S. M. Park, L. Chen, P. Serles, R. A. Awni, B. Subedi, X. Zheng, C. Xiao, N. J. Podraza, T. Filleter, C. Liu, Y. Yang, J. M. Luther, S. De Wolf, M. G. Kanatzidis, Y. Yan, E. H. Sargent, *Nature* **2023**, *613*, 676.
[33] T. Moot, J. Werner, G. E. Eperon, K. Zhu, J. J. Berry, M. D. McGehee, J. M. Luther, *Advanced Materials* **2020**, *32*, 2003312.
[34] A. Kumar Jena, A. Kulkarni, T. Miyasaka, *Chem Rev* **2019**, *119*, 3036.
[35] CHR. KN. MØLLER, *Nature* **1958**, *182*, 1436.
[36] D. Weber, *Zeitschrift für Naturforschung B* **1978**, *33*, 1443.
[37] D. B. Mitzi, S. Wang, C. A. Feild, C. A. Chess, A. M. Guloy, *Science* **1995**, *267*, 1473.
[38] D. B. Mitzi, *Inorg Chem* **2000**, *39*, 6107.
[39] Q. Sun, W.-J. Yin, *J Am Chem Soc* **2017**, *139*, 14905.
[40] F. Zhang, H. Lu, J. Tong, J. J. Berry, M. C. Beard, K. Zhu, *Energy Environ Sci* **2020**, *13*, 1154.
[41] A. E. Maughan, A. M. Ganose, M. A. Almaker, D. O. Scanlon, J. R. Neilson, *Chemistry of Materials* **2018**, *30*, 3909.
[42] S. T. Umedov, D. B. Khadka, M. Yanagida, A. Grigorieva, Y. Shirai, *Solar Energy Materials and Solar Cells* **2021**, *230*, 111180.
[43] R. D. Nelson, K. Santra, Y. Wang, A. Hadi, J. W. Petrich, M. G. Panthani, *Chemical Communications* **2018**, *54*, 3640.
[44] J. Euvrard, X. Wang, T. Li, Y. Yan, D. B. Mitzi, *J Mater Chem A Mater* **2020**, *8*, 4049.
[45] M.-G. Ju, M. Chen, Y. Zhou, H. F. Garces, J. Dai, L. Ma, N. P. Padture, X. C. Zeng, *ACS Energy Lett* **2017**, acsenergylett.7b01167.
[46] S. M. Jain, T. Edvinsson, J. R. Durrant, *Commun Chem* **2019**, *2*, 91.
[47] B. Saparov, F. Hong, J. Sun, H. Duan, W. Meng, S. Cameron, I. G. Hill, Y. Yan, D. B. Mitzi, *Chemistry of Materials* **2015**, *27*, 5622.
[48] S. Weber, T. Rath, K. Fellner, R. Fischer, R. Resel, B. Kunert, T. Dimopoulos, A. Steinegger, G. Trimmel, *ACS Appl Energy Mater* **2019**, *2*, 539.
[49] D. Liu, C. M. Perez, A. S. Vasenko, O. V. Prezhdo, *J Phys Chem Lett* **2022**, *13*, 3645.
[50] A. Singh, R. Chaurasiya, A. Bheemaraju, J.-S. Chen, S. Satapathi, *ACS Appl Energy Mater* **2022**, *5*, 3926.

[51] G. Volonakis, A. A. Haghighirad, R. L. Milot, W. H. Sio, M. R. Filip, B. Wenger, M. B. Johnston, L. M. Herz, H. J. Snaith, F. Giustino, *Journal of Physical Chemistry Letters* **2017**, *8*, 772.
[52] W.-Y. Cong, C. Guan, Y.-B. Lu, P. Zhang, S. Xue, Q. Wu, *Journal of Physics: Condensed Matter* **2021**, *33*, 495501.
[53] M. Chen, Z. Shan, X. Dong, S. (Frank) Liu, Z. Xu, *Nanoscale Horiz* **2023**, DOI 10.1039/D2NH00499B.
[54] N. Wang, Y. Zhou, M.-G. Ju, H. F. Garces, T. Ding, S. Pang, X. C. Zeng, N. P. Padture, X. W. Sun, *Adv Energy Mater* **2016**, *6*, 1601130.
[55] W. Gao, C. Ran, J. Xi, B. Jiao, W. Zhang, M. Wu, X. Hou, Z. Wu, *ChemPhysChem* **2018**, *19*, 1696.
[56] F. Zhang, D. H. Kim, H. Lu, J.-S. Park, B. Larson, J. Hu, L. Gao, C. Xiao, O. Reid, X. Chen, Q. Zhao, P. F. Ndione, J. J. Berry, W. You, A. Walsh, M. C. Beard, K. Zhu, *J Am Chem Soc* **2019**, *19*, jacs. 9b00972.
[57] F. Igbari, R. Wang, Z.-K. Wang, X.-J. Ma, Q. Wang, K.-L. Wang, Y. Zhang, L.-S. Liao, Y. Yang, *Nano Lett* **2019**, *19*, 2066.
[58] W. Travis, E. N. K. Glover, H. Bronstein, D. O. Scanlon, R. G. Palgrave, *Chem Sci* **2016**, *7*, 4548.
[59] M. A. Green, A. Ho-Baillie, H. J. Snaith, *Nat Photonics* **2014**, *8*, 506.
[60] J. Even, L. Pedesseau, J.-M. Jancu, C. Katan, *J Phys Chem Lett* **2013**, *4*, 2999.
[61] W. J. Yin, T. Shi, Y. Yan, *Advanced Materials* **2014**, *26*, 4653.
[62] T. Baikie, Y. N. Fang, J. M. Kadro, M. Schreyer, F. X. Wei, S. G. Mhaisalkar, M. Graetzel, T. J. White, *J. Mater. Chem. A* **2013**, *1*, 5628.
[63] F. Yang, L. Dong, D. Jang, K. C. Tam, K. Zhang, N. Li, F. Guo, C. Li, C. Arrive, M. Bertrand, C. J. Brabec, H. Egelhaaf, *Adv Energy Mater* **2020**, *10*, 2001869.
[64] T. Liu, Y. Zong, Y. Zhou, M. Yang, Z. Li, O. S. Game, K. Zhu, R. Zhu, Q. Gong, N. P. Padture, *Chemistry of Materials* **2017**, *29*, 3246.
[65] J.-W. Lee, S. Tan, S. Il Seok, Y. Yang, N.-G. Park, *Science* **2022**, *375*, eabj1186.
[66] C. C. Stoumpos, C. D. Malliakas, M. G. Kanatzidis, *Inorg Chem* **2013**, *52*, 9019.
[67] F. Hao, C. C. Stoumpos, R. P. H. Chang, M. G. Kanatzidis, *J Am Chem Soc* **2014**, *136*, 8094.
[68] R. Prasanna, A. Gold-Parker, T. Leijtens, B. Conings, A. Babayigit, H. G. Boyen, M. F. Toney, M. D. McGehee, *J Am Chem Soc* **2017**, *139*, 11117.
[69] S. Tao, I. Schmidt, G. Brocks, J. Jiang, I. Tranca, K. Meerholz, S. Olthof, *Nat Commun* **2019**, *10*, DOI 10.1038/s41467-019-10468-7.
[70] A. Goyal, S. McKechnie, D. Pashov, W. Tumas, M. van Schilfgaarde, V. Stevanović, *Chemistry of Materials* **2018**, *30*, 3920.
[71] X. Zhou, L. Zhang, J. Yu, D. Wang, C. Liu, S. Chen, Y. Li, Y. Li, M. Zhang, Y. Peng, Y. Tian, J. Huang, X. Wang, X. Guo, B. Xu, *Advanced Materials* **2022**, *34*, 2205809.
[72] Y. Ogomi, A. Morita, S. Tsukamoto, T. Saitho, N. Fujikawa, Q. Shen, T. Toyoda, K. Yoshino, S. S. Pandey, T. Ma, S. Hayase, *J Phys Chem Lett* **2014**, *5*, 1004.
[73] J. Seo, T. Song, S. Rasool, S. Park, J. Y. Kim, *Advanced Energy and Sustainability Research* **2023**, 2200160.
[74] I. Levchuk, A. Osvet, X. Tang, M. Brandl, J. D. Perea, F. Hoegl, G. J. Matt, R. Hock, M. Batentschuk, C. J. Brabec, *Nano Lett* **2017**, *17*, 2765.
[75] P. Brenner, T. Glöckler, D. Rueda-Delgado, T. Abzieher, M. Jakoby, B. S. Richards, U. W. Paetzold, I. A. Howard, U. Lemmer, *Opt Mater Express* **2017**, *7*, 4082.
[76] M. Karlsson, Z. Yi, S. Reichert, X. Luo, W. Lin, Z. Zhang, C. Bao, R. Zhang, S. Bai, G. Zheng, P. Teng, L. Duan, Y. Lu, K. Zheng, T. Pullerits, C. Deibel, W. Xu, R. Friend, F. Gao, *Nat Commun* **2021**, *12*, 361.
[77] D. B. Khadka, Y. Shirai, M. Yanagida, T. Noda, K. Miyano, *ACS Appl Mater Interfaces* **2018**, *10*, 22074.
[78] M. Pitaro, E. K. Tekelenburg, S. Shao, M. A. Loi, *Advanced Materials* **2022**, *34*, 2105844.
[79] Z. Yang, X. Zhang, W. Yang, G. E. Eperon, D. S. Ginger, *Chemistry of Materials* **2020**, *32*, 2782.
[80] G. Kim, H. Min, K. S. Lee, D. Y. Lee, S. M. Yoon, S. Il Seok, *Science* **2020**, *370*, 108.
[81] J. Zhang, S. Wu, T. Liu, Z. Zhu, A. K. Y. K. - Y. Jen, *Adv Funct Mater* **2019**, *29*, 1808833.
[82] H. Lu, Y. Liu, P. Ahlawat, A. Mishra, W. R. Tress, F. T. Eickemeyer, Y. Yang, F. Fu, Z. Wang, C. E. Avalos, B. I. Carlsen, A. Agarwalla, X. Zhang, X. Li, Y. Zhan, S. M. Zakeeruddin, L. Emsley, U. Rothlisberger, L. Zheng, A. Hagfeldt, M. Grätzel, *Science* **2020**, *370*, DOI 10.1126/science.abb8985.
[83] J. Jeong, M. Kim, J. Seo, H. Lu, P. Ahlawat, A. Mishra, Y. Yang, M. A. Hope, F. T. Eickemeyer, M. Kim, Y. J. Yoon, I. W. Choi, B. P. Darwich, S. J. Choi, Y. Jo, J. H. Lee, B. Walker, S. M. Zakeeruddin, L. Emsley, U. Rothlisberger, A. Hagfeldt, D. S. Kim, M. Grätzel, J. Y. Kim, *Nature* **2021**, *592*, 381.
[84] M. Jung, T. J. Shin, J. Seo, G. Kim, S. Il Seok, *Energy Environ Sci* **2018**, *11*, 2188.

[85] Y. Kong, W. Shen, H. Cai, W. Dong, C. Bai, J. Zhao, F. Huang, Y. Cheng, J. Zhong, *Adv Funct Mater* **2023**, 2300932.
[86] G. Duan, K. Zhang, W. Zhang, H. Shu, Y. Yang, X. Zhou, C. Liu, L. Yu, X. Yu, Y. Huang, X. Wu, C. Peng, S. Yang, M. Liang, W. Zhang, H. Tan, *ACS Energy Lett* **2023**, 2308.
[87] W. Shen, H. Cai, Y. Kong, W. Dong, C. Bai, G. Liang, W. Li, J. Zhao, F. Huang, Y. Cheng, J. Zhong, *Small* **2023**, 2302194.
[88] Y. Liu, S. Akin, L. Pan, R. Uchida, N. Arora, J. V Milić, A. Hinderhofer, F. Schreiber, A. R. Uhl, S. M. Zakeeruddin, A. Hagfeldt, M. I. Dar, M. Grätzel, *Sci Adv* **2019**, *5*, eaaw2543.
[89] B. Yang, J. Suo, F. Di Giacomo, S. Olthof, D. Bogachuk, Y. Kim, X. Sun, L. Wagner, F. Fu, S. M. Zakeeruddin, A. Hinsch, M. Grätzel, A. Di Carlo, A. Hagfeldt, *ACS Energy Lett* **2021**, *6*, 3916.
[90] Z. Li, B. Li, X. Wu, S. A. Sheppard, S. Zhang, D. Gao, N. J. Long, Z. Zhu, *Science* **2022**, *376*, 416.
[91] S. Wang, P. Wang, B. Shi, C. Sun, H. Sun, S. Qi, Q. Huang, S. Xu, Y. Zhao, X. Zhang, *Advanced Materials* **2023**, *35*, 2300581.
[92] R. Azmi, E. Ugur, A. Seitkhan, F. Aljamaan, A. S. Subbiah, J. Liu, G. T. Harrison, M. I. Nugraha, M. K. Eswaran, M. Babics, Y. Chen, F. Xu, T. G. Allen, A. ur Rehman, C.-L. Wang, T. D. Anthopoulos, U. Schwingenschlögl, M. De Bastiani, E. Aydin, S. De Wolf, *Science* **2022**, *376*, 73.
[93] S. Tan, B. Yu, Y. Cui, F. Meng, C. Huang, Y. Li, Z. Chen, H. Wu, J. Shi, Y. Luo, D. Li, Q. Meng, *Angewandte Chemie International Edition* **2022**, *61*, e202201300.
[94] J. Peng, D. Walter, Y. Ren, M. Tebyetekerwa, Y. Wu, T. Duong, Q. Lin, J. Li, T. Lu, M. A. Mahmud, O. L. C. Lem, S. Zhao, W. Liu, Y. Liu, H. Shen, L. Li, F. Kremer, H. T. Nguyen, D.-Y. Choi, K. J. Weber, K. R. Catchpole, T. P. White, *Science* **2021**, *371*, 390.
[95] W. Peng, K. Mao, F. Cai, H. Meng, Z. Zhu, T. Li, S. Yuan, Z. Xu, X. Feng, J. Xu, M. D. McGehee, J. Xu, *Science* **2023**, *379*, 683.
[96] S. Zhang, F. Ye, X. Wang, R. Chen, H. Zhang, L. Zhan, X. Jiang, Y. Li, X. Ji, S. Liu, M. Yu, F. Yu, Y. Zhang, R. Wu, Z. Liu, Z. Ning, D. Neher, L. Han, Y. Lin, H. Tian, W. Chen, M. Stolterfoht, L. Zhang, W.-H. Zhu, Y. Wu, *Science* **2023**, *380*, 404.
[97] S. Wang, M.-H. Li, Y. Zhang, Y. Jiang, L. Xu, F. Wang, J.-S. Hu, *Energy Environ Sci* **2023**, *16*, 2572.
[98] D. W. Boukhvalov, I. S. Zhidkov, A. F. Akbulatov, A. I. Kukharenko, S. O. Cholakh, K. J. Stevenson, P. A. Troshin, E. Z. Kurmaev, *J Phys Chem A* **2020**, *124*, 135.
[99] A. Dualeh, P. Gao, S. Il Seok, M. K. Nazeeruddin, M. Grätzel, *Chemistry of Materials* **2014**, *26*, 6160.
[100] Y. Hu, M. F. Aygüler, M. L. Petrus, T. Bein, P. Docampo, *ACS Energy Lett* **2017**, *2*, 2212.
[101] D. J. Kubicki, D. Prochowicz, A. Hofstetter, S. M. Zakeeruddin, M. Grätzel, L. Emsley, P. Péchy, S. M. Zakeeruddin, M. Grätzel, L. Emsley, *J Am Chem Soc* **2017**, *139*, 14173.
[102] D. J. Kubicki, D. Prochowicz, A. Hofstetter, P. Péchy, S. M. Zakeeruddin, M. Grätzel, L. Emsley, *J Am Chem Soc* **2017**, *139*, 10055.
[103] B. Yu, J. Shi, S. Tan, Y. Cui, W. Zhao, H. Wu, Y. Luo, D. Li, Q. Meng, *Angewandte Chemie International Edition* **2021**, *60*, 13436.
[104] S. Valastro, G. Mannino, E. Smecca, C. Bongiorno, S. Sanzaro, I. Deretzis, A. La Magna, A. K. Jena, T. Miyasaka, A. Alberti, *Solar RRL* **2022**, *6*, 2200008.
[105] A. Polman, M. Knight, E. C. Garnett, B. Ehrler, W. C. Sinke, *Science* **2016**, *352*, DOI 10.1126/science.aad4424.
[106] W. Xiang, S. (Frank) Liu, W. Tress, *Energy Environ Sci* **2021**, *14*, 2090.
[107] D. Liu, D. Luo, A. N. Iqbal, K. W. P. Orr, T. A. S. Doherty, Z.-H. Lu, S. D. Stranks, W. Zhang, *Nat Mater* **2021**, *20*, 1337.
[108] M. Liu, L. Duan, T. J. Jacobsson, J. Luo, *Solar RRL* **2023**, *7*, 2300022.
[109] A. Chen, M. Yossef, C. Zhang, *Solar Energy* **2018**, *163*, 243.
[110] C. Yang, K. Song, X. Xu, G. Yao, Z. Wu, *Solar Energy* **2020**, *195*, 121.
[111] B. L. Watson, N. Rolston, A. D. Printz, R. H. Dauskardt, *Energy Environ Sci* **2017**, *10*, 2500.
[112] M. Abdi-Jalebi, Z. Andaji-Garmaroudi, S. Cacovich, C. Stavrakas, B. Philippe, J. M. Richter, M. Alsari, E. P. Booker, E. M. Hutter, A. J. Pearson, S. Lilliu, T. J. Savenije, H. Rensmo, G. Divitini, C. Ducati, R. H. Friend, S. D. Stranks, *Nature* **2018**, *555*, 497.
[113] L. Qiao, W. Fang, R. Long, O. V. Prezhdo, *Angewandte Chemie* **2020**, *132*, 4714.
[114] W.-J. Yin, Y. Yan, S.-H. Wei, *J Phys Chem Lett* **2014**, *5*, 3625.
[115] B. Walker, G. Kim, J. Y. Kim, *Advanced Materials* **2019**, *31*, 1807029.

[116] T. Singh, T. Miyasaka, *Adv Energy Mater* **2018**, *8*, 1700677.
[117] Q. Han, Y. Bai, J. Liu, K. Du, T. Li, D. Ji, Y. Zhou, C. Cao, D. Shin, J. Ding, A. D. Franklin, J. T. Glass, J. Hu, M. J. Therien, J. Liu, D. B. Mitzi, *Energy Environ Sci* **2017**, *10*, 2365.
[118] H. F. Zarick, N. Soetan, W. R. Erwin, R. Bardhan, *J Mater Chem A Mater* **2018**, *6*, 5507.
[119] E. T. Hoke, D. J. Slotcavage, E. R. Dohner, A. R. Bowring, H. I. Karunadasa, M. D. McGehee, *Chem. Sci.* **2015**, *6*, 613.
[120] A. J. Knight, J. Borchert, R. D. J. Oliver, J. B. Patel, P. G. Radaelli, H. J. Snaith, M. B. Johnston, L. M. Herz, *ACS Energy Lett* **2021**, *6*, 799.
[121] D. P. McMeekin, G. Sadoughi, W. Rehman, G. E. Eperon, M. Saliba, M. T. Horantner, A. Haghighirad, N. Sakai, L. Korte, B. Rech, M. B. Johnston, L. M. Herz, H. J. Snaith, *Science* **2016**, *351*, 151.
[122] J. Xu, C. C. Boyd, Z. J. Yu, A. F. Palmstrom, D. J. Witter, B. W. Larson, R. M. France, J. Werner, S. P. Harvey, E. J. Wolf, W. Weigand, S. Manzoor, M. F. A. M. A. M. Van Hest, J. J. Berry, J. M. Luther, Z. C. Holman, M. D. McGehee, *Science* **2020**, *367*, 1097.
[123] L. Gil-Escrig, C. Momblona, M.-G. La-Placa, P. P. Boix, M. Sessolo, H. J. Bolink, *Adv Energy Mater* **2018**, *8*, 1703506.
[124] J. Tao, X. Liu, J. Shen, S. Han, L. Guan, G. Fu, D.-B. Kuang, S. Yang, *ACS Nano* **2022**, *16*, 10798.
[125] L. Chu, *Matter* **2021**, *4*, 1762.
[126] D. Kim, H. J. Jung, I. J. Park, B. W. Larson, S. P. Dunfield, C. Xiao, J. Kim, J. Tong, P. Boonmongkolras, S. G. Ji, F. Zhang, S. R. Pae, M. Kim, S. B. Kang, V. Dravid, J. J. Berry, J. Y. Kim, K. Zhu, D. H. Kim, B. Shin, *Science* **2020**, *368*, 155.
[127] J. Chen, S.-G. Kim, N.-G. Park, *Advanced Materials* **2018**, *30*, 1801948.
[128] Z. Yao, Z. Jin, X. Zhang, Q. Wang, H. Zhang, Z. Xu, L. Ding, S. (Frank) Liu, *J Mater Chem C Mater* **2019**, *7*, 13736.
[129] M. Birkholz, R. Rudert, *physica status solidi (b)* **2008**, *245*, 1858.
[130] Q. Tai, P. You, H. Sang, Z. Liu, C. Hu, H. L. W. Chan, F. Yan, *Nat Commun* **2016**, *7*, 11105.
[131] W. Ke, C. Xiao, C. Wang, B. Saparov, H.-S. Duan, D. Zhao, Z. Xiao, P. Schulz, S. P. Harvey, W. Liao, W. Meng, Y. Yu, A. J. Cimaroli, C.-S. Jiang, K. Zhu, M. Al-Jassim, G. Fang, D. B. Mitzi, Y. Yan, *Advanced Materials* **2016**, *28*, 5214.
[132] R. Zhang, M. Li, Y. Huan, J. Xi, S. Zhang, X. Cheng, H. Wu, W. Peng, Z. Bai, X. Yan, *Inorg Chem Front* **2019**, *6*, 434.
[133] S. Yang, W. Liu, L. Zuo, X. Zhang, T. Ye, J. Chen, C.-Z. Li, G. Wu, H. Chen, *J Mater Chem A Mater* **2016**, *4*, 9430.
[134] S. Yang, S. Chen, E. Mosconi, Y. Fang, X. Xiao, C. Wang, Y. Zhou, Z. Yu, J. Zhao, Y. Gao, F. De Angelis, J. Huang, *Science* **2019**, *365*, 473 LP.
[135] D.-K. Lee, N.-G. Park, *Appl Phys Rev* **2023**, *10*, 011308.
[136] D. Bi, X. Li, J. V Milić, D. J. Kubicki, N. Pellet, J. Luo, T. LaGrange, P. Mettraux, L. Emsley, S. M. Zakeeruddin, M. Grätzel, *Nat Commun* **2018**, *9*, 4482.
[137] P.-W. Liang, C.-Y. Liao, C.-C. Chueh, F. Zuo, S. T. Williams, X.-K. Xin, J. Lin, A. K.-Y. Jen, *Advanced Materials* **2014**, *26*, 3748.
[138] T. Niu, L. Chao, W. Gao, C. Ran, L. Song, Y. Chen, L. Fu, W. Huang, *ACS Energy Lett* **2021**, 1453.
[139] F. Wang, C. Ge, D. Duan, H. Lin, L. Li, P. Naumov, H. Hu, *Small Struct* **2022**, *3*, 2200048.
[140] L. Chao, Y. Xia, X. Duan, Y. Wang, C. Ran, T. Niu, L. Gu, D. Li, J. Hu, X. Gao, J. Zhang, Y. Chen, *Joule* **2022**, *6*, 2203.
[141] S. Bai, P. Da, C. Li, Z. Wang, Z. Yuan, F. Fu, M. Kawecki, X. Liu, N. Sakai, J. T.-W. Wang, S. Huettner, S. Buecheler, M. Fahlman, F. Gao, H. J. Snaith, *Nature* **2019**, *571*, 245.
[142] W. Shen, H. Cai, Y. Kong, W. Dong, C. Bai, G. Liang, W. Li, J. Zhao, F. Huang, Y. Cheng, J. Zhong, *Small* **2023**, DOI 10.1002/smll.202302194.
[143] J. Chen, S.-G. Kim, X. Ren, H. S. Jung, N.-G. Park, *J Mater Chem A Mater* **2019**, *7*, 4977.
[144] P. Schulz, D. Cahen, A. Kahn, *Chem Rev* **2019**, *119*, 3349.
[145] S. Fu, J. Le, X. Guo, N. Sun, W. Zhang, W. Song, J. Fang, *Advanced Materials* **2022**, *34*, 2205066.
[146] Y. Guo, H. Liu, W. Li, L. Zhu, H. Chen, *Solar RRL* **2020**, *4*, 2000380.
[147] Q. Jiang, J. Tong, Y. Xian, R. A. Kerner, S. P. Dunfield, C. Xiao, R. A. Scheidt, D. Kuciauskas, X. Wang, M. P. Hautzinger, R. Tirawat, M. C. Beard, D. P. Fenning, J. J. Berry, B. W. Larson, Y. Yan, K. Zhu, *Nature* **2022**, *611*, 278.

[148] K. T. Cho, Y. Zhang, S. Orlandi, M. Cavazzini, I. Zimmermann, A. Lesch, N. Tabet, G. Pozzi, G. Grancini, M. K. Nazeeruddin, *Nano Lett* **2018**, *18*, 5467.
[149] J. Suo, B. Yang, E. Mosconi, H.-S. Choi, Y. Kim, S. M. Zakeeruddin, F. De Angelis, M. Grätzel, H.-S. Kim, A. Hagfeldt, *Adv Funct Mater* **2021**, *31*, 2102902.
[150] M. A. Ruiz-Preciado, D. J. Kubicki, A. Hofstetter, L. McGovern, M. H. Futscher, A. Ummadisingu, R. Gershoni-Poranne, S. M. Zakeeruddin, B. Ehrler, L. Emsley, J. V. Milić, M. Grätzel, *J Am Chem Soc* **2020**, *142*, 1645.
[151] C. Zhang, X. Shen, M. Chen, Y. Zhao, X. Lin, Z. Qin, Y. Wang, L. Han, *Adv Energy Mater* **2023**, *13*, 2203250.
[152] S. Akin, B. Dong, L. Pfeifer, Y. Liu, M. Graetzel, A. Hagfeldt, *Advanced Science* **2021**, *8*, 2004593.
[153] G. Yang, Z. Ren, K. Liu, M. Qin, W. Deng, H. Zhang, H. Wang, J. Liang, F. Ye, Q. Liang, H. Yin, Y. Chen, Y. Zhuang, S. Li, B. Gao, J. Wang, T. Shi, X. Wang, X. Lu, H. Wu, J. Hou, D. Lei, S. K. So, Y. Yang, G. Fang, G. Li, *Nat Photonics* **2021**, *15*, 681.
[154] H. Kim, S. Lee, D. Y. Lee, M. J. Paik, H. Na, J. Lee, S. Il Seok, *Adv Energy Mater* **2019**, *9*, 1902740.
[155] S. Kajal, J. Jeong, J. Seo, R. Anand, Y. Kim, B. Bhaskararao, C. Beom Park, J. Yeop, A. Hagdfeldt, J. Young Kim, K. S. Kim, *Chemical Engineering Journal* **2023**, *451*, 138740.
[156] S. Gharibzadeh, P. Fassl, I. M. Hossain, P. Rohrbeck, M. Frericks, M. Schmidt, T. Duong, M. R. Khan, T. Abzieher, B. A. Nejand, F. Schackmar, O. Almora, T. Feeney, R. Singh, D. Fuchs, U. Lemmer, J. P. Hofmann, S. A. L. Weber, U. W. Paetzold, *Energy Environ Sci* **2021**, *14*, 5875.
[157] B. Liu, C. M. M. Soe, C. C. Stoumpos, W. Nie, H. Tsai, K. Lim, A. D. Mohite, M. G. Kanatzidis, T. J. Marks, K. D. Singer, *Solar RRL* **2017**, *1*, 1700062.
[158] H. Kim, M. Pei, Y. Lee, A. A. Sutanto, S. Paek, V. I. E. Queloz, A. J. Huckaba, K. T. Cho, H. J. Yun, H. Yang, M. K. Nazeeruddin, *Adv Funct Mater* **2020**, *30*, 1910620.
[159] Y.-W. Jang, S. Lee, K. M. Yeom, K. Jeong, K. Choi, M. Choi, J. H. Noh, *Nat Energy* **2021**, *6*, 63.
[160] A. H. Proppe, A. Johnston, S. Teale, A. Mahata, R. Quintero-Bermudez, E. H. Jung, L. Grater, T. Cui, T. Filleter, C.-Y. Kim, S. O. Kelley, F. De Angelis, E. H. Sargent, *Nat Commun* **2021**, *12*, 3472.
[161] M. Kim, J. Jeong, H. Lu, T. K. Lee, F. T. Eickemeyer, Y. Liu, I. W. Choi, S. J. Choi, Y. Jo, H.-B. Kim, S.-I. Mo, Y.-K. Kim, H. Lee, N. G. An, S. Cho, W. R. Tress, S. M. Zakeeruddin, A. Hagfeldt, J. Y. Kim, M. Grätzel, D. S. Kim, *Science* **2022**, *375*, 302.
[162] C. Bi, Q. Wang, Y. Shao, Y. Yuan, Z. Xiao, J. Huang, *Nat Commun* **2015**, *6*, 7747.
[163] Md. B. Islam, M. Yanagida, Y. Shirai, Y. Nabetani, K. Miyano, *ACS Omega* **2017**, *2*, 2291.
[164] S. Yuchuan, Y. Yuan, H. Jinsong, *Nat Energy* **2016**, *1*, 15001.
[165] L. Calió, S. Kazim, M. Grätzel, S. Ahmad, *Angewandte Chemie International Edition* **2016**, *55*, 14522.
[166] H. Pan, X. Zhao, X. Gong, H. Li, N. H. Ladi, X. L. Zhang, W. Huang, S. Ahmad, L. Ding, Y. Shen, M. Wang, Y. Fu, *Mater Horiz* **2020**, *7*, 2276.
[167] J. Peng, F. Kremer, D. Walter, Y. Wu, Y. Ji, J. Xiang, W. Liu, T. Duong, H. Shen, T. Lu, F. Brink, D. Zhong, L. Li, O. Lee Cheong Lem, Y. Liu, K. J. Weber, T. P. White, K. R. Catchpole, *Nature* **2022**, *601*, 573.
[168] I. R. Benmessaoud, A.-L. Mahul-Mellier, E. Horváth, B. Maco, M. Spina, H. A. Lashuel, L. Forró, *Toxicol Res (Camb)* **2016**, *5*, 407.
[169] E. K. Silbergeld, *Annu Rev Public Health* **1997**, *18*, 187.
[170] J. Li, H.-L. Cao, W.-B. Jiao, Q. Wang, M. Wei, I. Cantone, J. Lü, A. Abate, *Nat Commun* **2020**, *11*, 310.
[171] S. Y. Park, J.-S. Park, B. J. Kim, H. Lee, A. Walsh, K. Zhu, D. H. Kim, H. S. Jung, *Nat Sustain* **2020**, *3*, 1044.
[172] G. Nasti, A. Abate, *Adv Energy Mater* **2020**, *10*, 1902467.
[173] A. Kama, S. Tirosh, A. Itzhak, M. Ejgenberg, D. Cahen, *ACS Appl Energy Mater* **2022**, *5*, 3638.
[174] C. H. Ng, K. Nishimura, N. Ito, K. Hamada, D. Hirotani, Z. Wang, F. Yang, S. likubo, Q. Shen, K. Yoshino, T. Minemoto, S. Hayase, *Nano Energy* **2019**, *58*, 130.
[175] N. Ito, M. A. Kamarudin, D. Hirotani, Y. Zhang, Q. Shen, Y. Ogomi, S. Iikubo, T. Minemoto, K. Yoshino, S. Hayase, *Journal of Physical Chemistry Letters* **2018**, *9*, 1682.
[176] T. Krishnamoorthy, H. Ding, C. Yan, W. L. Leong, T. Baikie, Z. Zhang, M. Sherburne, S. Li, M. Asta, N. Mathews, S. G. Mhaisalkar, *J Mater Chem A Mater* **2015**, *3*, 23829.
[177] F. J. Amaya Suazo, S. Shaji, D. A. Avellaneda, J. A. Aguilar-Martínez, B. Krishnan, *Mater Sci Semicond Process* **2020**, *115*, 105115.
[178] A. E. Maughan, A. M. Ganose, A. M. Candia, J. T. Granger, D. O. Scanlon, J. R. Neilson, *Chemistry of Materials* **2018**, *30*, 472.
[179] T. Singh, A. Kulkarni, M. Ikegami, T. Miyasaka, *ACS Appl Mater Interfaces* **2016**, *8*, 14542.

[180] W. Ke, M. G. Kanatzidis, *Nat Commun* **2019**, *10*, 965.
[181] W. Shockley, H. J. Queisser, *J Appl Phys* **1961**, *32*, 510.
[182] C. Wang, F. Gu, Z. Zhao, H. Rao, Y. Qiu, Z. Cai, G. Zhan, X. Li, B. Sun, X. Yu, B. Zhao, Z. Liu, Z. Bian, C. Huang, *Advanced Materials* **2020**, *32*, 1907623.
[183] H. Xu, Y. Jiang, T. He, S. Li, H. Wang, Y. Chen, M. Yuan, J. Chen, *Adv Funct Mater* **2019**, *0*, 1807696.
[184] X. Meng, J. Lin, X. Liu, X. He, Y. Wang, T. Noda, T. Wu, X. Yang, L. Han, *Advanced Materials* **2019**, *31*, 1903721.
[185] X. Jiang, H. Li, Q. Zhou, Q. Wei, M. Wei, L. Jiang, Z. Wang, Z. Peng, F. Wang, Z. Zang, K. Xu, Y. Hou, S. Teale, W. Zhou, R. Si, X. Gao, E. H. Sargent, Z. Ning, *J Am Chem Soc* **2021**, *143*, 10970.
[186] X. Jiang, F. Wang, Q. Wei, H. Li, Y. Shang, W. Zhou, C. Wang, P. Cheng, Q. Chen, L. Chen, Z. Ning, *Nat Commun* **2020**, *11*, 1245.
[187] E. W.-G. Diau, E. Jokar, M. Rameez, *ACS Energy Lett* **2019**, 1930.
[188] W. Gao, C. Ran, J. Li, H. Dong, B. Jiao, L. Zhang, X. Lan, X. Hou, Z. Wu, *J Phys Chem Lett* **2018**, *9*, 6999.
[189] E. Jokar, C.-H. Chien, C.-M. Tsai, A. Fathi, E. W.-G. Diau, *Advanced Materials* **2019**, *31*, 1804835.
[190] D. B. Khadka, Y. Shirai, M. Yanagida, K. Miyano, *J Mater Chem C Mater* **2020**, *8*, 2307.
[191] K. Nishimura, M. A. Kamarudin, D. Hirotani, K. Hamada, Q. Shen, S. Iikubo, T. Minemoto, K. Yoshino, S. Hayase, *Nano Energy* **2020**, *74*, 104858.
[192] Y. Jiang, Z. Lu, S. Zou, H. Lai, Z. Zhang, J. Luo, Y. Huang, R. He, J. Jin, Z. Yi, Y. Luo, W. Wang, C. Wang, X. Hao, C. Chen, X. Wang, Y. Wang, S. Ren, T. Shi, F. Fu, D. Zhao, *Nano Energy* **2022**, *103*, 107818.
[193] H. Kim, Y. H. Lee, T. Lyu, J. H. Yoo, T. Park, J. H. Oh, *J Mater Chem A Mater* **2018**, *6*, 18173.
[194] D. B. Khadka, Y. Shirai, M. Yanagida, K. Miyano, *ACS Appl Energy Mater* **2021**, *4*, 12819.
[195] H. Jang, H. Y. Lim, Y. J. Yoon, J. Seo, C. B. Park, J. G. Son, J. W. Kim, Y. S. Shin, N. G. An, S. J. Choi, S. H. Kim, J. Jeong, Y. Jo, S. K. Kwak, D. S. Kim, J. Y. Kim, *Solar RRL* **2022**, *6*, 2200789.
[196] S. Shahbazi, M.-Y. Li, A. Fathi, E. W.-G. Diau, *ACS Energy Lett* **2020**, *5*, 2508.
[197] Z. Zhu, X. Jiang, D. Yu, N. Yu, Z. Ning, Q. Mi, *ACS Energy Lett* **2022**, *7*, 2079.
[198] H. Ban, T. Nakajima, Z. Liu, H. Yu, Q. Sun, L. Dai, Y. Shen, X.-L. Zhang, J. Zhu, P. Chen, M. Wang, *J Mater Chem A Mater* **2022**, *10*, 3642.
[199] J. Sanchez-Diaz, R. S. Sánchez, S. Masi, M. Krecîmarová, A. O. Alvarez, E. M. Barea, J. Rodriguez-Romero, V. S. Chirvony, J. F. Sánchez-Royo, J. P. Martinez-Pastor, I. Mora-Seró, *Joule* **2022**, *6*, 861.
[200] C.-H. Kuan, J.-M. Chih, Y.-C. Chen, B.-H. Liu, C.-H. Wang, C.-H. Hou, J.-J. Shyue, E. W.-G. Diau, *ACS Energy Lett* **2022**, *7*, 4436.
[201] S. Zou, S. Ren, Y. Jiang, Y. Huang, W. Wang, C. Wang, C. Chen, X. Hao, L. Wu, J. Zhang, D. Zhao, *ENERGY & ENVIRONMENTAL MATERIALS* **2023**, e12465.
[202] X. Liu, T. Wu, X. Luo, H. Wang, M. Furue, T. Bessho, Y. Zhang, J. Nakazaki, H. Segawa, L. Han, *ACS Energy Lett* **2022**, *7*, 425.
[203] D. B. Khadka, Y. Shirai, M. Yanagida, T. Tadano, K. Miyano, *Chemistry of Materials* **2023**, *35*, 4250.
[204] M. A. Kamarudin, D. Hirotani, Z. Wang, K. Hamada, K. Nishimura, Q. Shen, T. Toyoda, S. Iikubo, T. Minemoto, K. Yoshino, S. Hayase, *J Phys Chem Lett* **2019**, *10*, 5277.
[205] T. Nakamura, S. Yakumaru, M. A. Truong, K. Kim, J. Liu, S. Hu, K. Otsuka, R. Hashimoto, R. Murdey, T. Sasamori, H. Do Kim, H. Ohkita, T. Handa, Y. Kanemitsu, A. Wakamiya, *Nat Commun* **2020**, *11*, 3008.
[206] H. Li, B. Chang, L. Wang, Z. Wang, L. Pan, Y. Wu, Z. Liu, L. Yin, *ACS Energy Lett* **2022**, *7*, 3889.
[207] S. Shao, J. Liu, G. Portale, H.-H. Fang, G. R. Blake, G. H. ten Brink, L. J. A. Koster, M. A. Loi, *Adv Energy Mater* **2018**, *8*, 1702019.
[208] M. Li, M. Li, M. Li, W. W. Zuo, W. W. Zuo, Y. G. Yang, M. H. Aldamasy, M. H. Aldamasy, Q. Wang, S. H. T. Cruz, S. L. Feng, M. Saliba, M. Saliba, Z. K. Wang, A. Abate, A. Abate, *ACS Energy Lett* **2020**, *5*, 1923.
[209] E. Jokar, P.-Y. Cheng, C.-Y. Lin, S. Narra, S. Shahbazi, E. Wei-Guang Diau, *ACS Energy Lett* **2021**, *6*, 485.
[210] T. Wang, H. Loi, J. Cao, Z. Qin, Z. Guan, Y. Xu, H. Cheng, M. G. Li, C. Lee, X. Lu, F. Yan, *Advanced Science* **2022**, 2200242.
[211] G. Liu, Y. Zhong, W. Feng, M. Yang, G. Yang, J. Zhong, T. Tian, J. Luo, J. Tao, S. Yang, X. Wang, L. Tan, Y. Chen, W. Wu, *Angewandte Chemie International Edition* **2022**, *61*, e202209464.
[212] B. Li, X. Wu, H. Zhang, S. Zhang, Z. Li, D. Gao, C. Zhang, M. Chen, S. Xiao, A. K. - Y. Jen, S. Yang, Z. Zhu, *Adv Funct Mater* **2022**, *32*, 2205870.
[213] L. Wang, M. Chen, S. Yang, N. Uezono, Q. Miao, G. Kapil, A. K. Baranwal, Y. Sanehira, D. Wang, D. Liu, T. Ma, K. Ozawa, T. Sakurai, Z. Zhang, Q. Shen, S. Hayase, *ACS Energy Lett* **2022**, *7*, 3703.

[214] Z. Zhao, F. Gu, Y. Li, W. Sun, S. Ye, H. Rao, Z. Liu, Z. Bian, C. Huang, *Advanced Science* **2017**, *4*, 1700204.
[215] T. Nakamura, K. Otsuka, S. Hu, R. Hashimoto, T. Morishita, T. Handa, T. Yamada, M. A. Truong, R. Murdey, Y. Kanemitsu, A. Wakamiya, *ACS Appl Energy Mater* **2022**, *5*, 14789.
[216] M. Rameez, E. Y.-R. Lin, P. Raghunath, S. Narra, D. Song, M.-C. Lin, C.-H. Hung, E. W.-G. Diau, *ACS Appl Mater Interfaces* **2020**, *12*, 21739.
[217] M. Rameez, S. Shahbazi, P. Raghunath, M. C. Lin, C. H. Hung, E. W.-G. Diau, *J Phys Chem Lett* **2020**, *11*, 2443.
[218] F. Hao, C. C. Stoumpos, D. H. Cao, R. P. H. Chang, M. G. Kanatzidis, *Nat Photonics* **2014**, *8*, 489.
[219] S. Wang, C. Wu, L. Xie, L. Ding, F. Hao, *ACS Mater Lett* **2023**, *5*, 936.
[220] M. H. Kumar, S. Dharani, W. L. Leong, P. P. Boix, R. R. Prabhakar, T. Baikie, C. Shi, H. Ding, R. Ramesh, M. Asta, M. Graetzel, S. G. Mhaisalkar, N. Mathews, *Advanced Materials* **2014**, *26*, 7122.
[221] J. Pascual, M. Flatken, R. Félix, G. Li, S. Turren- Cruz, M. H. Aldamasy, C. Hartmann, M. Li, D. Di Girolamo, G. Nasti, E. Hüsam, R. G. Wilks, A. Dallmann, M. Bär, A. Hoell, A. Abate, *Angewandte Chemie International Edition* **2021**, *60*, 21583.
[222] W. Liao, D. Zhao, Y. Yu, C. R. Grice, C. Wang, A. J. Cimaroli, P. Schulz, W. Meng, K. Zhu, R.-G. Xiong, Y. Yan, *Advanced Materials* **2016**, *28*, 9333.
[223] S. Joy, H. R. Atapattu, S. Sorensen, H. Pruett, A. B. Olivelli, A. J. Huckaba, A.-F. Miller, K. R. Graham, *J Mater Chem A Mater* **2022**, *10*, 13278.
[224] B.-B. Yu, L. Xu, M. Liao, Y. Wu, F. Liu, Z. He, J. Ding, W. Chen, B. Tu, Y. Lin, Y. Zhu, X. Zhang, W. Yao, A. B. Djurišić, J.-S. Hu, Z. He, *Solar RRL* **2019**, *3*, 1800290.
[225] C. Wang, Y. Zhang, F. Gu, Z. Zhao, H. Li, H. Jiang, Z. Bian, Z. Liu, *Matter* **2021**, *4*, 709.
[226] Z. Zhu, Q. Mi, *Cell Rep Phys Sci* **2022**, *3*, 100690.
[227] W.-G. Choi, C.-G. Park, Y. Kim, T. Moon, *ACS Energy Lett* **2020**, *5*, 3461.
[228] J. Pascual, D. Di Girolamo, M. A. Flatken, M. H. Aldamasy, G. Li, M. Li, A. Abate, *Chemistry – A European Journal* **2022**, *28*, DOI 10.1002/chem.202103919.
[229] V. S. Kostko, O. V. Kostko, G. I. Makovetskii, K. I. Yanushkevich, *physica status solidi (b)* **2002**, *229*, 1349.
[230] C. Li, Z. Song, C. Chen, C. Xiao, B. Subedi, S. P. Harvey, N. Shrestha, K. K. Subedi, L. Chen, D. Liu, Y. Li, Y.-W. Kim, C. Jiang, M. J. Heben, D. Zhao, R. J. Ellingson, N. J. Podraza, M. Al-Jassim, Y. Yan, *Nat Energy* **2020**, *5*, 768.
[231] F. Li, Y. Xie, Y. Hu, M. Long, Y. Zhang, J. Xu, M. Qin, X. Lu, M. Liu, *ACS Energy Lett* **2020**, *5*, 1422.
[232] J. Qiu, Y. Xia, Y. Zheng, W. Hui, H. Gu, W. Yuan, H. Yu, L. Chao, T. Niu, Y. Yang, X. Gao, Y. Chen, W. Huang, *ACS Energy Lett* **2019**, *4*, 1513.
[233] H. Yao, W. Zhu, J. Hu, C. Wu, S. Wang, X. Zhao, X. Niu, L. Ding, F. Hao, *Chemical Engineering Journal* **2023**, *455*, 140862.
[234] J.-T. Lin, T.-C. Chu, D.-G. Chen, Z.-X. Huang, H.-C. Chen, C.-S. Li, C.-I. Wu, P.-T. Chou, C.-W. Chiu, H. M. Chen, *ACS Appl Energy Mater* **2021**, *4*, 2041.
[235] F. Wang, X. Jiang, H. Chen, Y. Shang, H. Liu, J. Wei, W. Zhou, H. He, W. Liu, Z. Ning, *Joule* **2018**, *2*, 2732.
[236] M. Hu, R. Nie, H. Kim, J. Wu, S. Chen, B. Park, G. Kim, H.-W. Kwon, S. Il Seok, *ACS Energy Lett* **2021**, *6*, 3555.
[237] N. Sun, W. Gao, H. Dong, Y. Liu, X. Liu, Z. Wu, L. Song, C. Ran, Y. Chen, *ACS Energy Lett* **2021**, *6*, 2863.
[238] H. Kang, C.-H. Cho, H.-H. Cho, T. E. Kang, H. J. Kim, K.-H. Kim, S. C. Yoon, B. J. Kim, *ACS Appl Mater Interfaces* **2012**, *4*, 110.
[239] M. Jošt, L. Kegelmann, L. Korte, S. Albrecht, *Adv Energy Mater* **2020**, *10*, 1904102.
[240] S. Hu, J. A. Smith, H. J. Snaith, A. Wakamiya, *Precision Chemistry* **2023**, *1*, 69.
[241] J. Tong, Q. Jiang, A. J. Ferguson, A. F. Palmstrom, X. Wang, J. Hao, S. P. Dunfield, A. E. Louks, S. P. Harvey, C. Li, H. Lu, R. M. France, S. A. Johnson, F. Zhang, M. Yang, J. F. Geisz, M. D. McGehee, M. C. Beard, Y. Yan, D. Kuciauskas, J. J. Berry, K. Zhu, *Nat Energy* **2022**, *7*, 642.
[242] J. Wang, M. A. Uddin, B. Chen, X. Ying, Z. Ni, Y. Zhou, M. Li, M. Wang, Z. Yu, J. Huang, *Adv Energy Mater* **2023**, *13*, 2204115.
[243] F. Yang, R. W. MacQueen, D. Menzel, A. Musiienko, A. Al- Ashouri, J. Thiesbrummel, S. Shah, K. Prashanthan, D. Abou- Ras, L. Korte, M. Stolterfoht, D. Neher, I. Levine, H. Snaith, S. Albrecht, *Adv Energy Mater* **2023**, *13*, 2204339.
[244] S. Hu, K. Otsuka, R. Murdey, T. Nakamura, M. A. Truong, T. Yamada, T. Handa, K. Matsuda, K. Nakano, A. Sato, K. Marumoto, K. Tajima, Y. Kanemitsu, A. Wakamiya, *Energy Environ Sci* **2022**, *15*, 2096.

[245] Y. Zhu, P. Lv, M. Hu, S. R. Raga, H. Yin, Y. Zhang, Z. An, Q. Zhu, G. Luo, W. Li, F. Huang, M. Lira- Cantu, Y. Cheng, J. Lu, *Adv Energy Mater* **2023**, *13*, 2203681.
[246] G. Kapil, T. Bessho, Y. Sanehira, S. R. Sahamir, M. Chen, A. K. Baranwal, D. Liu, Y. Sono, D. Hirotani, D. Nomura, K. Nishimura, M. A. Kamarudin, Q. Shen, H. Segawa, S. Hayase, *ACS Energy Lett* **2022**, *7*, 966.
[247] J. Wang, Z. Yu, D. D. Astridge, Z. Ni, L. Zhao, B. Chen, M. Wang, Y. Zhou, G. Yang, X. Dai, A. Sellinger, J. Huang, *ACS Energy Lett* **2022**, *7*, 3353.
[248] S. Hu, P. Zhao, K. Nakano, R. D. J. Oliver, J. Pascual, J. A. Smith, T. Yamada, M. A. Truong, R. Murdey, N. Shioya, T. Hasegawa, M. Ehara, M. B. Johnston, K. Tajima, Y. Kanemitsu, H. J. Snaith, A. Wakamiya, *Advanced Materials* **2023**, *35*, 2208320.
[249] L. Huerta Hernandez, M. A. Haque, A. Sharma, L. Lanzetta, J. Bertrandie, A. Yazmaciyan, J. Troughton, D. Baran, *Sustain Energy Fuels* **2022**, *6*, 4605.
[250] Z. Zhang, J. Liang, Y. Zheng, X. Wu, J. Wang, Y. Huang, Y. Yang, Z. Zhou, L. Wang, L. Kong, K. M. Reddy, C. Qin, C.-C. Chen, *J Mater Chem A Mater* **2021**, *9*, 17830.
[251] C. Peng, C. Li, M. Zhu, C. Zhang, X. Jiang, H. Yin, B. He, H. Li, M. Li, S. K. So, Z. Zhou, *Angewandte Chemie International Edition* **2022**, *61*, e202201209.
[252] J. Li, N. Yan, Z. Fang, S. F. Liu, *ACS Appl Energy Mater* **2022**, *5*, 6936.
[253] Z. Yu, X. Chen, S. P. Harvey, Z. Ni, B. Chen, S. Chen, C. Yao, X. Xiao, S. Xu, G. Yang, Y. Yan, J. J. Berry, M. C. Beard, J. Huang, *Advanced Materials* **2022**, *34*, 2110351.
[254] L. Huang, H. Cui, W. Zhang, D. Pu, G. Zeng, Y. Liu, S. Zhou, C. Wang, J. Zhou, C. Wang, H. Guan, W. Shen, G. Li, T. Wang, W. Zheng, G. Fang, W. Ke, *Advanced Materials* **2023**, 2301125.
[255] X. Jiang, C. Li, X. Wang, C. Peng, H. Jiang, H. Bu, M. Zhu, H. Yin, B. He, H. Li, S. Pang, Z. Zhou, *ACS Energy Lett* **2023**, *8*, 1068.
[256] Q. Wen, C. Duan, F. Zou, D. Luo, J. Li, Z. Liu, J. Wang, K. Yan, *Chemical Engineering Journal* **2023**, *452*, 139697.
[257] S. Hu, M. A. Truong, K. Otsuka, T. Handa, T. Yamada, R. Nishikubo, Y. Iwasaki, A. Saeki, R. Murdey, Y. Kanemitsu, A. Wakamiya, *Chem Sci* **2021**, *12*, 13513.
[258] Z. Liang, H. Xu, Y. Zhang, G. Liu, S. Chu, Y. Tao, X. Xu, S. Xu, L. Zhang, X. Chen, B. Xu, Z. Xiao, X. Pan, J. Ye, *Advanced Materials* **2022**, *34*, 2110241.
[259] J. Luo, R. He, H. Lai, C. Chen, J. Zhu, Y. Xu, F. Yao, T. Ma, Y. Luo, Z. Yi, Y. Jiang, Z. Gao, J. Wang, W. Wang, H. Huang, Y. Wang, S. Ren, Q. Lin, C. Wang, F. Fu, D. Zhao, *Advanced Materials* **2023**, *35*, 2300352.
[260] W. Zhang, H. Yuan, X. Li, X. Guo, C. Lu, A. Liu, H. Yang, L. Xu, X. Shi, Z. Fang, H. Yang, Y. Cheng, J. Fang, *Advanced Materials* **2023**, 2303674.
[261] M. Wei, K. Xiao, G. Walters, R. Lin, Y. Zhao, M. I. Saidaminov, P. Todorović, A. Johnston, Z. Huang, H. Chen, A. Li, J. Zhu, Z. Yang, Y. Wang, A. H. Proppe, S. O. Kelley, Y. Hou, O. Voznyy, H. Tan, E. H. Sargent, *Advanced Materials* **2020**, *32*, 1907058.
[262] J. Zhang, H. Hu, Y. Zhang, Z. Liang, P. Zhu, Z. Li, D. Wang, J. Chen, J. Zeng, Z. Jiang, J. Wu, L. Zhang, B. Hu, X. Pan, X. Wang, B. Xu, *ACS Appl Mater Interfaces* **2023**, *15*, 15321.
[263] Y. Ma, F. Zheng, S. Li, Y. Liu, J. Ren, Y. Wu, Q. Sun, Y. Hao, *ACS Appl Mater Interfaces* **2023**, *15*, 34862.
[264] G. Kapil, T. Bessho, C. H. Ng, K. Hamada, M. Pandey, M. A. Kamarudin, D. Hirotani, T. Kinoshita, T. Minemoto, Q. Shen, T. Toyoda, T. N. Murakami, H. Segawa, S. Hayase, *ACS Energy Lett* **2019**, *4*, 1991.
[265] L. Chen, C. Li, Y. Xian, S. Fu, A. Abudulimu, D. Li, J. D. Friedl, Y. Li, S. Neupane, M. S. Tumusange, N. Sun, X. Wang, R. J. Ellingson, M. J. Heben, N. J. Podraza, Z. Song, Y. Yan, *Adv Energy Mater* **2023**, 2301218.
[266] C. Li, Z. Song, D. Zhao, C. Xiao, B. Subedi, N. Shrestha, M. M. Junda, C. Wang, C. S. Jiang, M. Al-Jassim, R. J. Ellingson, N. J. Podraza, K. Zhu, Y. Yan, *Adv Energy Mater* **2019**, *9*, DOI 10.1002/aenm.201803135.
[267] D. Zhao, C. Chen, C. Wang, M. M. Junda, Z. Song, C. R. Grice, Y. Yu, C. Li, B. Subedi, N. J. Podraza, X. Zhao, G. Fang, R.-G. Xiong, K. Zhu, Y. Yan, *Nat Energy* **2018**, *3*, 1093.
[268] M. H. Futscher, B. Ehrler, *ACS Energy Lett* **2016**, *1*, 863.
[269] R. W. Crisp, G. F. Pach, J. M. Kurley, R. M. France, M. O. Reese, S. U. Nanayakkara, B. A. MacLeod, D. V. Talapin, M. C. Beard, J. M. Luther, *Nano Lett* **2017**, *17*, 1020.
[270] Y. Zhao, C. Wang, T. Ma, L. Zhou, Z. Wu, H. Wang, C. Chen, Z. Yu, W. Sun, A. Wang, H. Huang, B. Zou, D. Zhao, X. Li, *Energy Environ Sci* **2023**, *16*, 2080.
[271] F. Fu, J. Li, T. C. Yang, H. Liang, A. Faes, Q. Jeangros, C. Ballif, Y. Hou, *Advanced Materials* **2022**, *34*, 2106540.
[272] A. De Vos, *J Phys D Appl Phys* **1980**, *13*, 839.

[273] Y. Hou, E. Aydin, M. De Bastiani, C. Xiao, F. H. Isikgor, D.-J. Xue, B. Chen, H. Chen, B. Bahrami, A. H. Chowdhury, A. Johnston, S.-W. Baek, Z. Huang, M. Wei, Y. Dong, J. Troughton, R. Jalmood, A. J. Mirabelli, T. G. Allen, E. Van Kerschaver, M. I. Saidaminov, D. Baran, Q. Qiao, K. Zhu, S. De Wolf, E. H. Sargent, *Science* **2020**, *367*, 1135.

[274] K. Sveinbjörnsson, B. Li, S. Mariotti, E. Jarzembowski, L. Kegelmann, A. Wirtz, F. Frühauf, A. Weihrauch, R. Niemann, L. Korte, F. Fertig, J. W. Müller, S. Albrecht, *ACS Energy Lett* **2022**, *7*, 2654.

[275] M. Spence, R. Hammond, A. Pockett, Z. Wei, A. Johnson, T. Watson, M. J. Carnie, *ACS Appl Energy Mater* **2022**, *5*, 5974.

[276] Z. Li, Y. Zhao, X. Wang, Y. Sun, Z. Zhao, Y. Li, H. Zhou, Q. Chen, *Joule* **2018**, *2*, 1559.

[277] J. Thiesbrummel, F. Peña- Camargo, K. O. Brinkmann, E. Gutierrez- Partida, F. Yang, J. Warby, S. Albrecht, D. Neher, T. Riedl, H. J. Snaith, M. Stolterfoht, F. Lang, *Adv Energy Mater* **2023**, *13*, 2202674.

[278] Y. Wang, R. Lin, X. Wang, C. Liu, Y. Ahmed, Z. Huang, Z. Zhang, H. Li, M. Zhang, Y. Gao, H. Luo, P. Wu, H. Gao, X. Zheng, M. Li, Z. Liu, W. Kong, L. Li, K. Liu, M. I. Saidaminov, L. Zhang, H. Tan, *Nat Commun* **2023**, *14*, 1819.

[279] R. He, W. Wang, Z. Yi, F. Lang, C. Chen, J. Luo, J. Zhu, J. Thiesbrummel, S. Shah, K. Wei, Y. Luo, C. Wang, H. Lai, H. Huang, J. Zhou, B. Zou, X. Yin, S. Ren, X. Hao, L. Wu, J. Zhang, J. Zhang, M. Stolterfoht, F. Fu, W. Tang, D. Zhao, *Nature* **2023**, *618*, 80.

[280] R. Lin, J. Xu, M. Wei, Y. Wang, Z. Qin, Z. Liu, J. Wu, K. Xiao, B. Chen, S. M. Park, G. Chen, H. R. Atapattu, K. R. Graham, J. Xu, J. Zhu, L. Li, C. Zhang, E. H. Sargent, H. Tan, *Nature* **2022**, *603*, 73.

[281] R. Lin, Y. Wang, Q. Lu, B. Tang, J. Li, H. Gao, Y. Gao, H. Li, C. Ding, J. Wen, P. Wu, C. Liu, S. Zhao, K. Xiao, Z. Liu, C. Ma, Y. Deng, L. Li, F. Fan, H. Tan, *Nature* **2023**, DOI 10.1038/s41586-023-06278-z.

Table of Contents Graphics

Recent progress on the strategies to fabricate Pb, Sn, and Pb-Sn perovskite based- solar cells is reviewed. This report discusses the fundamental aspects of crystal structure and perovskite chemistry along with advancements in device performance and operational stability using the crystal lattice modulation, molecular passivation, and carrier transport engineering.

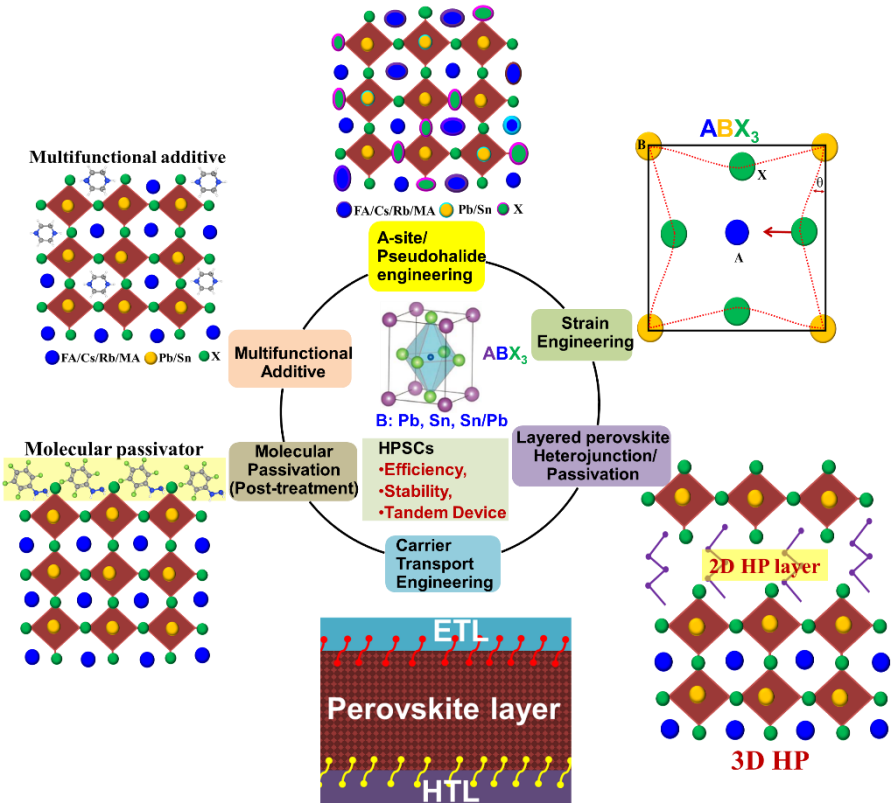

Authors-Bio

Table of Contents Graphics

Recent progress on the strategies to fabricate Pb, Sn, and Pb-Sn perovskite based- solar cells is reviewed. This report discusses the fundamental aspects of crystal structure and perovskite chemistry along with advancements in device performance and operational stability using the crystal lattice modulation, molecular passivation, and carrier transport engineering.